AALBORG UNIVERSITET

Student report

Department of Energy Technology-Pontoppidanstraede 101

Aalborg University, Denmark

Optimal Sizing and Operation of Battery Storages in Stand-Alone Hybrid Power Systems

Ioannis Kyriakidis

M.Sc. Wind Power Systems

MASTER THESIS

SPRING SEMESTER 2012

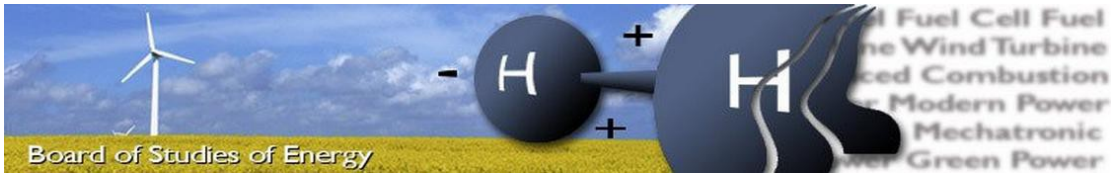

Title:	Optimal sizing and operation of battery storages in stand-alone hybrid power systems
Semester:	10th
Semester theme:	Master thesis
Project period:	7th February – 31st May 2012
ECTS:	30
Supervisor:	Jayakrishnan R. Pillai (Assistant Professor), Sanjay K. Chaudhary (Assistant Professor)

Ioannis Kyriakidis

_____

Copies: 3

Pages, total: 70

Appendices: 3

Supplements: 3 CDs

SYNOPSIS:

The electrification of many remote islands in Greece is satisfied by autonomous diesel-fueled power stations. The operation of those stations brings a number of environmental and economic drawbacks. It is proven that integration of renewable-based systems along with storage technologies can contribute to limitation of those problems. The scope of this thesis is to investigate the optimal size and operation of a battery storage technology for the hybrid power system of Agios Efstratios. The optimization procedure is done with respect to the net present cost (NPC) of the system. Additionally, the feasibility of incorporating different battery technologies is evaluated and an interconnection scenario with a nearby island is assessed. Furthermore, the island's network is analyzed under normal operation conditions, the optimal placement for the renewable and storage units is explored and finally, the dynamic behavior of the battery is analyzed under various generation/load conditions.

By signing this document, each member of the group confirms that all group members have participated in the project work, and thereby all members are collectively liable for the contents of the report. Furthermore, all group members confirm that the report does not include plagiarism.

Preface

The present Master thesis entitled "Optimal sizing and operation of battery storages in stand-alone hybrid power systems" was conducted by the author at the Department of Energy Technology, Aalborg University, between 7th of February – 31st of May 2012.

The main purpose of this thesis is the investigation of optimal ES technology, size, location and operation for the islanded hybrid renewable power system of Agios Efstratios.

Reading Instructions

In order to simplify the reading of the project some details about the way it is structured are presented. Detailed information about the literature used is illustrated at the bibliography. Figures and tables are numbered in arithmetical order. Equations are presented like (X.Y), where X is the chapter number and Y is the equation number. For the values, the point is used as decimal separator.

Acknowledgements

The author would like to express his special thanks to his supervisors, Assistant Professor Jayakrishnan R. Pillai and Assistant Professor Sanjay K. Chaudhary, for their endless support and guidance provided throughout the development of the thesis. Also I would like to thank the Public Power Corporation (PPC) and the Center for Renewable Energy Sources and Savings (CRES) for all the information and help provided during the entire project period.

Contents

Tables

Figures

Abbreviations

APS	Autonomous Power Systems
AVR	Automatic Voltage Regulator
BESS	Battery Energy Storage System
CAES	Compressed Air Energy Storage
COE	Cost of Electricity
CRES	Center for Renewable Energy Sources and Savings
CRF	Capital Recovery Factor
DG	Diesel Generators
DOD	Depth of Discharge
ES	Energy Storage
EU	European Union
FC	Fuel Cells
FES	Flywheel Energy Storage
HES	Hydrogen Energy Storage
ICE	Internal Combustion Engines
LA	Lead Acid
LI	Lithium Ion
LVRT	Low Voltage Ride Through
NaS	Sodium Sulphur
NiCd	Nickel Cadmium
NPC	Net Present Cost
NREL	National Renewable Energy Laboratory
OHL	Overhead Line
PHES	Pumped Hydro Energy Storage
PPC	Public Power Corporation
PSB	Polyshulphide Bromide
PV	Photovoltaic
RES	Renewable Energy Sources
SCES	Supercapacitor Energy Storage
SMES	Superconducting Magnetic Energy Storage
SOC	State of Charge
TES	Thermal Energy Storage
UPS	Uninterrupted Power Supply (UPS)
VRB	Vanadium Redox Battery
WT	Wind Turbines
ZEBRA	Sodium Nickel Chloride Battery Energy Storage
ZnBr	Zinc Bromine

Summary

Several remote islands in Greece are not interconnected to the central power network because of the high cost of the required infrastructure. As a result, their electricity demand is satisfied by diesel-fueled generators. Those kinds of units have high operational cost and are associated with various environmental drawbacks. Those problems can be limited through integration of renewable energy technologies such as wind and solar generation units. The greatest challenge in renewable-based networks is the negotiation of power fluctuations brought by the stochastic nature of renewable energy sources (RES). A commonly used method for balancing those variations is the implementation of energy storage (ES) devices in parallel to the renewable ones. Storages provide regulation and ancillary services and enable an increased RES penetration in the network. Agios Efstratios is one of the most remote islands located at the north part of the Aegean Sea. Due to the island's location, the price for the diesel fuel used in its autonomous power station (APS) is high and this fact increases the cost of electricity production. On the other hand, Agios Efstratios provides suitable environment for RES integration due to its abundant wind and solar power potential. The main goal of this thesis is to investigate the optimal size of an ES unit included in a hybrid renewable power plant at Agios Efstratios. For that scope, the initial step is to analyze the attributes and applications of various storage techniques in order to focus on those technologies which are most suitable for RES support. The comparison showed that batteries are suited for that purpose. In the following, simulation models are developed in HOMER software tool. Various RES and ES types and capacities are considered and the most feasible combinations with respect to the net present cost (NPC) are calculated. The results have been assessed according to three scenarios each of them representing a different policy and encountering several constraints. Moreover, this thesis evaluates the feasibility of addressing different battery types according to their cost, efficiency and cycle lifetime. An alternative option for the electrification of the island is the interconnection through submarine cable with the power network of Lemnos which the closest island to Agios Efstratios. Afterwards, steady-state analysis of the existing network topology is carried out considering typical cases of seasonal demand (summer- winter). The static model is developed in DIgSILENT PowerFactory simulator and the system's behavior is investigated (voltage profile, loading of lines and transformers). In the following, this thesis discusses the issue of optimal placement for the wind, solar and storage units. The main criterion which is used for this evaluation is the improvement of steady-state voltage magnitude and minimization of power losses. The final part of this study analyzes the hybrid system's stability. An aggregated dynamic model is constructed based on built-in models from DIgSILENT library. The results illustrate the battery's capability to manage the frequency and voltage variations under various cases of generation/load unbalance. Moreover, this study proves the importance of battery operation in systems with high RES penetration.

Chapter 1 – Introduction

1.1 Background and motivation

Among the 165 inhabited islands scattered over the Aegean and Ionian Archipelago region in Greece, there are 50 islands which are not interconnected to the central power network of the mainland due to their remote location and high cost of required infrastructures and so, their electrification is based on Autonomous Power Systems (APS). The annual electricity demand of those islands is around 2500 GWh (PPC 2011), as illustrated in Figure 1. The largest part of the energy production comes from diesel power stations and only a small fraction from renewables (wind and solar farms).

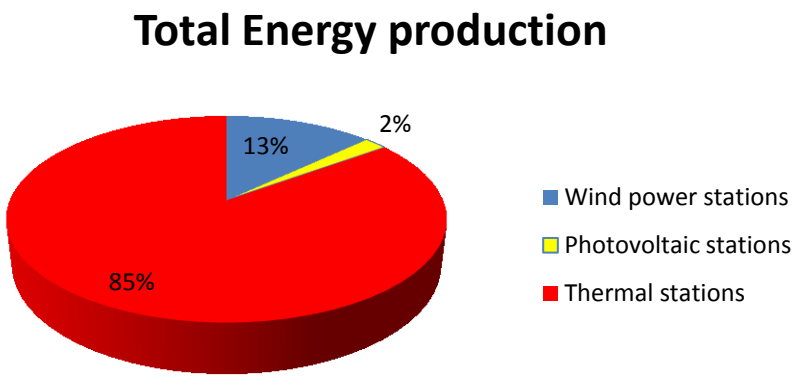

Figure 1 Total energy production share at non-interconnected islands for 2011 (PPC 2011)

There are a number of technical, environmental and economic drawbacks related to the operation of diesel stations that defy their sustainability and, for this reasons, the trend nowadays is to limit their participation in total energy production and gradually replace them with Renewable Energy Sources (RES) (Marin, Alves and Zervos 2005).

Technical inconveniencies such as low power quality and black outs are frequently being recorded at non interconnected islands, bringing economic losses and affecting the life of the locals. Also, most of the existing diesel power plants are rather old and insufficient to cover the expected electricity demand increase. Another factor that poses additional problems on the electricity power system of the islands is the seasonal demand. Summer peak load demand can be approximately five times more than the minimum winter demand, while load variations between ± 60% of the average daily demand can occur during the same day (Zafirakis and Kaldellis 2007).

Furthermore, regarding the economic part, the transportation cost of the fuel from the mainland to the remote locations in combination to the increasing prices of crude oil, raise the electricity generation cost significantly. As illustrated in Figure 2, energy production costs at some of the islands can be more than 1000 €/MWh.

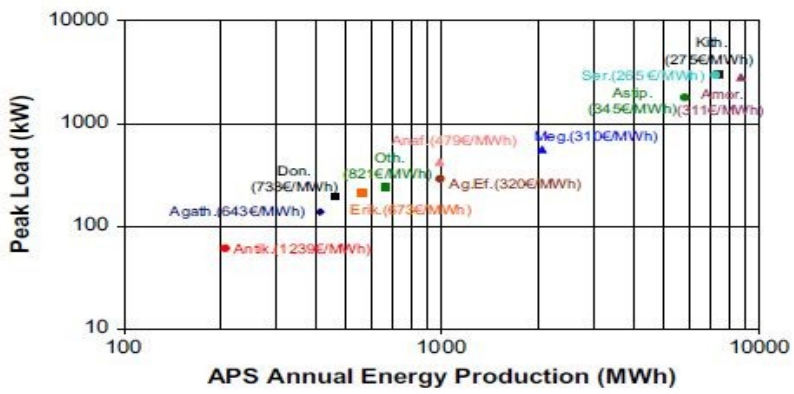

Figure 2 Small Greek island's peak load demand, APS annual energy production and electricity generation cost (kaldellis, et al. 2009)

Regarding the environmental aspect, it is well known that combustion of fossil fueled engines emits CO_2 gases enhancing the greenhouse effect, downgrading the environment and posing health risks for the inhabitants. The strategic targets that were set for year 2020 from the European Union (EU) needs to be followed by Greece which imposes reduction of greenhouse gases emissions by 20%, energy consumption of 20% from renewables and reduction in primary energy use by 20% (European Commission 2010).

In order to deal with the above mentioned drawbacks, at many non interconnected islands around the world, and in Greece as well, the system operators have started combing and/or replacing the existing conventional diesel station with hybrid ones based on Renewable Energy Sources (RES) such as wind turbines, photovoltaic (PV) panels and small hydro power stations. Due to their sustainability, reliability, long lifetime and technical maturity the aforementioned technologies consist a feasible and attractive solution for stand-alone applications when properly sized, located and suitable control strategies are implemented (Kaldellis, Zafirakis and Kavadias 2011). Most of the islands provide suitable environment for RES integration due to their abundant wind and solar potential as shown in Figure 3 and Figure 4.

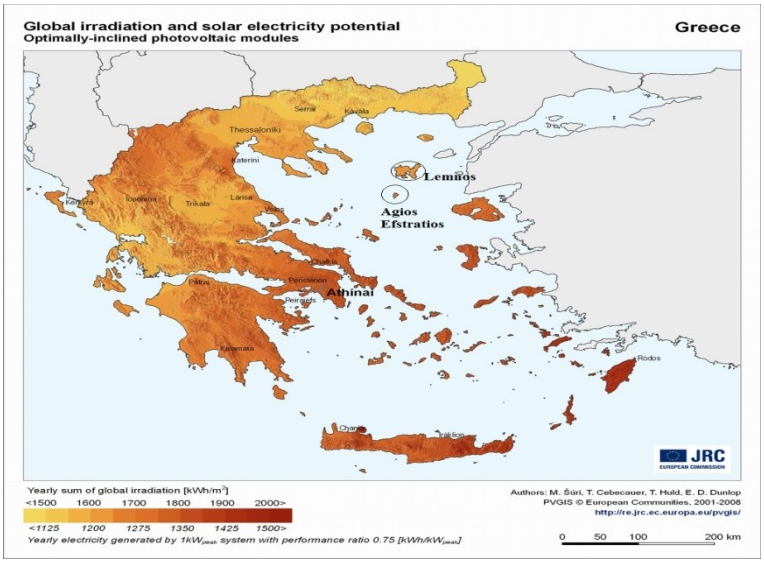

Figure 3 Solar potential distribution at Aegean - Ionian islands (Joint Research Centre 2012)

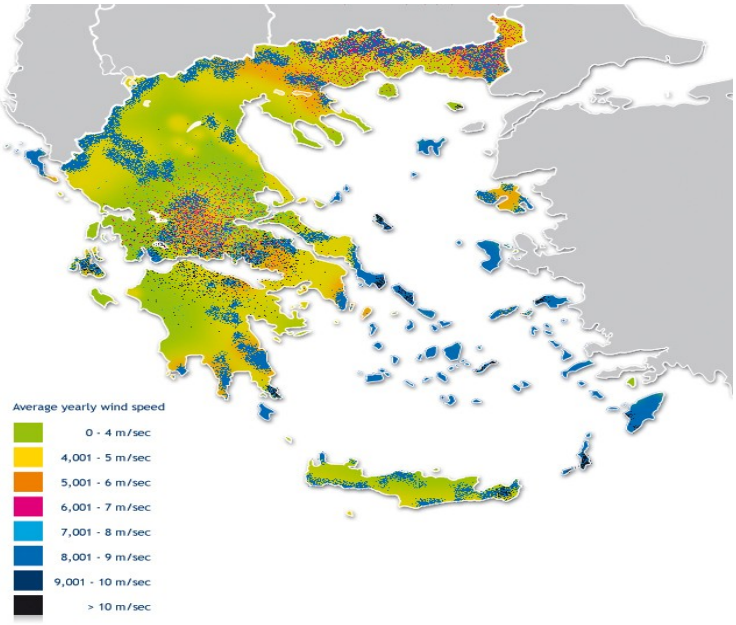

Figure 4 Wind energy potential in Greece (Global Energy Network Institute 2012)

It is worth being mentioned that connecting some of the Aegean Sea islands with the mainland and between them is also taken into consideration in order to take advantage of the renewable energy potential in the best possible way (Greek Transmission System Operator 2010).

Due to the fluctuating and intermittent characteristics of renewable resources, the RES power output is difficult to be predicted and because of the imbalances between power generation and demand, APS are subject to important frequency and voltage variations.

It is very crucial for any power system, including stand-alone networks, to maintaining the power quality at specific standardized levels. Specifically, frequency and voltage stability are the most important parts of this issue and for this reason the European Standard EN-50160 (EURELECTRIC 1995) has set limits for those two parameters, which for the case of non-interconnected power systems are:

- 50 Hz ± 1% (49.5 – 50.5 Hz) during 99.5% of a week / 50 Hz – 6%/+4% (47 – 52 Hz) during 100% of a week (mean value of fundamental frequency measured over 10 seconds)
- 230 V ± 10% (207 – 253 V) during 95% of a week / 230 V – 15% + 10% (195.5 – 207) during 100% of a week (mean 10 minutes rms values)
- 15 kV ± 10% (13.5 – 16.5 kV) during 95% of a week (mean 10 minutes rms values)

In order to sustain voltage and frequency levels within the limits, a very popular technique is the utilization of energy storage (ES) systems. Storage devices provide regulation and ancillary services, enable the integration of RES units at both interconnected and stand-alone systems and allow an increased penetration of renewables in the network. Furthermore, conventional diesel generator (DG) units may be also used either as a back-up solution or to cover unexpected high load demand.

The case of Agios Efstratios

As shown in Figure 3, Agios Efstratios is a small island located at the north part of the Aegean Sea. It covers a total area of 44 km^2 and is permanently inhabited by 270 people. During summer the population increases because of tourism. The electricity supply is based at a diesel power station consisting of five engines with 840 kW total power capacity. During the year 2010 the peak power demand was 360 kW and the annual energy demand was 1221 MWh. The electricity generation cost is 326 €/MWh, which is around four times more than the cost from conventional thermal plants in the mainland. The main generation and demand characteristics of Agios Efstratios are summarized in Table 1. Moreover, Agios Efstratios is included in the European ecological network NATURA 2000 because of its important ecosystems and species (European Environmental Agency (EEA) 2011).

The aforementioned high electricity generation cost and the negative impact of the diesel power station at the island's fragile environment has motivated the Greek Ministry of Environmental and Energy affairs to announce, at July 2011, a plan that will make the island of Agios Efstratios the first renewable island in Greece. The project called as "***Green Island – Agios Efstratios***" is pilot demonstration project which aims at the establishment of a *fossil-fuel-independent* energy profile through achievement of high RES penetration and significant reduction of diesel consumption. The project includes the implementation of a hybrid power station based on wind turbines and photovoltaic panels supported by ES systems and efficient energy management controllers (CRES 2011). Figure 5 presents a diagram of a possible configuration of the island's hybrid system.

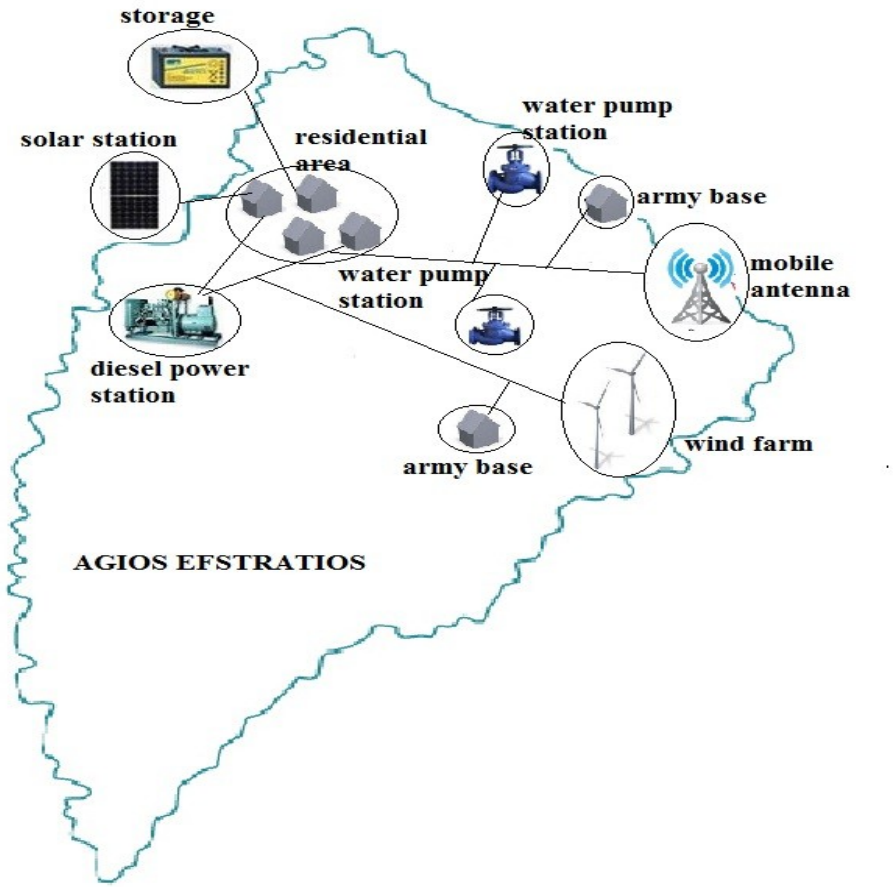

Figure 5 Diagram of Agios Efstratios hybrid Wind/PV/Diesel/Storage system

Table 1 General data for Agios Efstratios

Parameter	Value
Diesel power station capacity (kW)	840
Total annual energy demand (MWh)	1221
Average load (kW)	140
Peak load (kW)	360
Average wind speed (m/s)	8.65
Average solar power potential (kWh/m²/day)	4.43

1.2 Project objectives

The goal of this study is to investigate the optimal size and operation of an ES system included in a hybrid renewable-based plant for the islanded power system of Agios Efstratios. Furthermore, aims to optimize the hybrid system based on specific economic and policy criteria and evaluate the techno-economic feasibility of incorporating different battery ES types. Moreover, this thesis examines the economic feasibility of interconnecting the islanded system with the stronger network of the nearby island of Lemnos. Finally, another scope for this study is to analyze the steady-state behavior of the power network under normal operating conditions, find the optimal location for the RES and ES units and assess the battery impact in system stability under various generation-demand conditions.

1.3 Methodology

At first, various ES technologies and applications are analyzed in order to focus on those which are suitable for the islanded power system. Long-term simulation models of the power system network, RES (Wind and PV) units and storages are developed in HOMER. The most feasible types and capacities for RES and ES units are calculated considering different scenarios. The next step is to calculate the optimal location for the proposed hybrid system's components by performing load flow analysis for different scenarios (demand profiles) using DIgSILENT PowerFactory. Dynamic analysis is carried out, with the same software tool, in order to demonstrate the ES operation in stand-alone systems (including contingencies and the effect of variable demand). Apart from the technical, cost analysis for different types of storages is also done in order to find the most feasible solution from both technical and economic viewpoint. The scope of this project includes steady-state analysis of the base case (existing topology) islanded system under normal operation and cost evaluation of interconnecting Agios Efstratios with the power network of the nearby island of Lemnos.

1.4 Limitations

A number of limitations have been considered in this thesis as stated below.

- The time series of wind speed and demand which were used in the simulations, are provided from CRES and Public Power Corporation (PPC) respectively and have a time resolution of one hour.

- The diesel price is assumed to be constant for the lifetime period of the project.
- The optimization analysis is not considering any demand side management actions.
- A simplified radial model of the low-voltage (LV) distribution network is used for the steady-state analysis. This model does not represent every individual consumer.
- The dynamic analysis considers an aggregated model of the hybrid power system.
- The dynamic modelling is based on DIgSILENT standard models and is not within the scopes of this study to build detailed models for the renewable and storage units or to evaluate their configuration parameters.

1.5 Project outline

This thesis is divided in six different chapters. Chapter 1 contains the background and motivation of this thesis, sets the objectives, describes the methodology and project limitations. Chapter 2 presents a literature overview on various ES technologies and applications, focusing on those who are suitable for the islanded power system of Agios Efstratios. Further, describes similar cases and studies for island networks. Chapter 3 describes the optimization analysis for the RES and ES units regarding different policy scenarios and evaluates the feasibility of interconnecting Agios Efstratios through submarine cable with a stronger grid. Chapter 4 presents the steady-state model development of the current power network in DIgSILENT and illustrates its voltage profile for different seasonal demand. Also, investigates the optimal placement for the proposed renewable and storage units. In chapter 5, DIgSILENT standard models are used for the dynamic model of the proposed hybrid system and illustrate the ES operation under different RES fractions, contingencies and generation/load variations. Chapter 6 summarizes the main conclusions of the thesis and proposes topics for future work. The Appendices contain additional results, model diagrams and parameters.

Chapter 2 - State of Art for Energy Storage Technologies and Applications

2.1 Introduction

Electricity can be stored in various Energy Storage (ES) devices after being converted into mechanical, electromagnetic, electrochemical or thermal energy. The aim of this chapter is to describe the ES technologies that are currently available or under development and evaluate their suitability to mitigate RES variability. Figure 6 presents the most typical technologies and a classification for each type of storage.

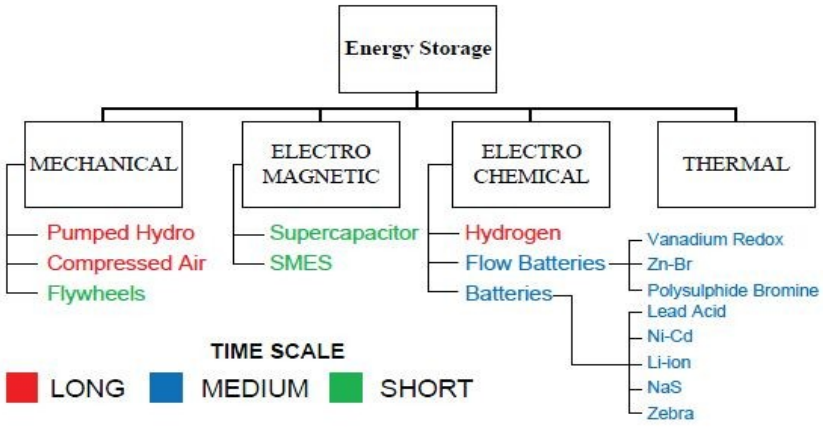

Figure 6 Classification of ES technologies (Swierczynski, et al. 2010)

The operation principle and main technical characteristics of each ES technology are illustrated and compared, namely power rating, discharge times, response time, round-trip efficiency, lifetime, and investment and operation costs. Furthermore, this chapter describes the main ES applications and presents some cases and studies regarding ES utilization at existing island systems.

2.2 Overview of ES technologies

2.2.1 Pumped Hydro Energy Storage (PHES)

Pumped Hydro ES is the most mature and widespread large-scale ES technology among the available ones (Connolly 2009). A typical PHES system comprises of two water reservoirs at different elevations connected by a system of waterways including a number of pump/turbine units. During off-peak electricity demand, excess energy is used to pump water to the upper reservoir. When the demand is high, water from the upper reservoir is released back into the lower one through turbines that generate electricity. Typical roundtrip efficiency of such kind of facilities is around 70% - 85% (E.S.A. 2009).

PHES systems are able to provide reliable power supply within a few minutes and are suitable for frequency regulation, load leveling, and black-start and energy management. Because of these capabilities, PHES can be utilized at stand-alone systems, where renewable energy technologies are used, in order to improve power quality and increase the RES penetration level. The major drawbacks of this technology are the long construction times and its dependence on geographical, ecological and environmental restrictions. Moreover, although the cost per kWh is relatively low in comparison to the rest storage technologies (up to 20 €/kWh), the high initial construction cost for the facility which is between 500 – 1500 €/kW can sometimes make PHES plants economically unattractive (Connolly 2009).

2.2.2 Compressed Air Energy Storage (CAES)

PHES and CAES are the only commercially available large-scale storage technologies. CAES systems use exceeding energy (usually at off-peak hours) taken from RES or the grid to compress air and store it in large storage reservoirs. There are many geological formations such as naturally occurring aquifers, solution-mined salt caverns and constructed rock caverns that can be used to store compressed air (Chen, et al. 2009). The typical power capacity of a CAES system is between 50 MW – 300 MW and its efficiency is around 70% - 80%. Although this technology, due to high power and energy capacity, can be a good storage solution for grids with RES integration, there is a serious disadvantage related to the dependence from geographical location. Moreover, even though the cost per kWh produced is low (3 – 5 €/kWh), the initial cost for the plant is relatively high (300 – 600 €/kW).

2.2.3 Flywheel Energy Storage (FES)

A FES system is also a mechanical form of storage and operates by storing energy in the form of kinetic energy in a rotating mass. The central shaft of a flywheel rotates on two magnetic bearings in order to reduce friction and is placed inside vacuum in order to minimize the windage losses (Naish, et al. 2008). During the charging process, the flywheel is accelerated by a motor to very high speed and maintains the energy in the system as kinetic energy. The faster a flywheel rotates the more energy it stores. On the other hand, during discharging, the stored energy is retrieved by returning the kinetic energy to the motor which in this case is used as a generator. As the flywheel discharges, the rotor slows down until it stops.

The typical efficiency of a FES system is around 85%. Furthermore the dynamic response of this storage technology is very fast, it requires only little maintenance, and its lifetime is tens of thousands of cycles and doesn't depend on the depth of discharge. On the contrary, the main disadvantage is the short discharge time. Consequently, they are suitable for power quality applications such as frequency regulation but only for a small time scale (Swierczynski, et al. 2010). Finally, the cost per kWh is between 750 – 3800 €/kWh and the initial cost of the system varies from 200 to 250 €/kW (Chen, et al. 2009).

2.2.4 Lead Acid Battery Energy Storage (LAES)

Lead Acid (LA) batteries are the most developed, common and mature battery storage technology. There are two types of LA batteries: flooded (FLA) and valve-regulated (VRLA).

FLA batteries consist of an anode (positive electrode) and a cathode (negative electrode). The electrodes are lead plates which are immersed in a mixture of water and sulphuric acid. When the battery is charged, the electrodes sit in a sulphuric acid electrolyte. During discharging, the electrodes turn into lead sulphate and the electrolyte losses its dissolved sulphuric acid and becomes mainly water (Chen, et al. 2009) (Martin 2010). The operational principle of VRLA batteries is similar to that of FLA. The difference is that the first ones have smaller weight and volume and lower maintenance cost but, on the opposite, they have shorter lifetime and higher initial cost.

The average efficiency of a LA battery is up to 85% and they are able to respond within milliseconds. Consequently, they are able to support RES devices at stand alone systems for both short term and long term applications such as energy management and frequency regulation. Some of the main drawbacks are the reduced lifetime and its dependence from the depth of discharge, the low power density and high sensitivity in temperature changes. The capital cost is around 1000 €/kWh and 150 to 200 €/kW (Espinar and Mayer 2011).

2.2.5 Lithium Ion Battery Energy Storage (LIES)

Likewise LAES, Lithium ion batteries are electrochemical cells. When the battery is charged, lithium oxide in the cathode is turned into lithium ions and move through the electrolyte towards the carbon anode where they combine to external electrons and are placed between the carbon layers. In the case of discharging, the aforementioned process is reversed and lithium moves from anode to cathode.

LIES systems have fast response, very high efficiency that can reach up to 100%, high energy density (100 – 150 Wh/kg), long lifetime (around 3000 charging/discharging cycles for 80% DOD) and minimum environmental impact. Consequently, they can be utilized for hybrid RES systems to improve the power quality and also for energy management. The main disadvantage of this technology is its high cost (around 500 €/kWh and 250 - 300 €/kW) because they require special packaging and internal overvoltage protection circuits (Schoenung 2011).

2.2.6 Nickel Cadmium Battery Energy Storage (NCES)

Nickel Cadmium is a mature and popular type of electrochemical battery. A typical NiCd battery consists of a positive electrode plate made of nickel oxyhydroxide and a negative electrode made of metallic cadmium. There are two types of NiCd batteries: the sealed and the vented ones. Sealed batteries are the common rechargeable batteries for small-scale applications and gases are not released from them. Vented batteries work in the same way as the sealed ones but gases are released through a low-pressure valve during overcharging or rapid discharging. This difference between them makes the vented batteries more robust, economical and safe compared to sealed ones (Connolly 2009).

Comparing this type of electrochemical battery with LAES, it has higher energy density (50 – 75 Wh/kg), longer lifetime (2000 – 2500 cycles) and are able to operate in wider temperature range. Moreover their efficiency varies from 60% to 70%, they are reliable, their response time is fast and they don’t require much maintenance. The cost of this storage technology is

around 190 €/kWh and 750 €/kW (Steward, et al. 2009) . Furthermore, the environmental impact of these batteries is serious since cadmium is a toxic material and brings issues regarding their disposal. Another disadvantage is the fact that they suffer from "memory effect". Consequently, it is not much possible that NCES will be used for large-scale projects and is not an important candidate for RES integration compared to other battery technologies.

2.2.7 Sodium Sulphur Battery Energy Storage (NaSES)

Sodium Sulphur (NaS) batteries are made of electrochemical cells constructed in cylindrical form. The positive electrode consists of liquid (molten) sulphur and the negative electrode is made of liquid (molten) sodium. During discharging, electrons are removed from sodium metal causing the formation of sodium ions that are transferred to the positive electrode through the electrolyte. The electrons move through the electric circuit and return back at the positive electrode. During charging, this process is reversed and as the sodium polyshulphides decompose, positive sodium ions are released back through the electrolyte to reform as elemental sodium. NaS are characterized as high temperature batteries since they operate at a range between 320 – 340 °C in order to keep the sodium and the sulphur molten in the battery and also to maintain the conductivity of the electrolyte (Divya and Ostergaard 2009).

The average round-trip efficiency of a NaS battery is up to 90%, the lifetime is approximately 2500 cycles and the energy density within the range 150 – 240 Wh/kg. Moreover it has the potential to respond within milliseconds and is also designed for long discharge cycles (8 hours). As a result, NaSES is suitable for power quality applications, peak shaving and energy management. Their major drawback is the fact that NaS battery needs to operate at high temperature so, a heat source is required which uses the battery's stored energy and reduces its performance (Chen, et al. 2009). The initial cost for this technology is also high (around 1500 €/kW and 250 €/kWh) but is expected to fall with mass production and NaSES can become an attractive and viable option for RES integration and large-scale applications.

2.2.8 Sodium Nickel Chloride Battery Energy Storage (ZEBRA)

The sodium nickel chloride batteries, also known as ZEBRA batteries, evolved from the sodium sulphur ones and operate at high temperature (around 300 °C) likewise NaS. The negative electrode consists of liquid sodium while the positive electrode is made of nickel and sodium chloride. The two electrodes are separated by a sodium ion-conducting solid electrolyte, beta – alumina. During charging, sodium ions from the central positive electrode move through the beta – alumina electrolyte to form the liquid sodium negative electrode (Sudworth 2001) (Turconi). During discharging, the opposite procedure takes place. The energy density of a typical ZEBRA battery is 120 Wh/kg, the lifetime is 2500 cycles and the round-trip efficiency can reach 90%. In comparison to other battery technologies, the cost is relatively low (around 80 €/kWh and 200 €/kW). The major drawback is related to the fact that ZEBRA batteries are manufactured exclusively by one factory in the world. Another disadvantage is the energy they have to spend in order to keep their temperature high. This storage technology is suitable for large capacity batteries and has the potential to be used for integration of renewables since it has already been used at electric vehicles (Electropaedia).

2.2.9 Vanadium Redox Battery Energy Storage (VRBES)

Vanadium Redox is a kind of flow battery that stores energy by interconnecting two forms of vanadium ions (V^{2+}/V^{3+} in the negative electrode and V^{4+}/V^{5+}) in a sulphuric acid electrolyte at each electrode. Hydrogen ions are transferred between the two electrolyte tanks through a hydrogen-ion-permeable polymer membrane. Moreover, through the electrochemical conversion all chemicals are dissolved in the electrolyte and so, within the battery, no deposit of materials takes place during the charging and discharging processes (Makarov, et al. 2008). The power capacity (kW) of the Vanadium Redox battery is determined by the size of the cell stack while the energy capacity (kWh) is indicated by the volume of the electrolyte. During discharging, the two electrolytes flow from the negative and positive tank to the cell stack where hydrogen ions pass between the two electrolytes through the permeable membrane. This process is reversed during charging. VRBES has fast response, can reach efficiency level up to 90% and its lifetime is approximately 10000 cycles. Their major disadvantages are the low energy density (25-45 Wh/kg) and the complexity of its structure. The power cost for this technology is around 1500 €/kW and the energy cost is in the range 250 – 750 €/kWh, depending on system design and application. Vanadium Redox batteries are highly versatile and, consequently, suitable for various energy storage applications such as power quality, peak shaving, Uninterrupted Power Supply (UPS) and integration of RES (Connolly 2009).

2.2.10 Polyshulphide Bromide Battery Energy Storage (PSBES)

Another type of flow battery is the Polyshulphide Bromide battery. This battery type is made up of a cell stack and an electrolyte tank system. The electrolytes utilized for PSB are sodium bromide as the positive electrolyte and sodium polysulphide as the negative electrolyte. A polymer membrane separates the two electrolytes at the cell, only allowing sodium ions to go through it during charging / discharging and, creates voltage around 1.5 V across the cell (Divya and Ostergaard 2009). The power cost is approximately 750 €/kW and the energy cost is 140 €/kWh.

The efficiency of PSBES is around 75% and the lifetime is estimated at around 2000 cycles depending on the application. The main disadvantage of this technology is the maintenance required to remove the small amounts of hydrogen, bromine and sodium sulphate that are produced during the chemical reactions. Characteristic feature of PSB batteries is their very fast response. Specifically, they are able to react within a few milliseconds and that makes them suitable for frequency and voltage regulation. They can be used for integration of RES and other ES requirements such as peak shaving, load leveling, black start and forecast improvement.

2.2.11 Zinc Bromine Battery Energy Storage (ZnBrBES)

The structure of this battery is similar to the other types of flow battery but does not operate in the same way as PSB and VR since material is deposited as solids within the cell during charging and discharging (Makarov, et al. 2008). During charging, zinc and bromine ions flow to the cell stack where they are separated by a microporous membrane. During discharging, Zn and Br ions are dissolved in both electrodes and combine into ZnBr,

generating 1.8 V across each cell (Chen, et al. 2009). The efficiency of the ZnBrBES system is around 75%, the energy density is between 75 – 85 Wh/kg and every 2000 cycles the membrane needs replacement. The power capacity cost is around 500 €/kW and the energy capacity cost is 400 €/kWh. Furthermore, this battery does not suffer from memory effect and can be 100% discharged without drawbacks (Connolly 2009). ZnBrBES is suitable for frequency regulation and support of RES in stand-alone/interconnected systems and are already being used at existing wind power plants.

2.2.12 Superconducting Magnetic Energy Storage (SMES)

SMES system consists of a superconductive coil, a power conditioning system, a cryogenic refrigerator and a vacuum vessel that preserve the coil's temperature low. Its operation is based on storing energy in the form of magnetic field produced by the flow of direct current through the circular superconducting coil. Materials such as lead, vanadium or mercury which have very low resistance are normally used for the coil and consequently, energy can be stored with practically no losses. Furthermore, it is kept in superconducting temperature (-269 °C) by being immersed in liquid helium or nitrogen. At that temperature, resistance of the material against electric currents is eliminated (Naish, et al. 2008).

Typical power capacity cost is 200 €/kW and energy capacity cost is around 400 €/kWh. The round-trip efficiency of SMES systems is approximately 97% and has very fast discharging times (within ms) but takes only a few minutes to discharge completely (Ibrahim, Ilinca and Perron 2008). Moreover, one of the greatest advantages of this technology is its long lifetime. It lasts for tens of thousands of cycles without wear of the magnet and this attribute makes SMES suitable for power quality applications. It has so far been employed for industrial applications but due to its low energy density, low discharging duration and high energy consumption of the refrigeration system, it is not much likely that it can play an important role for RES integration.

2.2.13 Supercapacitor Energy Storage (SCES)

In supercapacitors energy is stored in the form of electric field between two electrodes that hold opposite charges. The energy stored within the supercapacitor is a function of the voltage applied at and its capacity. A SCES device consists of two parallel electrodes which are separated by an electrolyte solution. The electrode plates are usually made of porous carbon material while the electrolyte can be either aqueous or organic (Chen, et al. 2009).

Typical efficiency of SCES systems is around 95% and they have very long lifetime (around 100,000 cycles). Other advantages are their quick response, the absence of memory effect and fast charge/discharge operation. On the contrary, they have low energy density (up to 5 Wh/kg) and high self-discharge rate. Typical power capacity cost of a SCES system is 200 €/kW and energy capacity cost can be up to 1500 €/kWh. Due to the aforementioned attributes, supercapacitors are suitable for small-scale (<250 kW) power quality applications but not for long-term applications such as energy management. Moreover, they can be considered as a technology that can support intermittent RES but on condition that they are combined with a battery system.

2.2.14 Thermal Energy Storage (TES)

TES systems store energy by using materials that can be kept at high/low temperatures in thermal insulated reservoirs and recover it for electricity generation using heat engine cycles. Moreover, TES systems are categorized into high-temperature and low-temperature TES depending on whether the operating temperature of the thermal reservoir is maintained at a temperature above or below that of the room. According to (Ibrahim, Ilinca and Perron 2008) there are three main types of high-temperature TES and two types of low-temperature TES.

High-temperature TES (HT-TES)

- Latent-fusion-heat TES
- Sensible heat TES
- Concrete storage

Low-temperature TES (LT-TES)

- Aquiferous low-temperature TES (AL-TES)
- Cryogenic Energy Storage (CES)

Most of the types mentioned above are under development so there is a lack of available data regarding their characteristics. Those that have been utilized so far, mostly at peak shaving applications, have demonstrated high energy density (100-200 Wh/kg), long storage periods and round-trip efficiency around 60%. Furthermore although the energy capacity cost is low, the investment cost for the initial infrastructure is high (Chen, et al. 2009). Summarizing, this technology is not considered yet to be suitable for RES integration due to its immaturity.

2.2.15 Hydrogen Energy Storage (HES)

Although hydrogen systems are still technologically immature and economically unattractive due to their high investment costs, they are expected to be one of the most promising storage techniques since they can be utilized both in stationary power systems and the transportation sector. Hydrogen produced by RES is totally emission free and can be produced at remote locations, thus increasing power supply security and contribute to energy independence (Zoulias and Lymperopoulos 2008). There are three stages comprising the operation process of a HES system:

- Create hydrogen
- Store hydrogen
- Use hydrogen for energy production

There are three main techniques to create hydrogen: extract it from fossil fuels, by electrolysis and through reacting steam with methane. Producing hydrogen from electrolyzers is the most economic and ecologic solution among the others. Production from fossil fuels is more expensive than using the fuel itself and production from steam reacting with methane pollutes the environment. Electrolyzers consist of an anode and a cathode separated by an electrolyte. During electrolysis, the electrolyzer divides water into hydrogen and oxygen. Oxygen is released in the atmosphere and hydrogen is stored for electricity generation when needed.

Storing of hydrogen can be done either by compressing it into containers, by liquefying it or by metal hydride (Connolly 2009). The first method is the most common one although there is the drawback of the energy required for the compression. The other two methods are not so popular since they require extra costs and energy consumption.

There are two main methods used to produce electricity from hydrogen: with Fuel Cells (FC) and Internal Combustion Engines (ICE). H2ICEs are modified gas engines that operate with hydrogen and their average efficiency is around 35% (Boretti 2011). FC converts the stored chemical energy into electricity and consists of two electrodes that are separated by an electrolyte.

At the cell's anode, electrons and protons of hydrogen are separated. The electrons travel through a circuit, generating electrical power. At the cathode, a catalytic process takes the electrons back in, combining them with the protons, which have travelled through the electrolyte. The greatest advantages of FC are their higher efficiency compared to ICEs, reliability, no emissions and higher power density. On the contrary, they require high initial costs because they are still under development (Connolly 2009).

2.2.16 Comparison of ES technologies

At this section, an overall comparison of the ES technologies is presented regarding their main characteristics.

Table 2 Comparison of technical and economic characteristics of ES technologies (Chen, et al. 2009) (Connolly 2009) (Swierczynski, et al. 2010) (Gonzalez, et al. 2012) (Ibrahim, Ilinca and Perron 2008) (Yang, et al. 2010) (E.S.A. 2009) (Steward, et al. 2009) (Schoenung 2011).

Characteristic / Technology	Power rating	Discharge duration	Response time	Efficiency (%)	Energy density (Wh/kg)	Lifetime (cycles)	Power capacity cost (€/kW)	Energy capacity cost (€/kWh)	Self discharge per day
PHES	100-5000 MW	1-24h +	minutes	70-85	0.5-1.5	12000-35000	500-1500	< 20	very small
CAES	50-300 MW	1-24h +	minutes	70-80	30-60	9000-20000	300-600	3-5	small
FES	tens of MW	< 15 min	milliseconds	85	10-30	20000+	200-250	750-3800	100%
LAES	< 20 MW	sec-hours	milliseconds	85	30-50	500-1500	1000	150-200	0.1-0.3%
LIES	tens of MW	sec-hours	milliseconds	90-100	100-150	1000-10000	250-300	500	0.1-0.3%
NCES	tens of MW	sec-hours	milliseconds	60-70	50-75	2000-2500	750	190	0.2-0.6
NaSES	few MW	sec-hours	milliseconds	75-90	150-240	2500	1500	250	20%
ZEBRA	few MW	sec-hours	milliseconds	80-90	120	2500	200	80	15%
VRBES	few MW	sec-hours	milliseconds	70-90	25-45	10000	1500	250-750	small
PSBES	1-15 MW	sec-hours	milliseconds	75	n/a	2000	750	140	small
ZnBrBES	< 2MW	sec-hours	seconds	75-80	75-85	2000	500	400	small
SMES	< 10 MW	seconds	milliseconds	97	0.5-5	100000+	200	400	10-15%
SCES	< 250 kW	sec-minutes	milliseconds	95	0.05-5	100000+	200	1500	20-40%
TES	tens of MW	1-24h +	minutes	60	100-200	n/a	200	30	1%
HES	few MW	sec-24h +	seconds	35-40	1000+	1000+	1000+	5-10	very small

2.3 Overview of ES applications

The aim of this section is to present an overview of the most significant ES potential applications for renewable energy integration and accommodation of network requirements.

Due to the intermittency of renewables, rapid fluctuations at the power output of wind and solar farms are likely to occur, bringing a mismatch between generation and load and a number of issues related to power quality and system stability. Especially at stand-alone systems with high RES penetration and reduced participation of conventional generation units that often supply regulation capacity, utilization of ES devices has a major importance. The following Figure 7 describes the operation of a typical ES device in such a system.

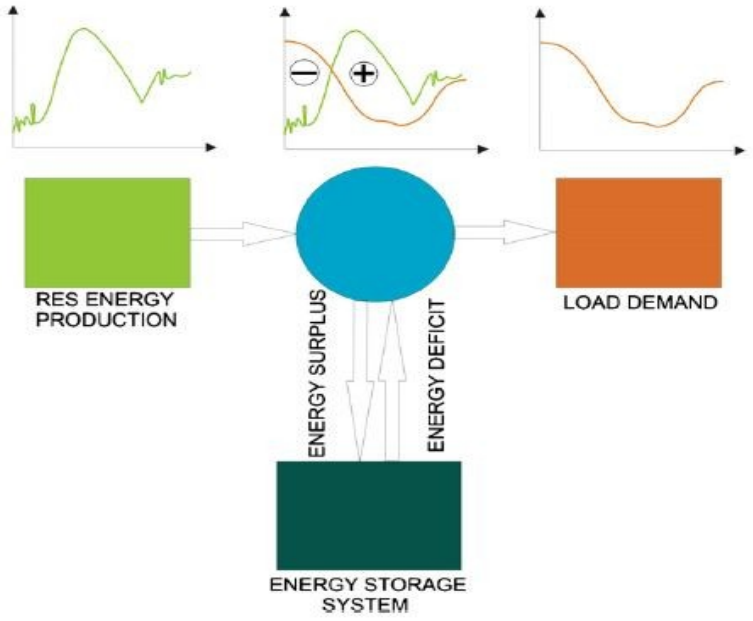

Figure 7 Operation of a typical ES system

The ES applications to be investigated here are: frequency regulation, low voltage ride through (LVRT), voltage control support, oscillation dumping, load following, load levelling, transmission curtailment, black start and energy arbitrage.

Frequency regulation

In order to balance the network frequency variations, ES systems can be employed and provide all three levels of frequency regulation (primary, secondary and tertiary). Storage technologies suitable for this application demonstrate good cycling capability and fast response (especially for the primary control). Thus, most batteries and other short time scale techniques such as FES and SCES are well suited for the primary control (fast response spinning reserve) while further technologies, such as PHES,CAES and HES, can provide secondary and tertiary control (conventional spinning reserve) as well (Gonzalez, et al. 2012).

Low voltage ride through (LVRT)

At the point of interconnection between the external grid and wind turbines, voltage control is required in order to keep them connected during a voltage dip. At every country there are grid codes, also known as LVRT requirements, which specify the level (% of the rated voltage)

and duration of voltage dips that wind turbines must withstand (Gonzalez, et al. 2012). Normally, the power converters which are connected to the wind generators regulate the reactive power injection into the grid during these situations (Gomis-Bellmunt, et al. 2008). Consequently, ES systems are not required for reactive power compensation but are utilized in order to maintain the voltage of the converter's dc-link in a specific range and also protect them against overvoltage by being charged during fault. Storage technologies with fast power response, like those mentioned for the frequency regulation, are suitable for this application.

Voltage control support

The voltage level of a power network is an illustration of its reactive power balance. Too high voltage means surplus of reactive power and vice versa (Singh and Hussain 2010). As mentioned above, the power electronics interface between wind turbines and the grid regulates the reactive power flow and is able to sustain the voltage levels stable. Apart from power converters, ES systems can also be used for this purpose and improve the dynamics of the voltage control. Batteries and other short time scale ES devices are well suited for this application due to their response time.

Oscillation damping

At stable grids without perturbations, relative angular positions of synchronous machines rotors remain constant. Since wind power penetration in a power system network can create disturbances, the generators that are connected to the grid can lose synchronism. According to grid requirements imposed by future grid codes, wind power plants will be required to assist generators to maintain their synchronism against power oscillations. ES systems can be utilized for this application by absorbing/injecting active power at frequencies of 0.5 – 1 Hz (EPRI DOE 2004). Since this application requires fast response times, batteries, FES, SMES and SCES can be suitable.

Load following

In order to deal with the drawbacks of RES output uncertainty, ES systems can be used to store and provide electrical power in a time frame of minutes to hours, acting as a source when power required is more than production and as a tank when there is power surplus (Barton and Infield 2004). Storage devices that are suitable for this application are: batteries (electrochemical and flow) and HES.

Load levelling

Load leveling is a long term application that requires ES devices able to operate within the time frame of 1-10 h. The operation strategy is to store cheap energy during off-peak hours (during nighttime) and supply it back to the network during times of high electricity demand as illustrated in Figure 8. The result is that the typical "mountain and valley" shape of the load curve flattens, which practically means that utilization of efficient and cheaper baseload generation is maximized and less spinning reserves are required. ES technologies that are suitable for this application are: batteries (electrochemical and flow), HES, PHES and CAES (Gonzalez, et al. 2012).

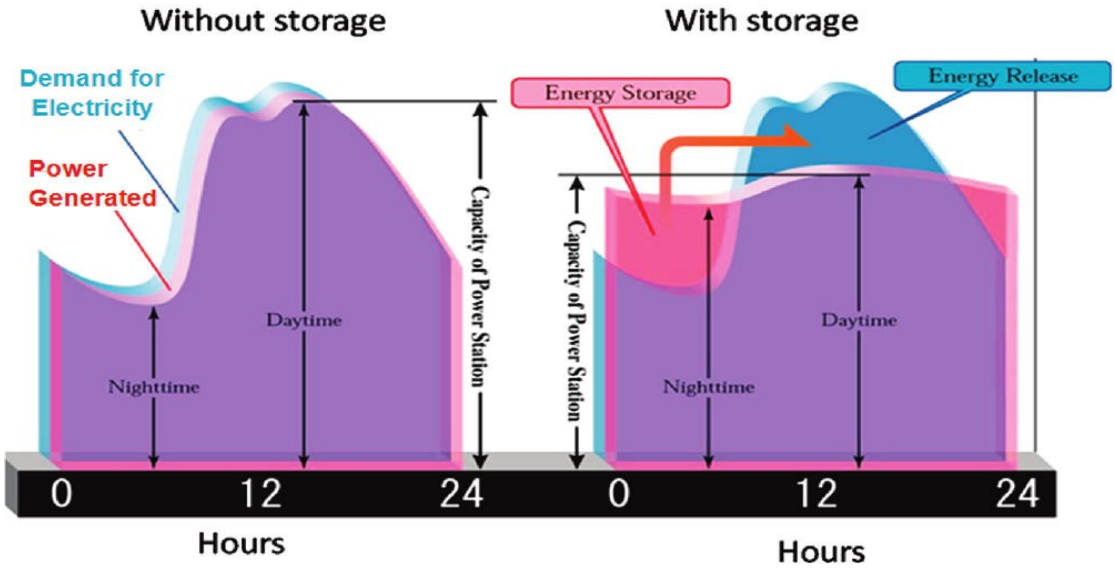

Figure 8 Schematic for a typical load levelling case

Transmission curtailment

RES power units must sometimes be disconnected from the grid due to reasons related to the stability of the electrical system or technical limitations of the transmission lines. ES devices can be utilized storing energy for hours and supply it back to the network according to the capacity of transmission lines and the system's stability. In such way, disconnection of RES units can be avoided. Transmission curtailment is a long term application and thus, suitable technologies are: batteries, CAES, PHES and hydrogen-based systems.

Black start

Black start is the ability of a power unit to go from shutdown state to operating condition without being assisted from the grid. Afterwards, the energized grid is able to help other generating units to start after a blackout occurs (EPRI 2002). This application can be particularly useful in case of remote stand-alone networks and can be provided for ES devices such as batteries, CAES, PHES and HES.

Energy arbitrage

The electricity price can vary from hour to hour at many grid areas. Utilization of ES devices can bring revenues by purchasing inexpensive electricity when its cost and demand are at low levels and sell it when price and demand are high. ES systems that are suitable for this application can operate on a daily charge/discharge cycle, have the capacity to store large amounts of energy and interact with the power grid at the transmission level (E.S.A. 2009). Some types of battery technologies can be used for this application but those that are considered as more suitable are PHES and CAES since they don't suffer from degradation like batteries do and they have low operation cost.

The type of application that each ES technology can provide is summarized in Table 3.

Table 3 Combination of ES technologies with their applications (Barton and Infield 2004) (EPRI DOE 2004) (Gonzalez, et al. 2012) (Singh and Hussain 2010) (Swierczynski, et al. 2010)

Technology / Application	PHES	CAES	FES	LAES	LIES	NCES	NaSES	ZEBRA	VRBES	PSBES	ZnBrBES	SMES	SCES	TES	HES
Primary Reserve			●	●	●	●	●	●	●	●	●		●		●
Secondary Reserve	●	●		●	●	●	●	●	●	●	●				●
Tertiary Reserve	●	●	●	●	●	●	●	●	●	●	●				●
LVRT			●	●	●	●	●	●	●	●	●	●	●		●
Voltage Control			●	●	●	●	●	●	●	●	●	●	●		●
Oscillation Damping			●	●	●	●	●	●	●	●	●	●	●		●
Load Following				●	●	●	●	●	●	●	●				●
Load Levelling	●	●		●	●	●	●	●	●	●	●			●	●
Transmission Curtailment	●	●		●	●	●	●	●	●	●	●				●
Black Start	●	●		●	●	●	●	●	●	●	●				●
Energy Arbitrage	●	●													

To summarize, according to the information provided in this chapter, there are various ES devices that are able to support RES integration in stand-alone systems. Specific ES selection depends on specific applications as well as other factors such as their cost, technical maturity, reliability and geographical dependence. PHES and CAES are not considered as suitable for the island of Agios Efstratios due to geological boundaries, large initial costs and incapability to provide short time scale regulation services. Although currently it is not a very attractive option, HES seems to have a very good future potential, specifically in case that the improvements at energy infrastructure at the island will consider the transportation sector as well. Moreover, ES technologies such as FES, SMES and SCES are not considered a good option due to their incapability to provide long term applications and can be utilized only if combined with another technology. TES is also not suitable because of its technical immaturity. On the other hand, most battery technologies seem to be a good option for RES integration. LAES are more technically mature, compared to LIES, NCES, NaSES, ZEBRA and flow batteries, and the most commonly used ES technology at renewable energy applications. On the contrary, they have lower energy density and restricted lifetime.

2.4 ES applications in renewable energy systems

In general, islands are rich in renewable resources but in order to overcome issues caused by intermittent renewable energy in their weak grids, ES can be integrated in the system. Adding storage units in stand-alone systems provides a number of benefits such as reduction in diesel consumption, lower power production cost and increased level of energy autonomy. These benefits are clearly stated in literature where both studies and already implemented energy systems including storage worldwide emphasize their importance, as presented below (Kaldellis and Zafirakis 2007).

Studies

Several storage technologies are combined with energy generated by wind and sun in two Greek islands, namely Lesvos and Donousa, possessing a large and a very small electrical grid respectively. The examined storage technologies include pumped hydro, lead acid batteries and CAES for Lesvos while for Donousa hydrogen and batteries such as lead acid, NaS and flow batteries are used. The study indicates that in both islands, the proper sizing of storage can address effectively issues caused by intermittent wind and solar energy in the autonomous grids. More specifically, the level of renewable energy penetration is increased, while eliminating the environmental impact of the current diesel generators and maintaining power quality and grid stability (Kaldellis and Zafirakis 2007).

In the case of Portugal's Porto Santo, hydrogen storage combined with an electrolyzer and a fuel cell promise complete coverage of the electricity demand, assistance of the energy system (existing oil fired generators, wind turbines and PV) and further expects successful operation both in the case of peak shaving and 100% renewable operation (Marin, Alves and Zervos 2005).

Existing systems

Apart from the previously presented studies, already implemented systems around the world demonstrate the benefits of adding storage to an energy system.

In Canada's Bella Coola, the existing diesel-hydro system was characterized by high diesel consumption and difficulty to match supply and demand. Therefore, two storage technologies, flow batteries and hydrogen used in a fuel cell limit the generators' use and contribute to a generally successful operation of the energy system, even though the fuel cell requires additional experience. The battery is preferred for short term stability of the system while hydrogen for long term energy management (Komor and Glassmire 2012).

In Samoa's Apolima Island, the 100% renewable electricity system consisting of PV and lead acid batteries is able to provide constant electricity supply. Replacing the formerly used diesel generators with the PV-battery system led to lower diesel consumption, noise levels and emissions but, most importantly, it led to high security of supply in a remote and inaccessible island (Komor and Glassmire 2012).

In Australia's Kind Island, a vanadium redox battery was introduced to a wind-diesel energy system and managed to increase the contribution of renewable energy, reduced the high costs originating from fuel use and also stabilized the fluctuating wind power and enhanced the overall operation of the system (Karri, Yap and Titchen 2008).

2.5 Conclusions

This chapter described various ES technologies with respect to their operation and main technical characteristics and their applications in renewable-based energy systems. Specific ES selection depends from various characteristics and the applications which are required. Regarding the case of Agios Efstratios, battery technologies are considered as the most suitable ones due to their wide range of applications, their flexibility and level of maturity. The following chapter investigates the optimal size of the hybrid RES/ES system and evaluates its feasibility considering different battery technologies. Finally, explores the economic feasibility of interconnecting Agios Efstratios to another island.

Chapter 3 – Optimization of the hybrid power system

3.1 Introduction

The hybrid power system of Agios Efstratios is suggested by CRES to consist of wind and photovoltaic generators, batteries and the existing diesel power station. The integration of both wind and solar systems can take advantage of the island's abundant renewable resources and ensure better security of supply. Moreover, those two technologies can be complementary to each other (Rodrigues and Estanqueiro). Photovoltaics are suitable for the island because they have the ability to supply power close to their nominal rating at summer, which is the season of peak load demand. On the other hand, wind turbines can be much useful for the rest of the year since as shown in Figure 9 and Figure 10, when solar irradiation is weak, wind speed is larger. Normally, at wind/PV systems the largest part of energy comes from the wind generators since they have larger capacity factors and lower cost per kW in comparison to PV. For this study, in order to improve security of supply and reassure participation of both technologies in the energy mix, it is assumed that their energy production potential must be at least 10% of the annual demand.

As explained in chapter 2, batteries are more suitable for the specific autonomous system, compared to other ES technologies, due to their flexibility and ability to provide a wide range of applications. Lastly, the diesel generators remain as reserves to ensure the energy security during the prolonged periods of low RES power potential.

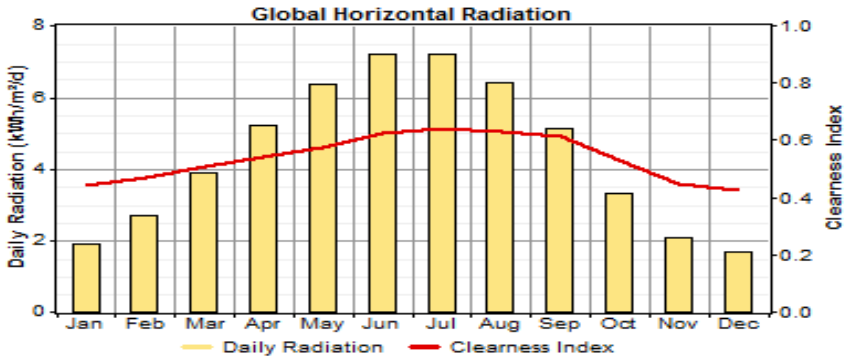

Figure 9 Yearly profile of solar irradiation for Agios Efstratios (HOMER online database)

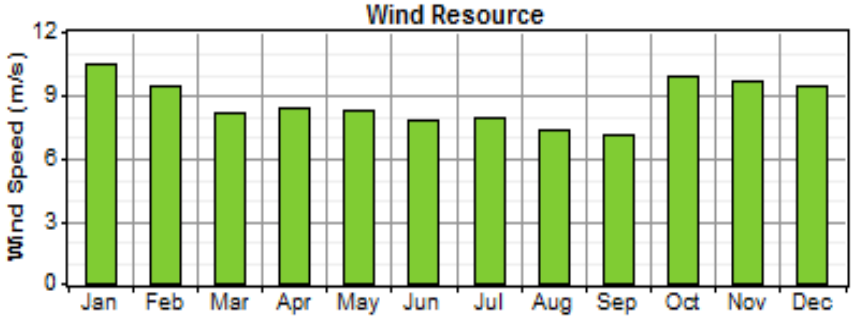

Figure 10 Yearly profile of wind speed for Agios Efstratios (provided by CRES)

In order to use solar and wind energy resources in an efficient and economical way, optimization of the hybrid wind/PV/battery system's sizing plays a major role.

The aim of this section is to optimize the size of RES and ES components, make a cost comparison between a stand-alone and interconnected system and evaluate the utilization of various battery technologies regarding their cost, efficiency and cycle lifetime.

3.2 Optimization of hybrid system

The goal of this section is to optimize the size of the hybrid system's components (WT, PV and ES) with respect to the net present cost (NPC). That factor is evaluated by calculating various costs and variables and is being optimized as described at the section below.

3.2.1 Objective function

The objective function for the system optimization is the NPC formula as stated below.

$$minimize\left(C_{NPC}=\frac{C_{ann,tot}}{CRF(i,R_{proj})}\right) \tag{3.1}$$

Where:

- $C_{ann,tot}$ is the total annualized cost (€/yr)
- i is the annual interest rate (discount rate) (%)
- R_{proj} is the project lifetime (yr)
- $CRF\ (i,N)$ is the capital recovery factor

The NPC includes all costs and revenues that occur within the project lifetime, with future cash flows discounted to the present using the discount rate. Specifically, the NPC includes the initial capital cost of the system components, the cost of any component replacements that occur within the project lifetime and the cost of maintenance and fuel. Any revenue from the sale of power to the grid or salvage value that occurs at the end of the project lifetime reduces the total NPC (National Renewable Energy Laboratory (NREL) 2012).

The $C_{ann,tot}$ is the hypothetical total annual cost value that if it occurred each year of the project lifetime would generate a NPC equal to the actual NPC and is described by equation (3.2).

$$C_{ann,tot}=C_{ann}^{cap}+C_{ann}^{rep}+C_{ann}^{O\&M}+C_{ann}^{f} \tag{3.2}$$

Where,C_{ann}^{cap}, C_{ann}^{rep}, $C_{ann}^{O\&M}$ and C_{ann}^{f} are the annualized capital, replacement, O&M and fuel costs respectively. The salvage value is included in the replacement cost.

The CRF converts a present value into a flow of equal annual payments over a specified time and is given by the following equation.

$$CRF(i,N) = \frac{i(i+1)^N}{(i+1)^N - 1} \quad (3.3)$$

Where, N is the number of years.

The calculation of salvage value, which is the value that remains at each component at the end of the project lifetime, is based on the equation below.

$$S = C_{rep} \frac{R_{rem}}{R_{comp}} \quad (3.4)$$

Where:

- C_{rep} is the replacement cost of the component (€)
- R_{rem} is the remaining life of the component (yr)
- R_{comp} is the lifetime of the component (yr)

3.2.2 Constraints

The aforementioned objective function is submitted to a number of technical constraints such as:

- The system active power balance

$$P_{battery} + P_{wind} + P_{PV} + P_{diesel} = P_{load} + P_{losses} \quad (3.5)$$

Where:

- P_{wind} is the power dispatched by the wind power plant (kW)
- P_{PV} is the power output from the photovoltaic station (kW)
- P_{diesel} is the power output from the diesel power station (kW)
- $P_{battery}$ is the power supplied (P_{disch}) or absorbed (P_{char}) from the battery (kW)
- P_{losses} is the system's power losses (kW)

The charging and discharging limit of the battery depends on its power rating and varies between the values ($-P_{max}$,P_{max}). The power losses are neglected at this optimization process.

- The power output of each generation unit (G_i) must be always positive and below a maximum generation limit ($P_{Gi,max}$). The generation units are the wind turbines, PV system and DG.

$$0 \leq P_{Gi} \leq P_{Gi,max} \quad (3.6)$$

There are also constraints related to governmental policy and stated below.

- The total NPC of the hybrid system (NPC_{hybrid}) must be less than the total cost of the diesel station for a time period equal to the project lifetime (25 years) and

assuming that diesel price is 0.8 €/L $\left(C_{total,diesel}\right)$. The diesel station NPC is 5,086,456 € and its calculation is presented in Figure 48 and Table 10 at Appendix A.

$$NPC_{hybrid} \leq C_{total,diesel} \tag{3.7}$$

- The annual energy production from photovoltaics E_{PV} must be at least 10% of the total annual demand$\left(E_{demand,annual}\right)$.

$$E_{PV} \geq E_{demand,annual} \tag{3.8}$$

3.2.3 Methodology

The simulations are performed with HOMER (National Renewable Energy Laboratory (NREL) 2012) which is a simulation and optimization tool suitable for modeling a hybrid power system's behavior and life-cycle cost in both grid-connected and autonomous model. HOMER comprises various energy components such as wind turbines, photovoltaics, hydro, batteries, diesel (and other fuels) generators, hydrogen storage and converters. Furthermore, it can evaluate the economical and technical feasibility for a large number of technology options, while considering alterations in availability of renewable resources and technology costs (Lund, et al. 2010).

Initially, the user defines the system configuration, sets the range of sizes for the components and provides input data such as capital, replacement, operation and maintenance (O&M) cost for the components, technical restraints, economic inputs for the hybrid system (fuel prices, annual interest rate and project lifetime). Moreover, annual time series for the load demand, wind speed and solar irradiation are required as well. Afterwards, as shown in Figure 11, HOMER starts an hourly simulation of every possible configuration, computing the available power from RES (P_{RES}), comparing it to the electric load (P_{load}) and deciding how to manage the surplus renewable power in times of excess (battery charging) or how to generate additional power in times of deficit (battery discharging / diesel station power supply). When simulations are over, it sorts the feasible combinations in order of increasing net present cost (NPC) which represents the life-cycle cost of the system (National Renewable Energy Laboratory (NREL) 2012).

The capital, maintenance, replacement and fuel costs along with the salvage value are used for the calculation of each component's annualized cost. The total annualized cost of the system derives from the summation of the annualized costs of each component and is an economic indice of major importance because it is used to compute the two principal economic figures of the system, the total NPC and the cost of electricity (COE). COE is the average cost per kWh of useful electrical energy produced by the system and is given as follows.

$$COE = \frac{C_{ann,tot} - C_{boiler} E_{thermal}}{E_{prim} + E_{def} + E_{grid,sales}} \tag{3.9}$$

Where E_{prim} and E_{def} are the total amounts of primary and deferrable load served (kWh/yr), C_{boiler} is the boiler marginal cost (€/kWh), $E_{thermal}$ is the total thermal load served (kWh/yr) and $E_{grid,sales}$ is the total grid sales (kWh/yr).

It is assumed that there are neither deferrable nor thermal loads and grid sales are zero. Since at the present study thermal loads have not been considered, the NPC can give a complete picture about the cost of the system and COE is not necessary to be analyzed.

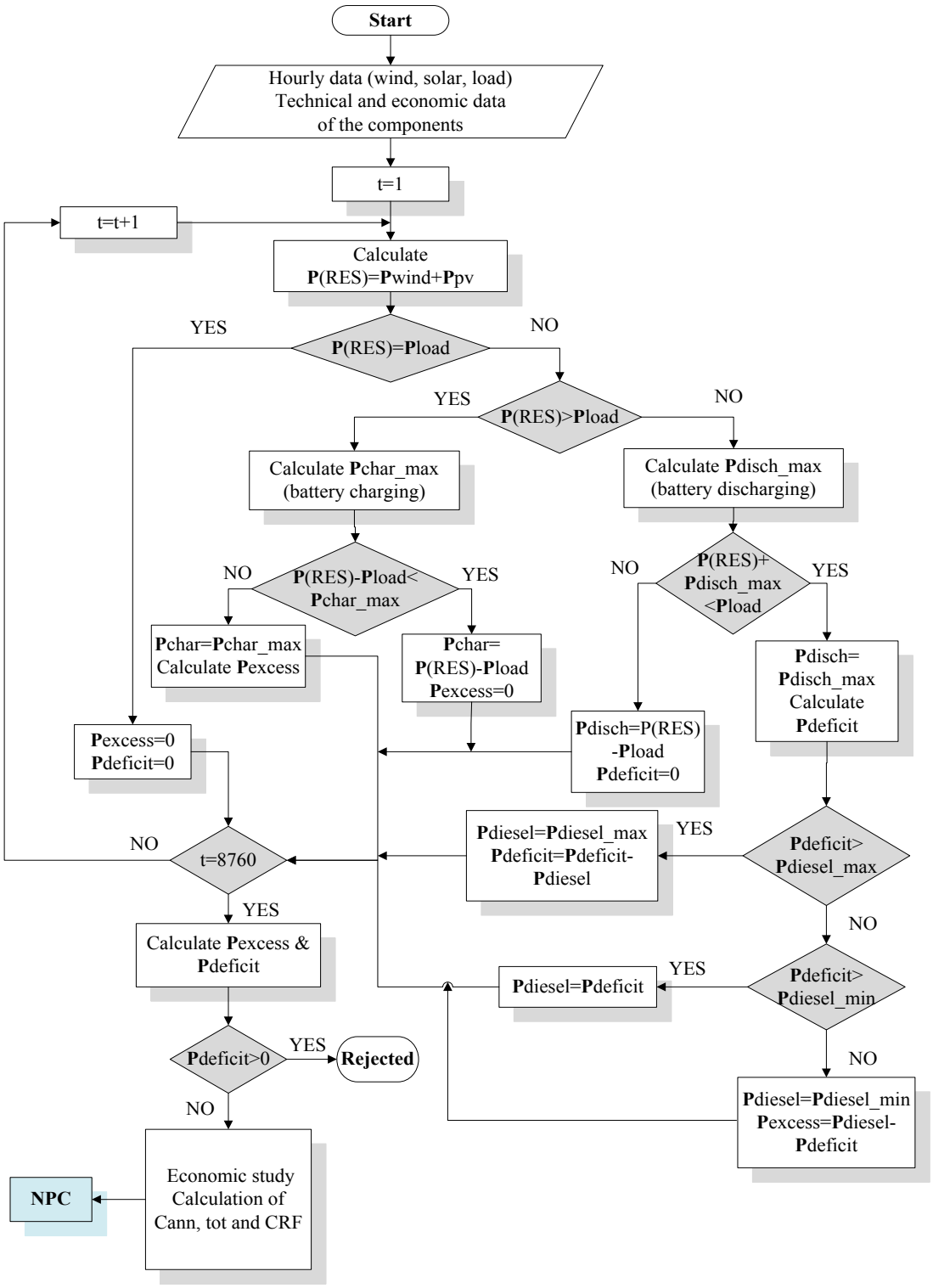

Figure 11 Optimization flowchart of the hybrid wind/PV/diesel/battery system (Souissi, Hasnaoui and Salami 2010)

Furthermore, within the scopes of this study is to investigate the cost of interconnecting Agios Efstratios with Lemnos through submarine power cable. The interconnection is an alternative solution for the island's power supply without requiring diesel units operation from the local station. A comparison between the cost of a 100% renewable stand-alone system and an interconnected system is performed by calculating the breakeven grid extension distance. This

is the distance from the grid which makes the NPC of extending the grid equal to the NPC of the stand-alone system.

$$D_{grid} = \frac{C_{NPC}\, CRF\,(i,R_{proj}) - c_{power} L_{tot}}{C_{cap}\, CRF\,(i,R_{proj}) + c_{om}} \quad (3.10)$$

Where:

- L_{tot} is the total primary and deferrable load (kWh/yr)
- c_{power} is the cost of power from the grid (€/kWh)
- c_{cap} is the capital cost of grid extension (€/km)
- C_{om} is the O&M cost of grid extension (€/yr/km)

Farther away from the grid, the remote system is optimal while closer to the grid, grid extension is optimal. The distance between the two islands is approximately 40 km and power can be transferred though a medium voltage level (15 kV) cable due to the low power demand. The advantage in the case of a medium voltage cable is that it doesn't require transformers at start and end point of the line since it is the same voltage level in both islands.

3.2.4 HOMER software input data

This section presents the data used as input parameters for the simulation of the hybrid system. The capacity range of renewable units was considered with respect to the island's power and energy demands.

3.2.4.1 Wind speed annual time series input data

The wind speed time series in hourly average values, as illustrated in Figure 49 at Appendix A, were measured with a 10m wind mast and have been provided by CRES.

3.2.4.2 Solar irradiation annual time series input data

Based on latitude and longitude of the island's location, HOMER accesses an online database that serves up data from either NREL's Climatological Solar Radiation (CSR) or NASA's Surface meteorology and Solar Energy (SSE) data set (National Renewable Energy Laboratory (NREL) 2012).

The latitude of Agios Efstratios is 39°30′ and longitude is 25°0′. The annual average solar irradiation for this area is 4.43 kWh/m²/day and Figure 9 illustrates the solar resource profile for a one-year period. At this level of solar potential, the energy output for every installed kW of PV is 1,446 kWh/yr.

3.2.4.3 Load demand annual time series input data

According to data provided by the Public Power Corporation (PPC) for 2010, the annual energy demand at the island was 1221 MWh and daily average demand was 3.349 kWh. Figure 12 shows the load profile in average monthly values. The peak demand was 360 kW during summer period. The average yearly power demand was 140 kW.

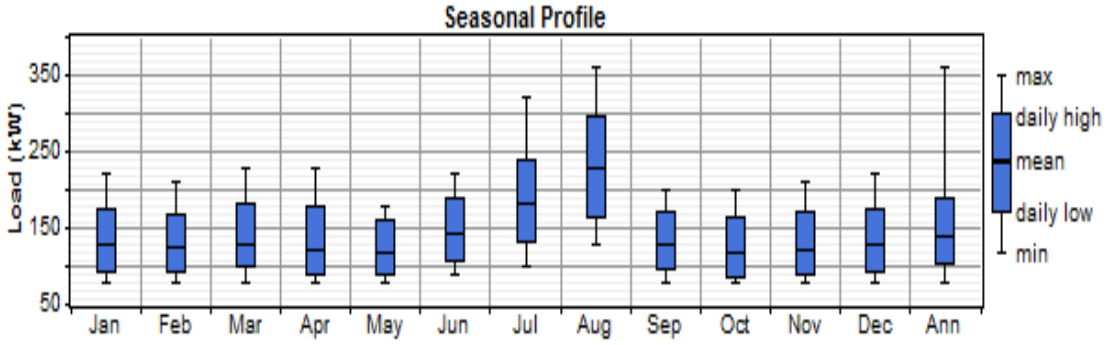

Figure 12 Yearly profile of load demand in average monthly values for Agios Efstratios

3.2.4.4 Economics

Since the construction of the island's energy infrastructure is based on PPC and relies on public funds, it is not subjected to any capital cost subsidies and tax reductions like private investments do (Vassillakos, et al. 2003). A real annual interest rate of 6% was assumed. The real interest rate is equal to the nominal interest rate (10%) minus the inflation rate (4%) (Giannoulis and Haralambopoulos 2011). The lifetime of the project is considered to be 25 years. Also, according to the PPC, the average price of diesel fuel is set at 0.8 €/L. This value is assumed to be constant and free from inflation due to software limitations. With respect to this diesel price, the COE is equal to 0.326 €/kWh and for a time period of 25 years the total NPC is 5,086,456 €. Finally, the CO_2 emission cost is 21 €/tn (Tsikalakis, et al. 2009).

Moreover, the cost for a medium voltage cable (15 kV) is around 100,000 €/km, excluding transportation cost, and the O&M cost is neglected (Wright, et al. 2002). Cable laying cost depends on the site, depth and length. Due to relatively low sea depth, approximately 100-150 m (Roussakis, et al. 2004), it is assumed that the laying cost is the same as the cable cost. The grid power price is approximately 0.1 €/kWh (PPC 2011).

3.2.4.5 Diesel Generators

The island's power station comprises of two types of engines as shown in Table 8 of the next chapter. According to data provided by PPC, the capital, replacement and O&M cost of the small units (MAN D2566/ME) are 22,500 €, 21,150 € and 0.5 €/hour respectively. For the other type of engine (HYUNDAI KD8AX) the same costs are 55,000 €, 51,700 € and 0.5 €/hour respectively. It must be noted that the capital cost of the HYUNDAI engines is not considered at the simulations since they have recently been replaced. On the other hand, the MAN engines will have to be replaced soon, so their capital cost is considered. The lifetime for both types of engines is 50,000 hours and the minimum load ratio is 50% as suggested by (Papathanasiou and Karamanou 2007).

3.2.4.6 Photovoltaic Panels

The power capacity range assumed for the simulation of the photovoltaic station of the island is between 100 kWp and 300 kWp. The minimum rating of 100 kWp is chosen so that the potential annual energy production can be more than 10% of the demand. Larger power capacities are not considered because of their cost. The capital and replacement costs of the PV panels are 4,000 €/kWp and 3,500 €/kWp respectively. The expected energy production of a typical crystalline silicon PV panel is between 1,300 – 1,400 kWh/kWp. The O&M cost is

usually so small that can be neglected. According to the guarantee of most PV producers, the derating factor is set to 80% (Bognar and Behrendt 2011). Moreover, it is assumed that the slope is 39.5°, Azimuth is 0° and the ground reflectance is 20%. The panels are modeled as fixed and the temperature effect is neglected.

3.2.4.7 Wind Turbine

The wind turbine that has recently been installed at the island (GEV 10/20) has capital/replacement cost 120,000 € and O&M cost 1,460 € (CRES 2011). The hub height is 25 m and its lifetime is 20 years. Apart from this wind turbine, larger ones need to be included at the hybrid system in order to satisfy the power/energy demands. Three popular and representative types of wind turbines and a number of combinations of units are tested in order to examine a wide range of wind power capacities. HOMER's library contains power curves for many types of wind generators and the ones considered at this study are described below:

- *Enercon E-33 / 330kW*: The maximum annual energy output of this type of generator is 2,891 MWh. The hub height is 50m and lifetime is 20 years. The capital is equal to the replacement cost (600,000 €) and the O&M cost is 12,000 €/year. The power curve of this wind turbine is shown in Figure 50 at Appendix A.

- *Fuhrlander 250 / 250kW*: For this type of wind generator, the maximum annual energy output is 2,190 MWh. The hub height is 45 m and lifetime is 20 years. The capital/replacement cost is 390,000 € and the O&M cost is 11,820 €/year (Lorax Energy Systems LLC 2004). The power curve is illustrated in Figure 51 at Appendix A.

- *Fuhrlander 100 / 100 kW*: This generator type has maximum annual energy output equal to 876 MWh. The hub height is 35 m and the lifetime is 20 years. The capital/replacement cost is 290,000 € and the 8,760 €/year (Lorax Energy Systems LLC 2004). The power curve is shown in Figure 52 at Appendix A.

3.2.4.8 Batteries

Conventional generic batteries are included in this study for storage of surplus energy and supply in cases of high demand. A commercial type, contained in the HOMER library, of a vented deep-cycle lead-acid battery (Hoppecke 24 OPzS 3000) is considered for the simulations. The capital and replacement costs per battery are 180 €/kWh and 150 €/kWh respectively. The O&M cost is 0.26 €/kWh/year. The minimum capacity assumed for the optimization analysis is 1 MWh and the depth of discharge (DOD) is 80%.

3.2.4.9 Converter

A power electronic AC/DC converter is required to maintain the energy flow between the AC side (grid) and the DC side, that are the PV array and the battery bank which are utilized at the island's hybrid system. The capacity level is chosen so that it can allow full power supply, even at peak demand periods, from the dc-side generators. For this study, the converter's size is considered to be 400 kW. The typical capital/replacement cost for a 1 kW system is around 650 € and the O&M cost can be neglected. The lifetime is estimated at 15 years and the efficiency is 90% (Khan and Iqbal 2004).

Table 4 Techno – economic data for the hybrid system in HOMER (Giannoulis and Haralambopoulos 2011) (Tsikalakis, et al. 2009) (Wright, et al. 2002) (PPC 2011) (Papathanasiou and Karamanou 2007) (Bognar and Behrendt 2011) (CRES 2011) (Lorax Energy Systems LLC 2004) (Khan and Iqbal 2004)

Technology	Model type	Size	Capital cost €	Repl. cost €	O&M cost	Lifetime	Min. load ratio
Diesel gen.	MAN D25666/ME	90 kW	22,500	21,150	0.5 €/hour	50,000 hours	50%
Diesel gen.	HYUNDAI KD8AX	220 kW	55,000	51,700	0.5 €/hour	50,000 hours	50%
PV	-	1 kW	4,000	3,500	0 €/yr	20 years	-
Wind gen.	GEV 10/20	20 kW	120,000	120,000	1460 €/yr	20 years	-
Wind gen.	Enercon E33	330 kW	600,000	600,000	12,000 €/yr	20 years	-
Wind gen.	Fuhrlander 250	250 kW	390,000	390,000	11,820 €/yr	20 years	-
Wind gen.	Fuhrlander 100	100 kW	290,000	290,000	8,760 €/yr	20 years	-
Batteries	Hoppecke 24 OPsZ 3000	1 kWh	180	150	0.26 €/yr	20 years	-
Converter	-	1 kW	650	650	0 €/yr	15 years	-

Economics and System Control			**Additional data**				
Economics			**PV**			**Wind turbine**	
Annual real interest race	6%		Derating factor	80%		GEV 10/20 hub height	25 m
Project lifetime	25 years		Slope	39.5°		E33 hub height	50 m
Diesel price	0.8 €/L		Azimouth	0		F250 hub height	45 m
Submarine cable capital cost	100,000 €/km		Ground reflectance	20%		F100 hub height	35 m
Submarine laying cost	100,000 €/km		Temperature effect	neglected			
Submarine cable O&M cost	0 €/km						
Grid power price	0.1 €/kWh						
CO_2 emission penalty	21 €/tn						
			Converter				
System Control			Efficiency	90%			
Dispatch strategy	Cycle charging						
Operating reserve as % of load	10%						
Maximum annual capacity shortage	0%						

3.3 Simulation results

The aim of this section is to calculate the RES and ES size for three different scenarios: an optimal one (scenario 1), a high RES penetration scenario (scenario 2) and a total (100%) renewable scenario (scenario 3). Also, the scope is to highlight the technical and economical differences between those scenarios and evaluate the advantages and disadvantages of each case. Furthermore, presents the results of the comparison between different types of batteries and between a stand-alone and an interconnected system.

Regarding scenario 2, it must be mentioned that according to the policy of the authorities which are responsible for the implementation of the project "Green Island – Agios Efstratios", the RES fraction F_{RES} must be very high in order to minimize the diesel fuel consumption as much as possible. For this study it is assumed that it must be at least 90% (CRES 2011).

$$F_{RES} = \frac{E_{wind}+E_{PV}}{E_{wind}+E_{PV}+E_{diesel}} \geq 0.9 \quad (3.11)$$

Where:

- E_{wind} is the annual energy production from wind turbines (kWh)
- E_{PV} is the annual energy production from photovoltaic farm (kWh)
- E_{diesel} is the annual energy production from the diesel power station (kWh)

The configuration of the hybrid power system as implemented in HOMER is shown in Figure 13.

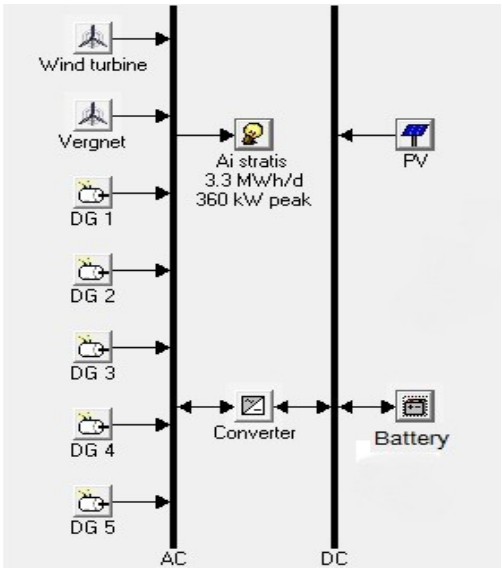

Figure 13 Configuration of Wind/PV/Diesel/Battery power system simulated at HOMER

The following figures show the simulation results with respect to the NPC of the hybrid system, the achieved RES fraction and excess electricity for various RES and storage capacities separated into three cases, each case corresponding to one of the WT types that were previously mentioned.

Case 1: E33 wind turbine type (330 kW)

Several RES and ES combinations are tested. PV power rating is between 100-300 kWp, wind power rating is from 330 to 660 kW and battery energy capacity from 1 MWh to tens of MWh. The optimization results are illustrated graphically in Fig. 13 – 15 and presented analytically in Table 11 at the Appendix A. As shown in Figure 14, when batteries are larger than 12 MWh, there is no feasible RES combination within the NPC policy constraints ($NPC_{hybrid} \leq$ 5,086,456 €) as stated in section 3.2.2 (eq. 3.7). Moreover, as PV power rating grows, the cost increases considerably. The optimal combination for scenario 1 is one WT, 100 kWp PV and 1 MWh ES capacity. The NPC for that combination is 2.966 M€, which is the smallest among the others. For the same RES ratings but larger batteries (3 MWh), the RES fraction is more than 90% as illustrated in Figure 15. This figure shows, only for the combinations that are economically feasible, the RES fractions that are achieved.

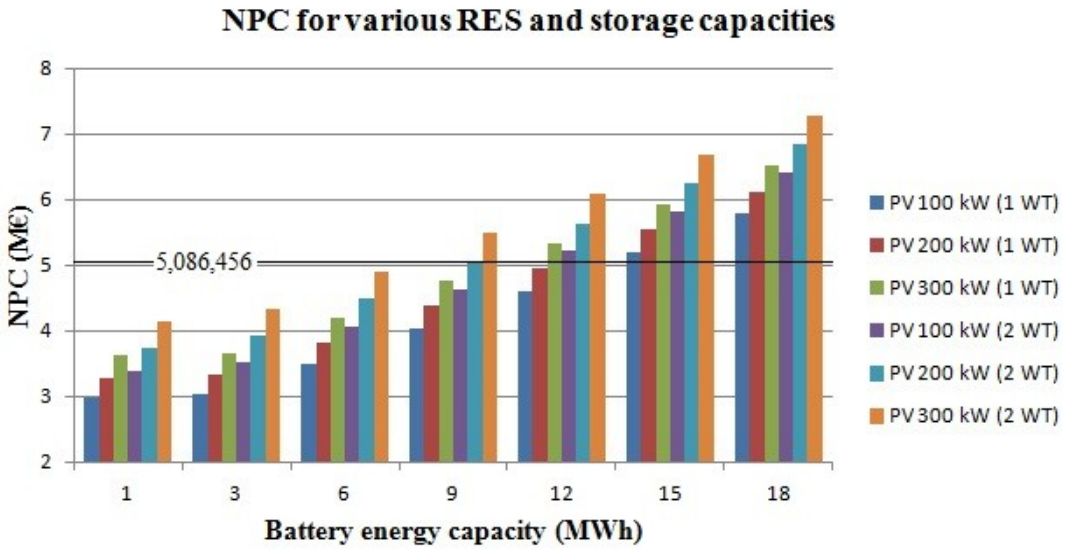

Figure 14 NPC for various combinations of RES and storage capacities for the case of E33 wind turbine

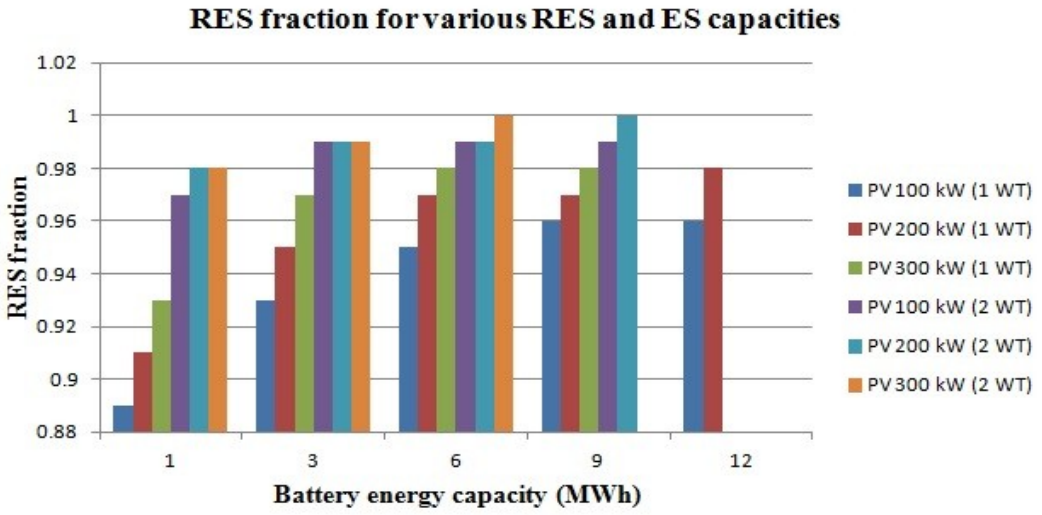

Figure 15 RES fraction for economically feasible combinations of RES and storage capacities for the case of E33 wind turbine

Moreover, the same figure shows that 100% RES fraction can be achieved, within the NPC constraint, with two WTs, 300 kW PV and 6 MWh battery unit.

Also, as illustrated in Figure 16 which shows the excess energy for all the scenarios, in scenarios 1 and 2 it is around 40% of the total production but in the 100% RES scenario the excess increases considerably at approximately 68%. Such amounts of exceeding energy are considered too high and are generated due to the size of the chosen RES units and the restrained capability of ES to absorb all the excess. In Figure 53 at the Appendix A, which illustrates the battery's SOC frequency histogram, it is shown that the battery is fully charged for more than half of the year. The energy that cannot be stored must be curtailed.

The capacity factor of WT is restrained because of the power curtailment. In the case of one WT (scenario 1 & 2), the capacity factor is 34.6% and for scenario 3 the capacity factor for each wind generator is 19%. Furthermore, the diesel consumption is 72,700 L/yr in the optimal scenario and decreases to 48,900 L/yr in scenario 2.

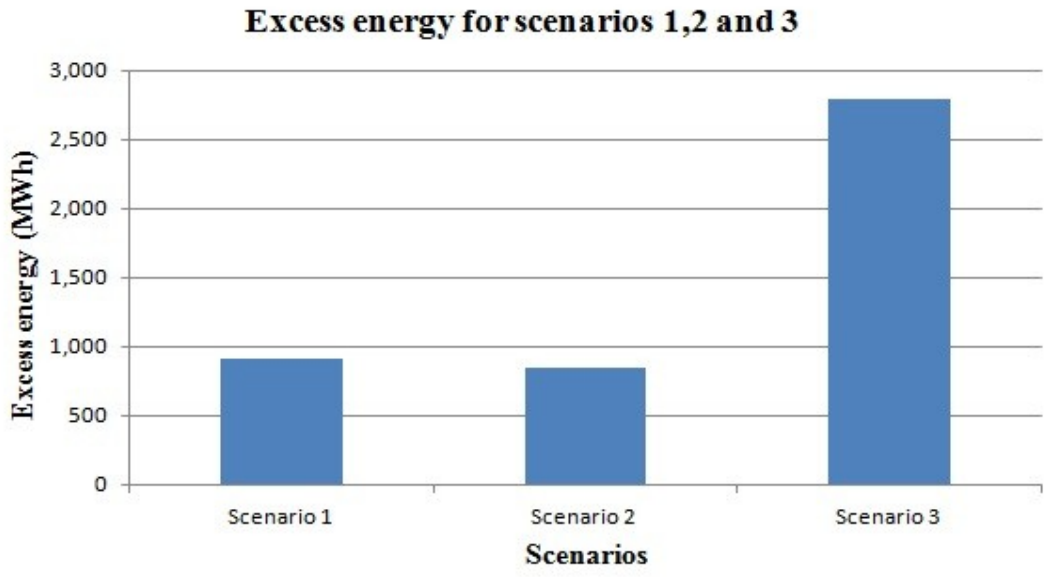

Figure 16 Energy excess of scenarios 1, 2 and 3 for the case of E33 wind turbine

Case 2: F250 wind turbine type (250 kW)

In this case it is considered that the wind power rating is in the range of 250-750 kW and capacity range for PV and storage is the same as in case 1. The results with respect to the NPC, RES fraction and excess electricity are illustrated graphically in Figures 16 – 18 and presented in Table 12 at Appendix A.

As illustrated in Figure 17, there are no feasible solutions when batteries are larger than 12 MWh because the NPC exceeds the constraint (eq. 3.7). As already explained in case 1, solar power capacities larger than 100 kWp raise the cost significantly but there is not any significant increase in RES fraction apart from the case of one WT. The optimal solution for scenario 1 is one WT with 100 kWp PV and 1 MWh battery unit. The NPC for this scenario is equal to 3.093 M€. The RES share for all the economically feasible combinations are

presented in Figure 18. For scenario 1, the RES penetration is 83% and diesel consumption is 103,500 L/yr. In the second scenario, RES share larger than 90% can be achieved with two WT and the same PV and battery capacity as in scenario 1. Furthermore, diesel consumption drops by 42%. The optimal size combination for 100% supply from RES is three WTs, 300 kWp PVs and 6 MWh batteries capacity.

In the third scenario, there is a large amount of exceeding energy which, as shown in Figure 19, is around 70% of the total production and the capacity factor of every wind turbine is very low (16.5%). In scenarios 2 and 1, the energy excess is 56% and 28% respectively. The capacity factor for each WT in those scenarios is 24.8% (scenario 2) and 41.3% (scenario 1).

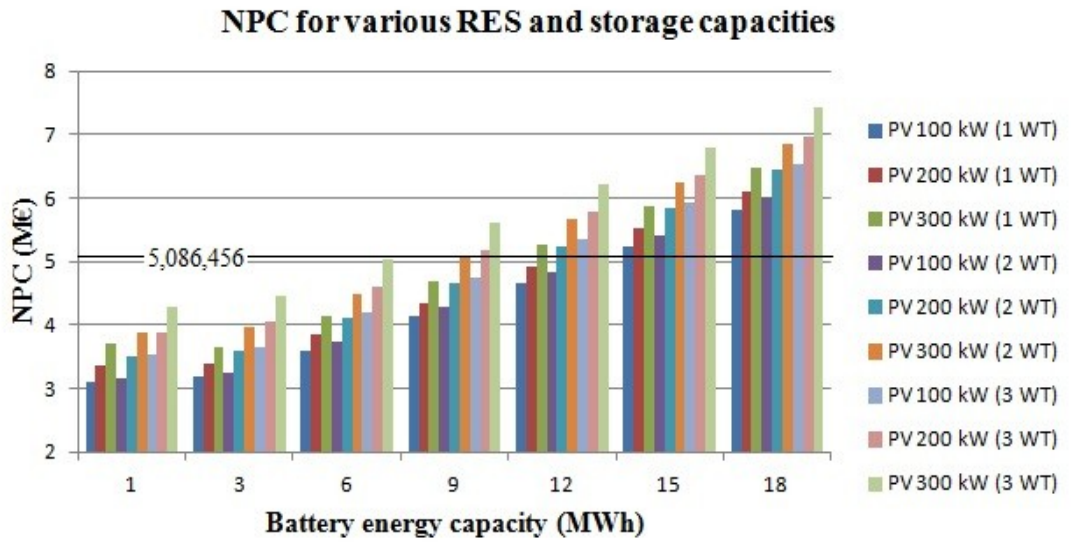

Figure 17 NPC for various combinations of RES and storage capacities for the case of F250 wind turbine

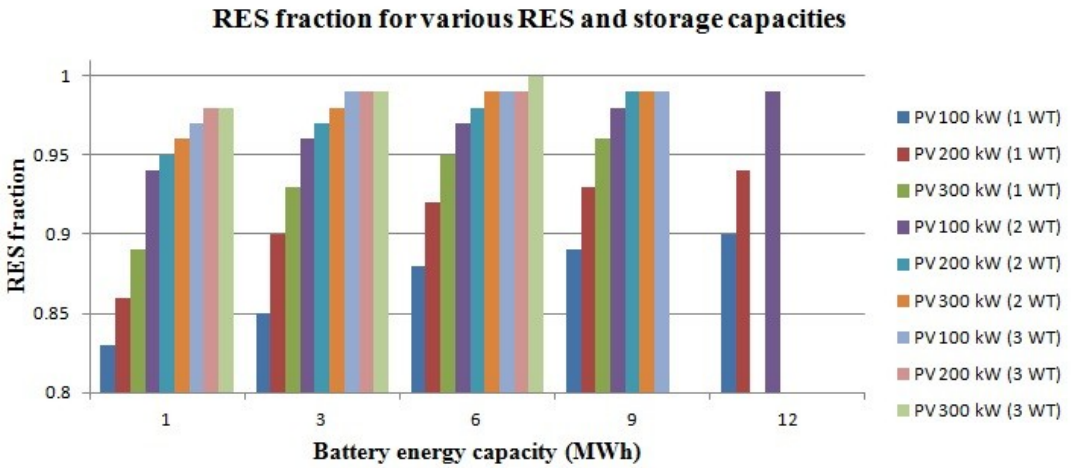

Figure 18 RES fraction for economically feasible combinations of RES and storage capacities for the case of F250 wind turbine

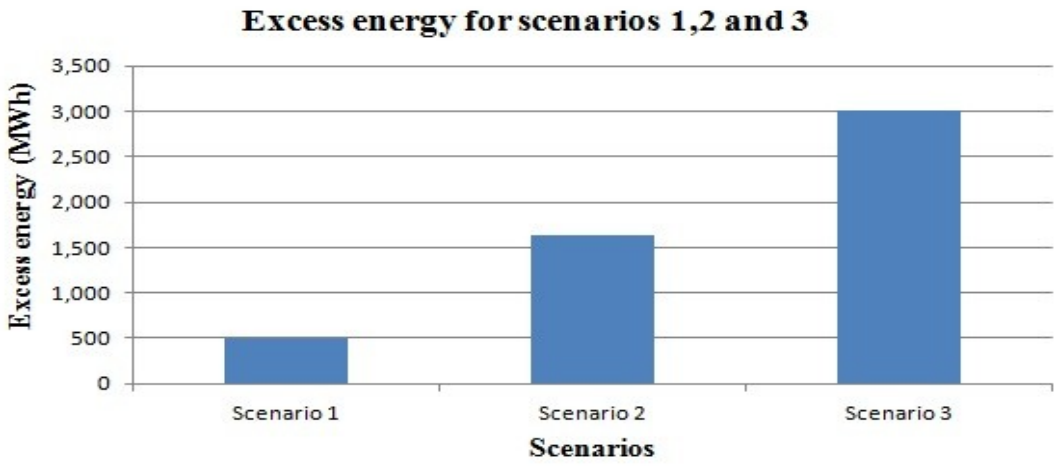

Figure 19 Energy excess of scenarios 1, 2 and 3 for the case of F250 wind turbine

Case 3:F100 wind turbine type (100 kW)

In this case the wind power rating varies from 100 to 700 kW. For simplicity reasons, the graphics will demonstrate only the combinations with WTs up to 400 kW. The results are illustrated in Figures 19 – 21 and in Table 13 at the Appendix A.

Figure 20 shows that for most RES combinations, when batteries are more than 9 MWh, the NPC values do not comply with the constraints. In case of low wind power rating (100 kW), the cost is higher than most of the other combinations due to high energy share from the diesel power station. Also, the increment of PV capacity brings the same impact over NPC and RES share as it did in cases 1 and 2. The optimal combination for scenario 1 is two WTs, 100 kWp PV and 1 MWh battery unit. The NPC for this combination is 3.483 M€. Moreover, the RES fraction is 81% and diesel consumption is 105,100 L/yr.

Additionally, as demonstrated in Figure 21, the effect of battery growth over RES fraction is more important in low RES capacities. Figure 22 shows that in scenario 1, the energy excess is relatively low. Therefore, the capacity factor of each WT is higher (49%) compared to cases 1 and 2.

The optimal solution for scenario 2 is three WTs, 100 kWp PV and 3 MWh battery units. That scenario brings a diesel consumption decrease by 44% and energy excess grows to 800 MWh (38% of total production). The capacity factor of each WT is 39%.

Another interesting point is the absence of solutions, within the constraints, that lead to 100% RES fraction. The most economic combination which can achieve that is seven WTs, 300 kWp PV and 6 MWh batteries. As Figure 22 shows, the exceeding energy at this scenario is 71% of total production. Finally, the capacity factor of each WT is 18%.

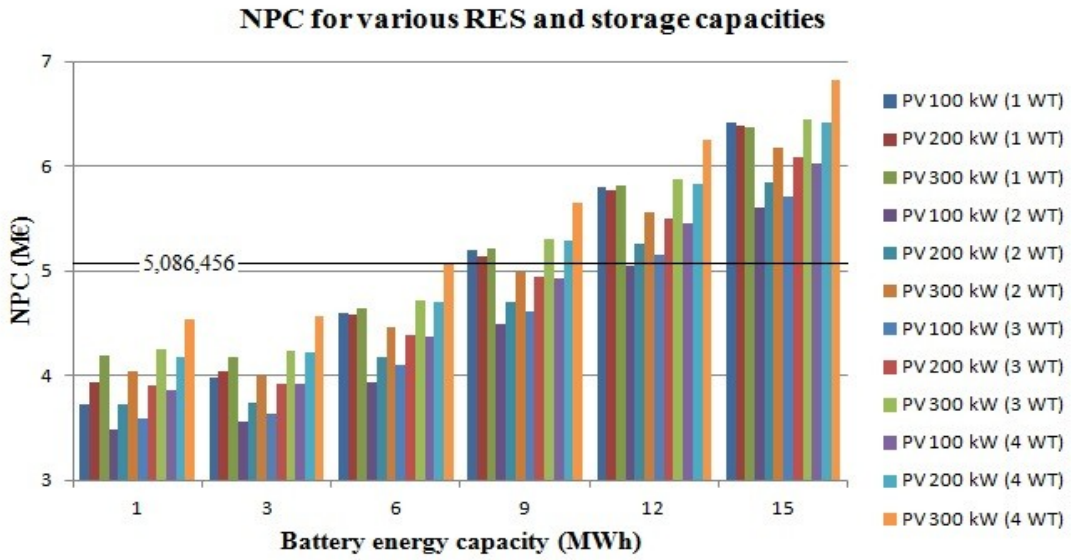

Figure 20 NPC for various combinations of RES and storage capacities for the case of F100 wind turbine

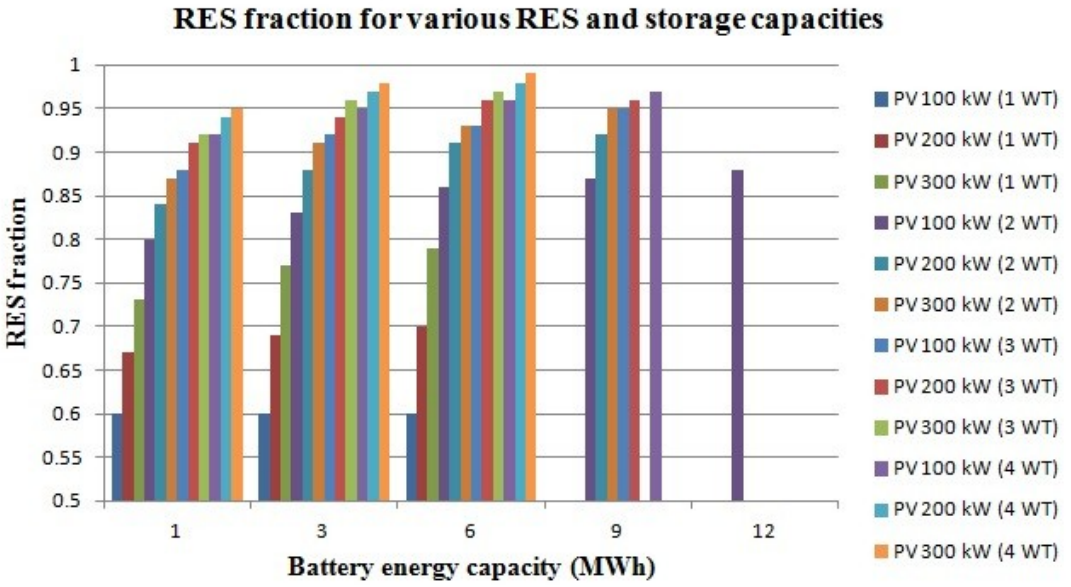

Figure 21 RES fraction for economically feasible combinations of RES and storage capacities for the case of F100 wind turbines

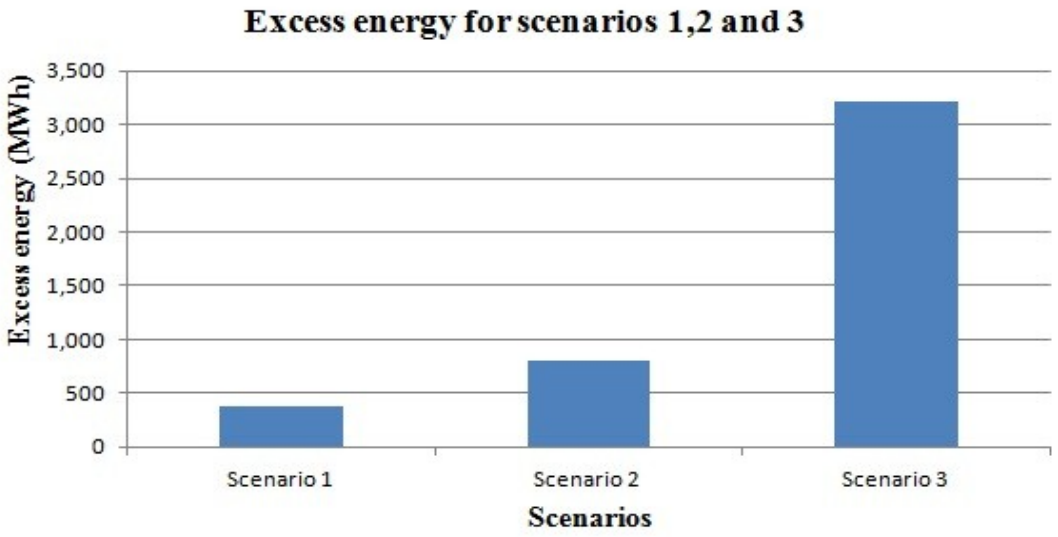

Figure 22 Energy excess of scenarios 1, 2 and 3 for the case of F100 wind turbine

In Table 5 below, the results for all the cases and scenarios are summarized. The total annualized costs of the hybrid system components are presented in Table 14 at Appendix A.

Table 5 Optimal RES and ES units' combinations for all cases and scenarios

Case	Scenario	Wind power (kW)	PV power (kWp)	ES capacity (MWh)	NPC (M€)	Diesel (L/yr)	RES fraction (%)	Excess energy (MWh)
Case 1	Optimal (Sc. 1)	1x330	100	1	2.966	72,709	89	937 (42%)
	High RES (Sc. 2)	1x330	100	3	3.033	48,945	93	846.5 (39%)
	100 RES (Sc. 3)	2x330	300	6	4.910	-	100	2,791(69%)
Case 2	Optimal (Sc. 1)	1x250	100	1	3.093	103,500	83	506.5 (28%)
	High RES (Sc. 2)	2x250	100	1	3.173	60,054	94	1639.6 (56%)
	100 RES (Sc. 3)	3x250	300	6	5,042	-	100	3,017 (70%)
Case 3	Optimal (Sc. 1)	2x100	100	1	3,483	105,100	81	383.9 (24%)
	High RES (Sc. 2)	3x100	100	3	3,628	58,680	92	800 (38%)
	100 RES (Sc. 3)	7x100	300	6	6,340	-	100	3,209 (71%)

As shown in Table 5, among the three cases the optimal solution for all the scenarios can be achieved in the first one. The NPC for scenario 1 is equal to 2.966 M€ and RES fraction is 89%. The extra cost in cases 2 and 3 for the same scenario is 127 k€ and 517 k€ respectively. Apart from the economic aspect, another advantage of case 1 compared to the other two is the reduction of diesel consumption and CO_2 emissions by approximately 30%. The drawback of case 1 in this scenario is the large energy excess and thus, limited capacity factor of the wind turbine.

The NPC for a hybrid system that satisfies the RES share policy constraint (RES fraction >90%) is 3.033 M€. That hybrid system costs 140 k€ less than the system in case 2 and 595

k€ less compared to case 3.Moreover, there is less diesel consumption in case 1. The energy excess is similar to case 3 and much less than case 2.

The cost difference between the optimal system (scenario 1) and a high RES system (scenario 2) is 67 k€. Practically, this is the extra cost that the government needs to pay in order to satisfy the policy constraint. On the other hand, the diesel consumption drops by 32% and there is a slight increase in the capacity factor of wind turbine.

In case 1, the financial cost for the implementation of a 100% renewable scenario is 4.910 M€ and the difference from the optimal one is 1.944 M€. In case 2 the difference is similar to case 1 and in case 3 it is 2.857 M€. The diesel consumption is not completely eliminated but is considered as insignificant and is being neglected.

Another fact that can be noticed in scenario 2 is that although the RES fraction in case 2 (94%) is greater than in case 1 (93%), the amount of diesel being consumed is 11,109 L/yr more. This can be explained by how frequently every DG is used, the loading ratio of each unit and its fuel consumption rate. The last one is shown in Table 8 of the following chapter.

The results which are stated in Table 5, derived with respect to the policy constraints referred to equations 3.7, 3.8 and 3.11. By removing those constraints and thus, without taking into account obligatory PV participation or considering any NPC and RES fraction limitations, the optimization results that appear are presented in Table 15 at Appendix A and compared to the previous ones of scenario1. The main conclusion from this comparison is that in all cases, by excluding the constraints, PV units are not included in the system and NPC drops. Moreover, in cases 1 and 3, the RES share decreases while in case 2 it grows.

Also, it is found that there is a large amount of excess electricity, especially in scenarios 2 and 3, which must be curtailed in order to keep an active power balance between generation and load. This large excess is created because of the hybrid system size and limited capability of battery to absorb it. In Figure 54 at the Appendix, a typical example of such case is illustrated. As soon as the battery's SOC approaches the upper limit and the energy produced is more than the demand, exceeding energy appears which must be rejected by the control systems of the generators. An alternative way to manage the excess and thus, further optimize the system is through demand side management actions.

Finally, the results for the calculation of breakeven distance are presented in Figure 23.

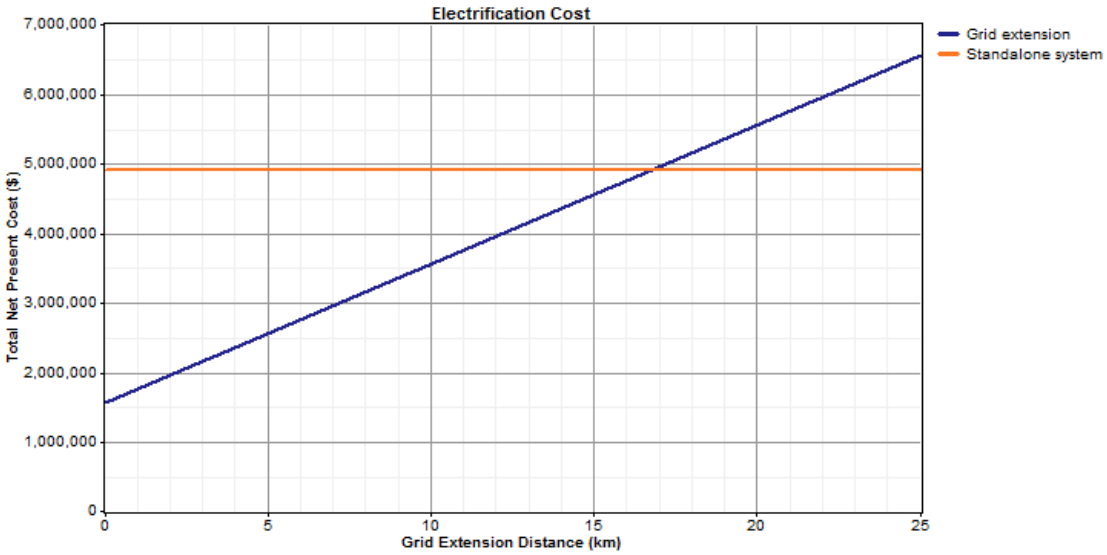

Figure 23 Breakeven grid distance extension for the 100% RES hybrid system of case 1

The cost of the 100% RES hybrid system of case 1 is compared to the cost of the interconnected system. The breakeven distance in is 16.7 km. Consequently, interconnection is more expensive and thus, a non-feasible option in comparison to the 100% RES scenario. The breakeven distance is extended at 17.4 km for the hybrid system of case 2 and at 23.9 km at case 3.

3.3.1 Verification using different types of batteries

So far in this study, lead acid batteries have been considered for the sizing of the renewable hybrid system. The aim of this section is to examine, for a given size of wind and solar farm (Case 1-scenario 2), the technical and economic impact of addressing various types of the most popular and promising battery storage technologies. In order to acquire comparable results, for all the following battery types, the nominal energy capacity is equal to 3 MWh.

Parameters for Vanadium Redox battery

Although Vanadium Redox battery storage is the most mature among flow batteries, it is relatively new and there is limited experience from its applications. The costs depend on the prices of materials and, for this reason, are subjected to uncertainty. According to (EPRI 2002), the capital cost for the battery stack is set at 1500 €/kW and for the electrolyte at 250 €/kWh. In its service life, only the pumps and the electrolyte should be replaced and consequently the replacement cost is 25 €/kWh (Hu, et al. 2012). The operation and maintenance cost is 1 €/kW per year for the cell stack and 0.02 €/kWh per year for the electrolyte. The expected lifetime for the stack and electrolyte is 15 and 30 years respectively and round-trip efficiency is 70% (EPRI 2002). As mentioned at chapter 2, the power and energy capacity are decoupled at this type of battery. Energy capacity is 3 MWh and power rating is 500 kW.

Parameters for NaS battery

The rated capacity of each cell is considered to be 628 Ah and the nominal voltage is 2 V (EPRI 2002). The energy to power ratio is six and typical efficiency for this battery

technology is 85%. The capital and replacement cost is 250 €/kWh and the O&M cost is 0.35 €/kWh/yr (Kintner-Meyer, et al. 2010). The service life of this battery is 15 years and the cycle life time is 2,500 cycles for 100% DOD, 4,500 cycles at 90% DOD and 6,500 cycles at 65%.

Parameters for Lithium ion battery

The lithium ion battery modeled in this study has nominal capacity equal to 99 Ah and its nominal voltage is 10.8 V. (Garimella and Nair 2009). It comprises of three parallel and three series cells. The capital and replacement cost of this battery technology is 500 €/kWh (Schoenung 2011). Due to lack of information regarding the O&M cost, it is assumed to be equal to 0.35 €/kWh/yr like in the case of NaSES. Furthermore, the lifetime is equal to 15 years and the cycle life is 2,000 cycles for 100% DOD, 3,000 cycles for 80% DOD, 4,000 cycles for 70% DOD and for very low DOD (3%) it can reach 500,000 cycles. The efficiency is 90% and the power to energy ratio is four (Braun, et al. 2011).

The characteristic which were used for the model development of those types of batteries are summarized in Table 6.

Table 6 Characteristics of battery technologies modeled in HOMER (EPRI 2002) (Hu, et al. 2012) (Kintner-Meyer, et al. 2010) (Garimella and Nair 2009) (Schoenung 2011) (Braun, et al. 2011)

Battery	Capital	Replacement	O&M per year	Efficiency (%)	Lifetime at 80% DOD	Energy to power ratio
Lead acid	180 (€/kWh)	150 (€/kWh)	0.26 (€/kWh)	86	1,600 cycles	6
NaS	250 (€/kWh)	250 (€/kWh)	0.35 (€/kWh)	85	5,000 cycles	6
Li-ion	500 (€/kWh)	500 (€/kWh)	0.35 (€/kWh)	90	3,000 cycles	0.25
VRB	1,500 (€/kW)	1,500 (€/kW)	1 (€/kW)	70	>10,000 cycles	6
	250 (€/kWh)	25 (€/kWh)	0.02 (€/kWh)		30 years	

As demonstrated in Figure 24, lead acid is the most attractive battery technology, among the investigated ones, from economic point of view. The NPC of the hybrid system, for the cases of NaS, Li-ion and VRB battery, increases by 13% (3,428 k€), 38% (4,184 k€) and 43% (4,335 k€) respectively.

Figure 25 shows that VRB has the largest energy losses (69.19 MWh/yr), in comparison to the other batteries, due to their lower efficiency. On the other hand, the energy losses at Li-ion batteries which are equal to 19.7 MWh/yr are the lowest among the other ones. At lead acid and NaS batteries the energy losses are 26.1 MWh/yr and 27.3 MWh/yr respectively. Practically, there are not major differences, regarding the losses, between LA, NaS and Li-ion. Also, it is worth to be mentioned that RES fraction, for the case of Li-ion, reaches 95% while for NaS and lead acid battery it is 93% and for VRB it is 92%.

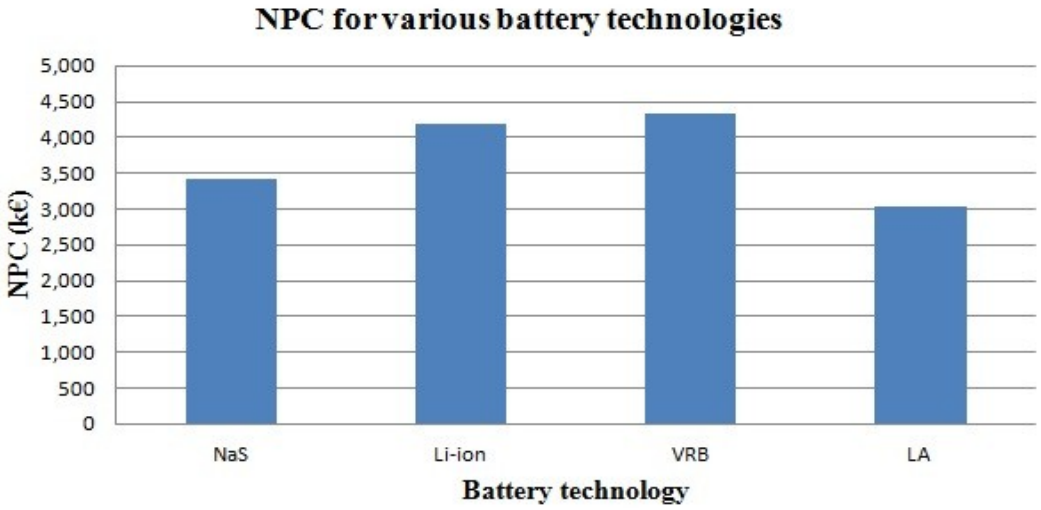

Figure 24 NPC of the hybrid system for different types of battery technologies

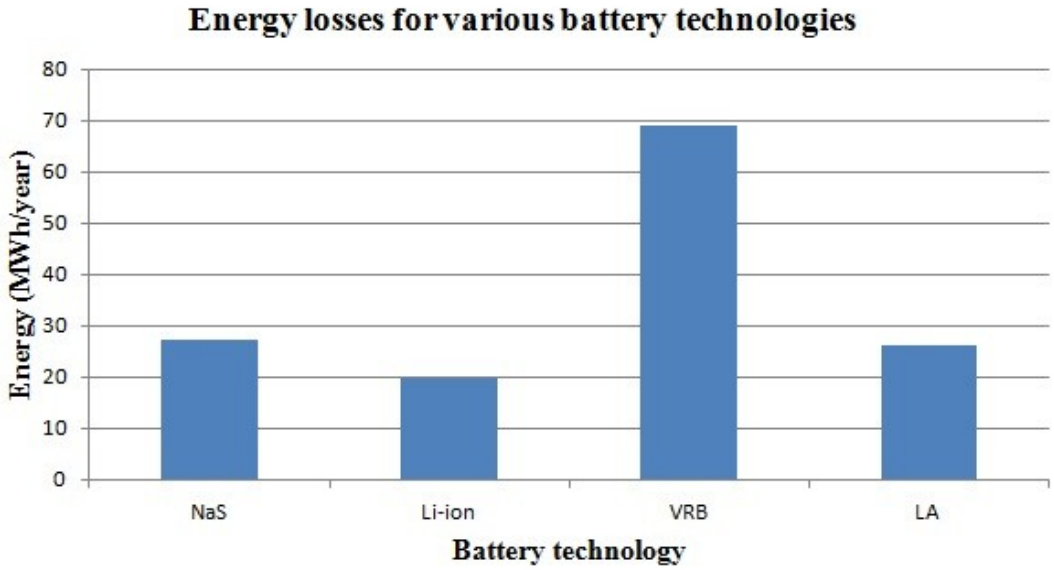

Figure 25 Energy losses for various battery technologies

3.3.2 Battery lifetime comparison

Apart from the cost and efficiency, this section performs a comparison between the lifetimes of each battery type. In HOMER, the battery bank lifetime can be limited either by the lifetime throughput or the battery float life and is given as follows.

$$R_{batt} = MIN\left(\frac{N_{batt}Q_{lifetime}}{Q_{thrpt}}, R_{batt,f}\right) \quad (3.12)$$

Where:

- R_{batt} is the battery bank life (yr)
- N_{batt} is the number of batteries in the battery bank

- $Q_{lifetime}$ is the lifetime throughput of a single battery (kWh)
- Q_{thrpt} is the annual battery throughput (kWh/yr)
- $R_{batt,f}$ is the battery float life (yr)

The battery's lifetime throughput ($Q_{lifetime}$) is the amount of energy that can be cycled through a battery before it needs replacement and is shown below.

$$Q_{lifetime} = fd\left(\frac{q_{max}V_{nom}}{1000\,W/kW}\right) \tag{3.13}$$

Where:

- f is the number of cycles to failure
- d is the depth of discharge (%)
- q_{max} is the maximum capacity of the battery (Ah)
- V_{nom} is the nominal voltage of the battery (V)

The results of the batteries cycle life time evaluation are presented in Table 7.

Table 7 Lifetime comparison for various battery technologies

Battery type	$Q_{lifetime}$ (kWh/yr)	Q_{thrpt} (kWh/yr)	$\frac{Q_{lifetime}}{Q_{thrpt}}$	Float life (yr)
LA	3,840,000	207,863	18.5	20
NaS	12,057,600	208,252	57.9	15
Li-ion	7,197,854	217,471	33.1	15
VRB	24,000,000	207,336	115.75	15

As illustrated in Table 7, the cycle lifetime of LA battery is close to its nominal float life. For the cases of NaS, Li-ion and VRB, the cycle life is much more than their float life. This fact happens because of the low annual throughput since there is neither charging nor discharging for more than 50% of the year. Practically, those three types of batteries are not likely to last more than what their float life suggests and thus, LA batteries have an advantage compared to them. Therefore, the best battery type option with respect to cost, efficiency and lifetime is the LA.

3.4 Conclusions

In conclusion, this chapter investigated the optimal size for a hybrid power system considering various RES and ES types and capacities. Three optimization scenarios were investigated each of them taking into account different policy constraints and approaches. Also, a comparison between the most promising battery technologies was performed regarding their cost, efficiency and cycle lifetime. Finally, this chapter evaluated the economic feasibility of submarine cable interconnection between Agios Efstratios and Lemnos. The following chapter will deal with the steady-state analysis of the existing network

configuration and also the proposed hybrid system with respect to the results of the optimization analysis. For the following chapter, it is assumed that the proposed system size is that of scenario 2.

Chapter 4 – Load flow analysis

4.1 Introduction

In the previous chapter, the optimal sizing of the hybrid system's units was discussed. The current chapter deals with the steady-state analysis of the power system during normal operation and the optimal location of WT, PV and ES plants.

Load flow analysis is a very useful tool for power system planning and design. Given supply voltages, system configuration and loading, a load flow analysis calculate voltages, active and reactive power flows and losses throughout the whole system (Saadat 2002). The load flow calculations are performed by DIgSILENT PowerFactory simulation tool. Since load flow analysis is a non-linear problem, DIgSILENT solves the system's equations by using an iterative procedure. One of the methods used for load flow analysis is the Newton Raphson's method.

4.2 Description of island's grid

As mentioned at the first chapter, the island's energy demand is covered by a conventional power station consisting of five diesel fueled generators. The nominal rating for two of those gensets is equal to 90 kW and the other three engines are rated at 220 kW. Their output voltage is 400 V and their technical characteristics are illustrated in Table 8. Apart from those engines, a small asynchronous wind turbine (20 kW) has recently been installed.

Table 8 Characteristics of diesel power generators

Unit	Installation year	Nominal power (kW)	Minimum operation point (kW)	Fuel consumption rate (g/kWh)		
				50%	75%	100%
MAN D2566/ME	1988	90	45	291.9	265.8	263.3
HYUNDAI KD8AX	2008	220	110	250.7	240.3	242.8

Two three-phase transformers raise the voltage level from 0.4 kV to 15 kV. As shown in Figure 26 at the single line diagram of the island's network, two separate overhead lines (OHL) start from each transformer and at the end of every line branch there is a transformer that steps down the voltage level at 400 V. The total length of the medium voltage (MV) OHL is 9 km and they are made of copper wire 3x35 mm². Individual cable lengths and characteristics are presented in Table 16 at Appendix B. A short line that starts from the transformer DPS TR-1(630 kVA) ends at the village where the majority of the households are located. The other transmission line starts from the second transformer DPS TR-2 (400 kVA) and goes to the smaller part of the village and to other loads which are spread at different parts of the island. The wind turbine is connected to this line through WPP TR (50 kVA). As shown in Table 9, the remote loads are two military bases (AB1-AB2), a station of

telecommunication network antennas (MNA) and two water pumping stations (PS1-PS2) that use induction motors. Characteristic load values for different periods are shown in Table 16. The power factor for the pumping stations is assumed to be 0.85 while for all the other loads it is equal to 0.95.

Table 9 List of the transformers' types, ratings and buses at MV/LV sides

Load type	Transformer type	Transformer rating	MV (15 kV) side bus	LV (400 V) side bus
Loads 1-7	R TR-1	250 kVA	BUS RL1-1	BUS RL1-2
Loads 8-11	R TR-2	250 kVA	BUS RL2-1	BUS RL2-2
AB1	AB TR-1	50 kVA	BUS AB1-1	BUS AB1-2
AB2	AB TR-2	100 kVA	BUS AB2-1	BUS AB2-2
MNA	NA TR	50 kVA	BUS NA-1	BUS NA-2
PS1	PS TR-1	50 kVA	BUS PS1-1	BUS PS1-2
PS2	PS TR-2	25 kVA	BUS PS2-1	BUS PS2-2

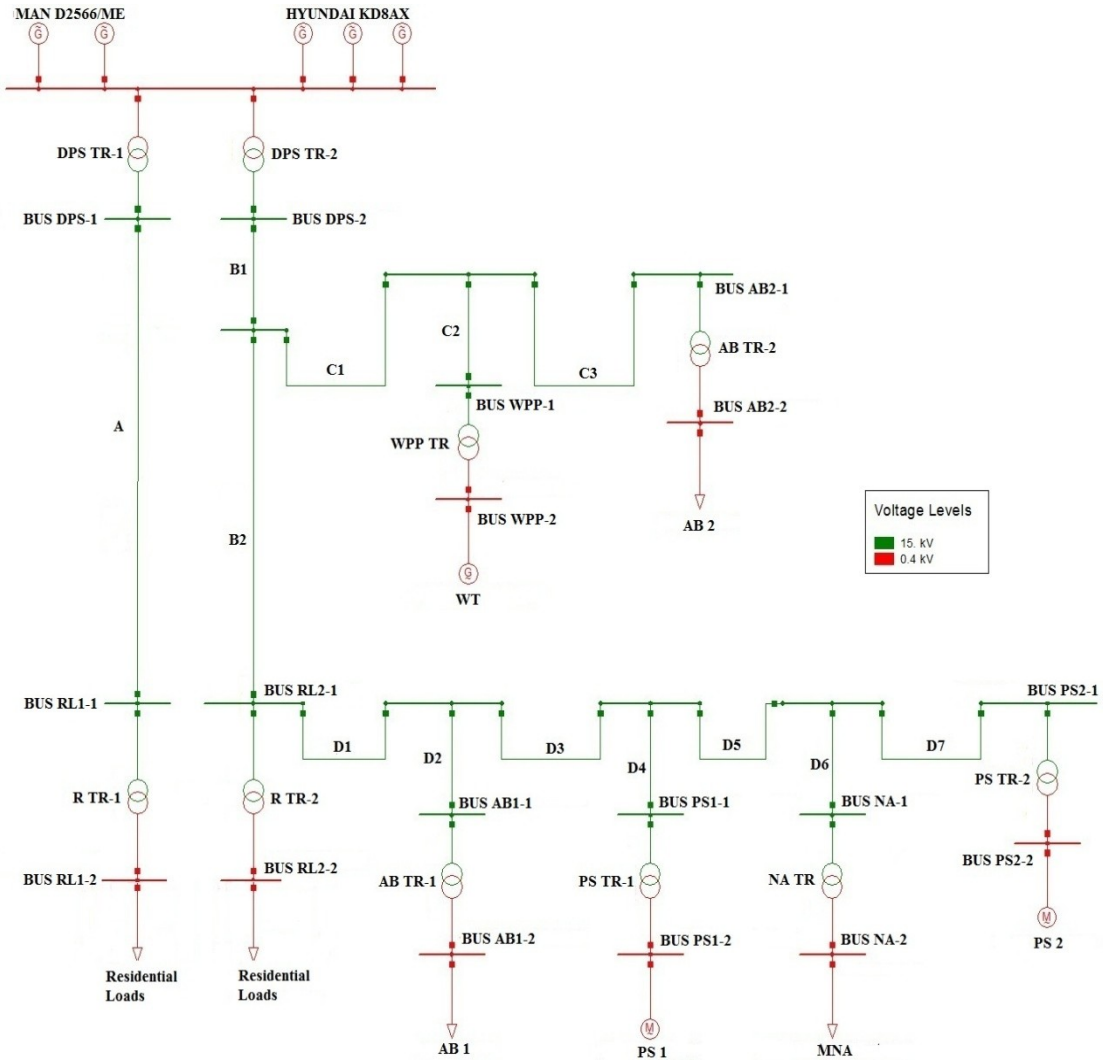

Figure 26 Single line diagram of the island's network

The total length of the low voltage (LV) OHL is around 1.5 km and the type of cable that uses is aerial bundled aluminum cable 4x120+25 mm². Its characteristics are shown in Table 17 at Appendix B.

Figure 27 illustrates a simplified schematic of the LV distribution network divided in 11 main branches. The feeders are arranged in radial configuration. The average length of the branches is between 100 – 150 m and separate lengths are stated, along with those of the MV line branches, in Table 16 at Appendix B. Also, at each branch there is a load which represents a group of households and buildings. The single line diagram and the data required for the model development were provided by the PPC.

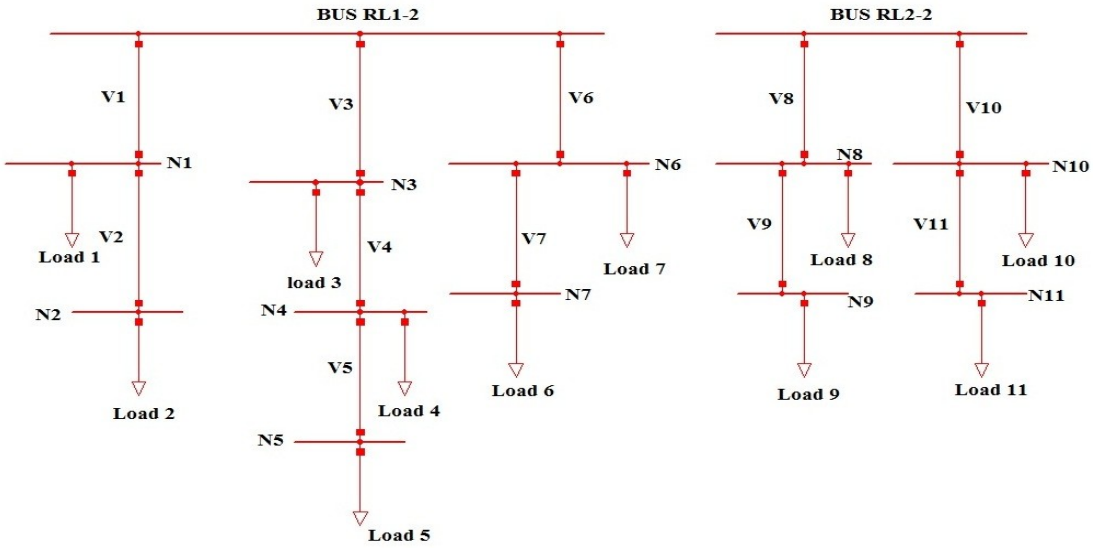

Figure 27 Single line diagram of the low voltage distribution network at the residential area

4.3 Load flow analysis of current electricity grid

At the current section, load flow analysis is performed for the existing (base) power system under different operating conditions.

The aim is to calculate the voltage magnitude at the buses and loading of lines and transformers. Moreover, the purpose of this load flow analysis is to compute the power system losses and investigate if the transmission and distribution system operates within acceptable ranges which are the voltage limits as stated in chapter 1, or if they are exceeded.

As being mentioned, the island's load profile is characterized by significant seasonal diversity. In summer, the electricity demand is greater because of the population growth (tourists) and usage of air-conditions for cooling. On the other hand, winters are mild and the villagers do not consume much power for heating or other domestic appliances. Figure 28 illustrates two different load profiles. The blue line represents the average daily demand of August and varies from 140 kW in the morning to more than 300 kW at night. The red line illustrates the average daily demand of January. At that case there is not important load deviation within a day and varies between 80 kW and 150 kW.

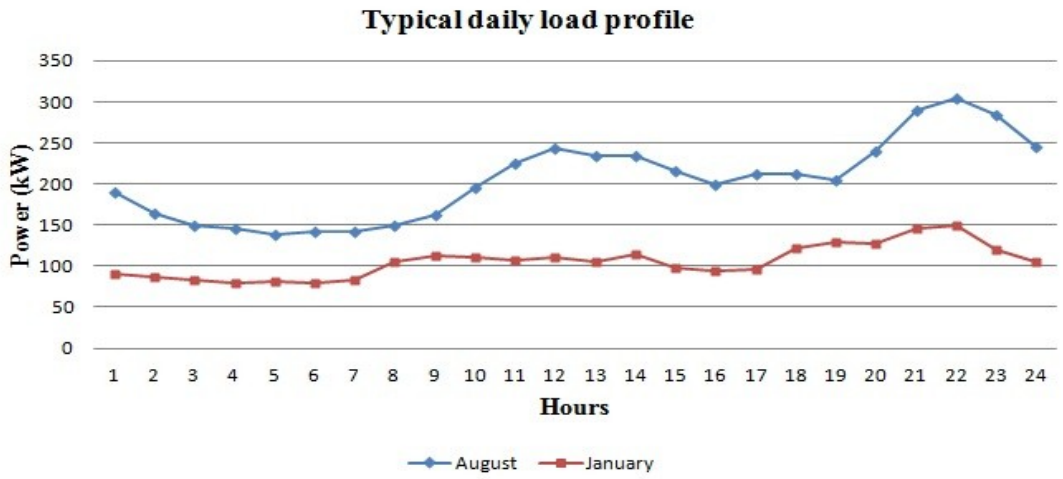

Figure 28 Typical daily load profiles for August and January

Three different cases (high demand – average demand – low demand) are considered for the load flow analysis of each season scenario. As shown in Figure 28, times of high demand take place during night while average and low demand take place at midday and morning hours respectively. Regarding August, the high demand case (case 1) demonstrates the system's maximum load conditions (360 kW) while case 2 represents average loading (225 kW) conditions. Case 3 is the zone of low load demand (150 kW). On the other hand, for the winter scenario (January), the load values for high (case 1), average (case 2) and low (case 3) demand are 150 kW, 110 kW and 80 kW respectively.

The load duration curve in Figure 29 illustrates that the demand is between 100 kW and 250 kW during 88% of the whole year. On the contrary, the load duration frequency for loads larger than 300 kW is less than 1% and for loads less than 100 kW it is around 8.7%.

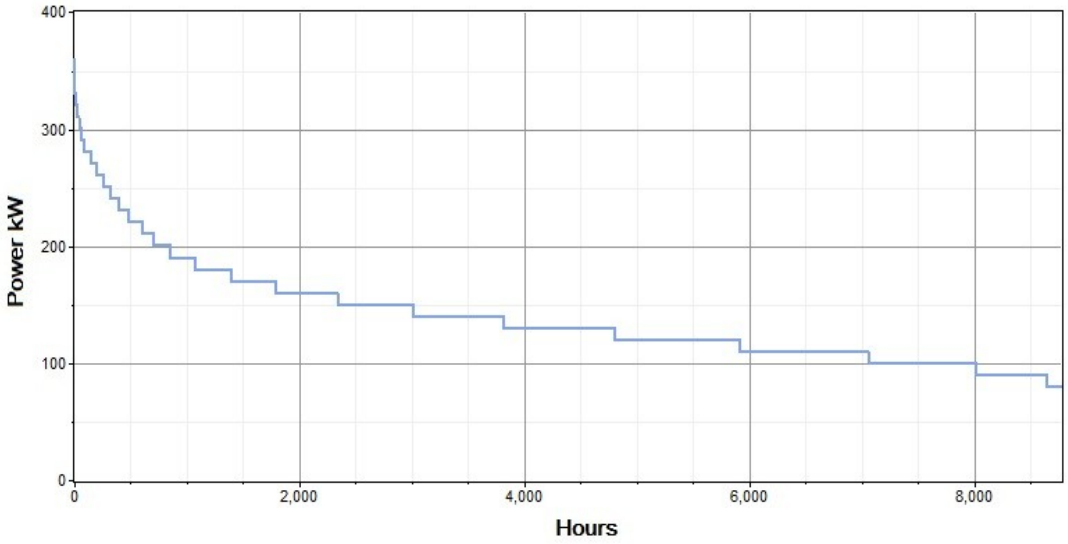

Figure 29 Load duration curve of Agios Efstratios for 2010

4.3.1 Base case simulation results

This section presents the simulation results for the base power system with respect to the previously mentioned cases and scenarios. In the following, the loading of lines and transformers and voltage magnitude at MV and LV buses is demonstrated.

Loading of lines

The rated current capacity is equal to 170 A for the MV OHL and 260 A for the LV OHL. For all cases the currents that flow through the lines are relatively low compared to their nominal capability.

As illustrated in Figure 30, the loading of MV OHL in August and January is less than 5% and 2% respectively. Lines A and B carry the largest part of the load and the loading difference between cases 1 and 3 at those lines is more significant compared to lines C and D. In August, this difference is up to 3.5% while in January it is around 1%. As indicated in Table 16, the remote loads connected to lines C and D are not subjected to major seasonal variations. On the contrary, there are more significant changes at the loads of the residential area.

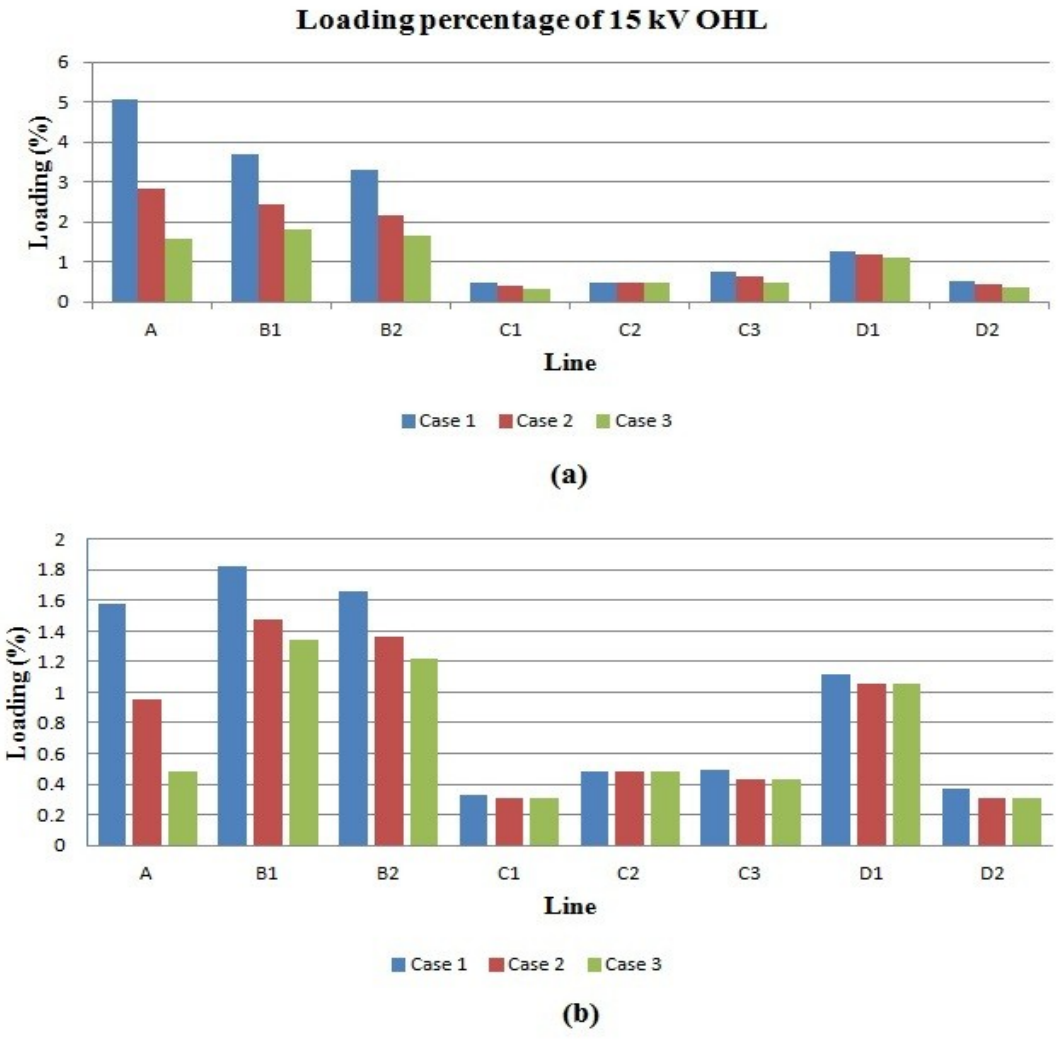

Figure 30 Loading of 15 kV OHL in August (a) and January (b) for different cases of demand

Regarding the loading of LV OHL, Figure 31 illustrates the important divergence between cases 1, 2 and 3. The line branches of the LV distribution network are not loaded more than 50% in August while in January it is less than 15%. Moreover, in case of August, loading varies up to 20% from case 1 to case 2 and 33% between cases 1 and 3. In January, that difference is up to 6% from case 1 to case 2 and 10% between cases 1 and 3. In general terms, during all cases, MV and LV lines are not imposed to high loading conditions.

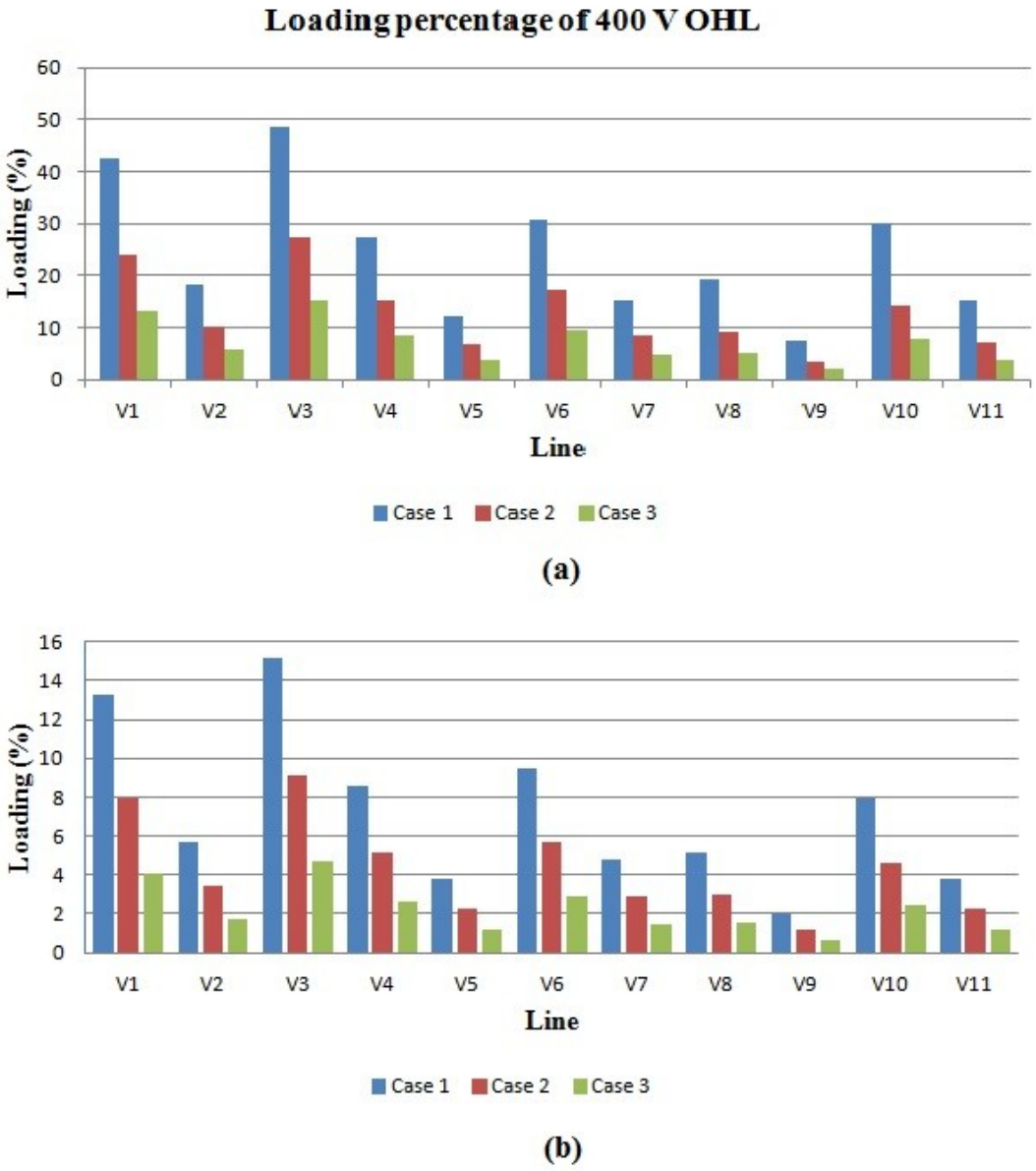

Figure 31 Loading of 400 V OHL in August (a) and January (b) for different cases of demand

Loading of transformers

As expected, in the period of August the loading at some of the transformers is higher compared to January. As shown in Figure 32, transformer R TR-1 which is connected to the

residential area, is highly loaded (up to 90%) in case 1. In cases 2 and 3, loading is 40% and 60% less compared to case 1. Similarly to the case of line loading, the most significant loading variations occur at the transformers between diesel station and the residential area (DPS TR, R TR) due to the fluctuations in demand profile of households. In January, those transformers are not loaded more than 27% in case 1 and 15% in case 3. The loading of those transformers which are located at the remote loads and generators (wind farm, army bases, pump stations and antennas) doesn't vary much between the cases and seasons.

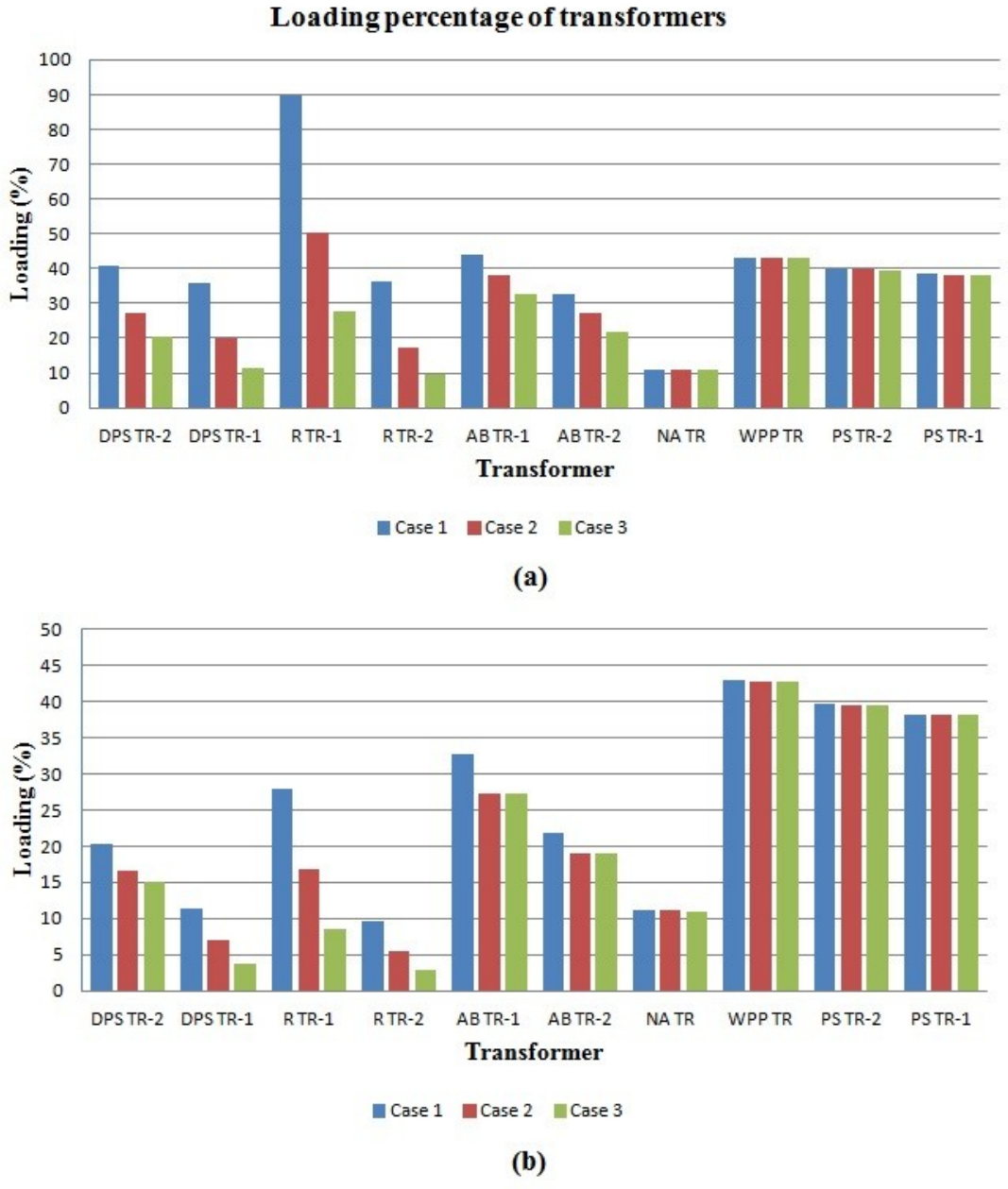

Figure 32 Loading percentages of transformers in August (a) and January (b) for different cases of demand

Voltage magnitude of buses

As shown in Figure 33 and for case 1, the steady-state voltage magnitude at the MV buses in August and January doesn't deviate from the nominal value (1 pu) by more than 1.5% and 1% respectively. In cases 2 and 3, voltage is closer to 1 pu. At buses connected to lines C and D, voltage level is almost the same for each case of demand.

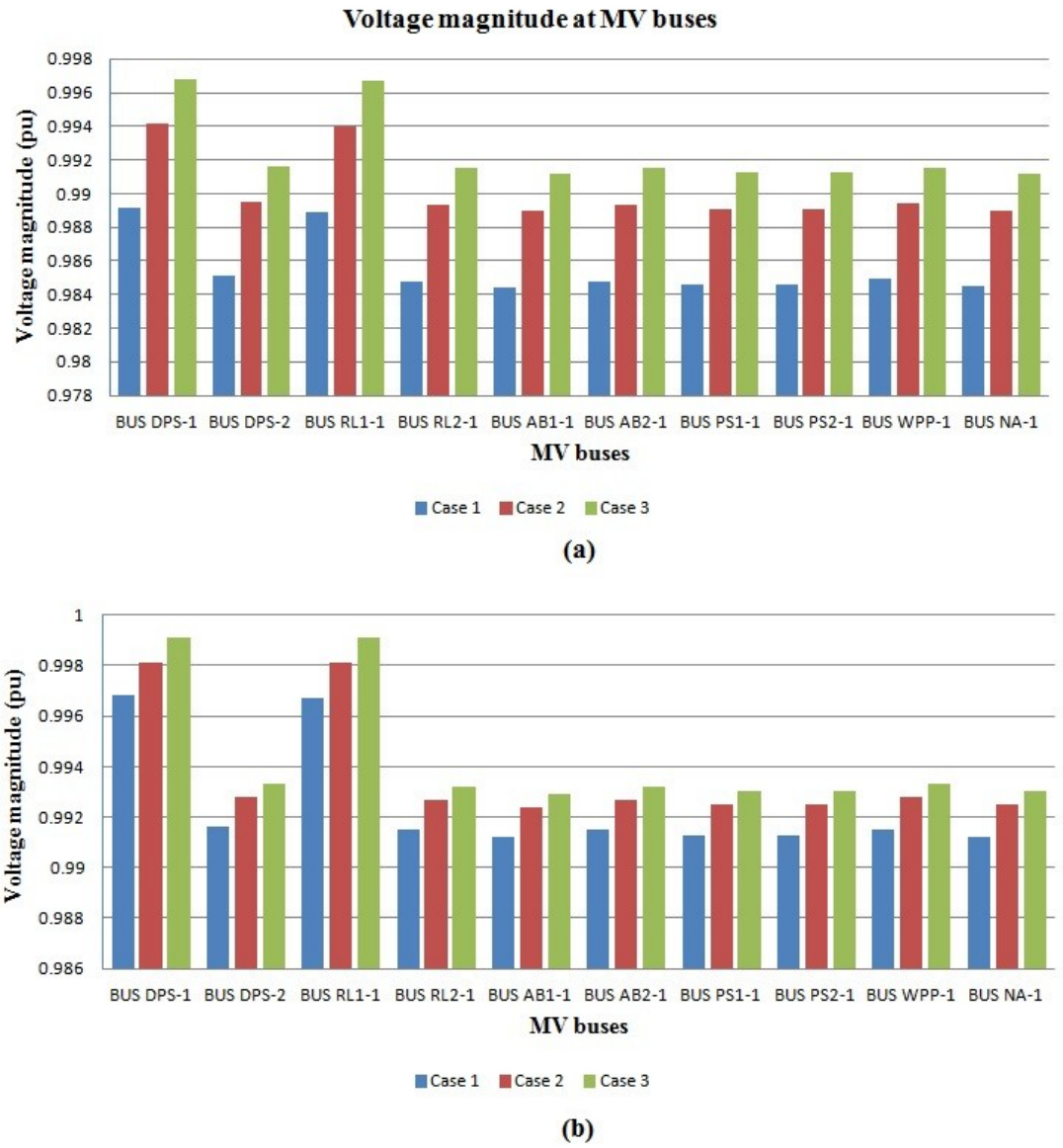

Figure 33 Voltage magnitudes at MV buses in August (a) and January (b) for different cases of demand

Figure 34 shows the voltage magnitude at LV buses in August and January for cases 1, 2 and 3. The voltage drop percentage depends on the length of the line that connects it with buses RL1-2 and RL2-2 and the loads along the line. In August the voltage magnitude drops by around 7% in case 1. In case 2 the voltage varies from 384 V to 392 V and in case 3 between 392 V and 396 V. As illustrated in Figure 34b, there is higher voltage magnitude in January and variations between the cases are not important.

In general, at all cases and buses, the steady-state value of voltage magnitude is maintained within the acceptable operational limits (±10%).

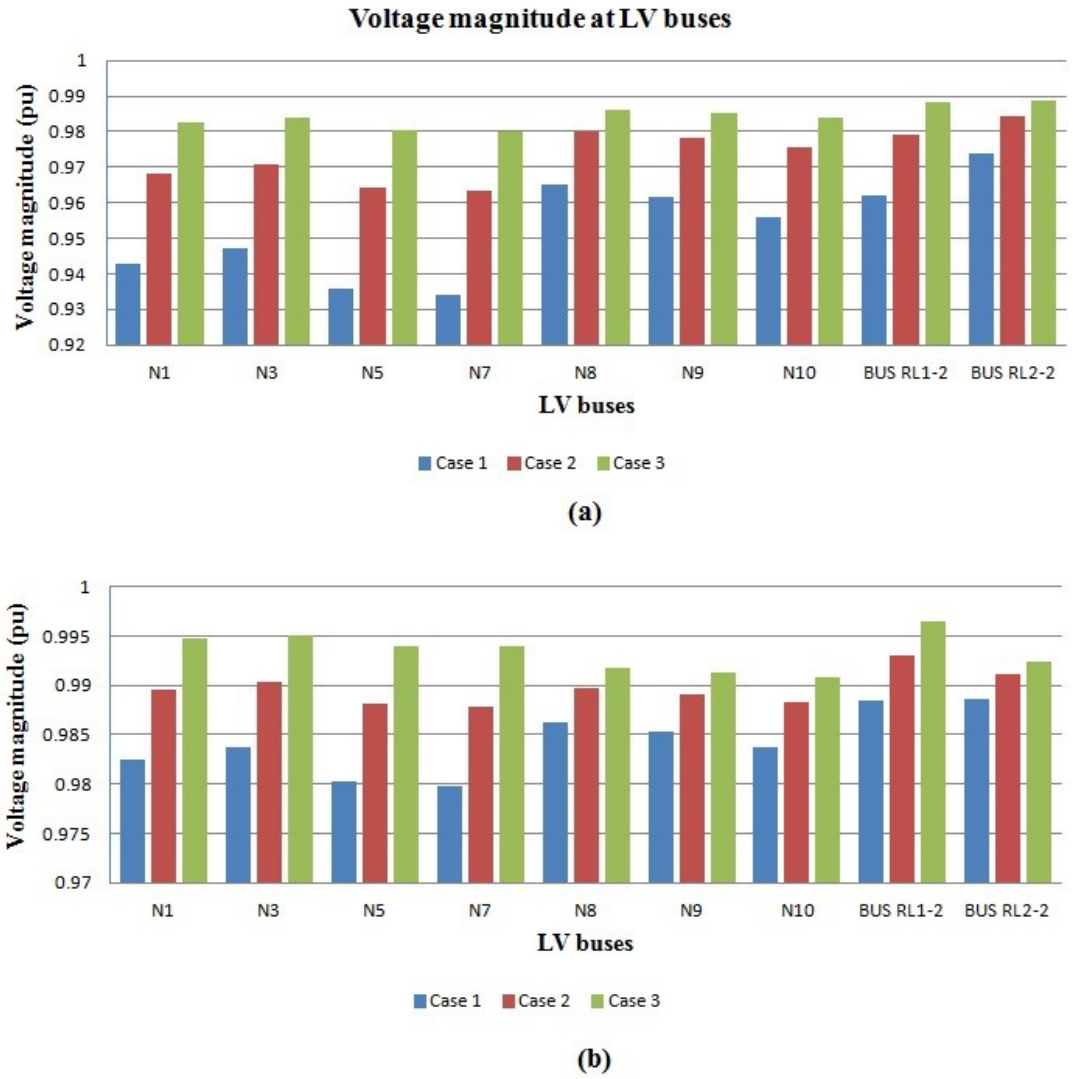

Figure 34 Voltage magnitudes at LV buses in August (a) and January (b) for different cases of demand

Finally, there are power losses at the system that occur at OHL and loads. The total losses of the power system in August are 17.5 kW in case 1, 9 kW in case 2 and approximately three times less compared to case 1 in the third case (6 kW). In high demand case (case 1) in January, power losses are 6 kW as well. In cases 2 and 3, the losses are 5.4 kW and 5 kW respectively. As expected, the losses are proportional to the demand.

4.4 Optimal location for the RES and ES units

The aim of this section is the investigation for the optimal placement of the renewable energy and storage units. The analysis is performed with respect to the hybrid system size as specified for high RES scenario (case 1-scenario 2) in chapter 3 (WT: 330 kW, PV: 100 kWp, ES: 3 MWh).

In general, the optimal placement of distributed generation units is the one that minimizes the electrical network losses, improves the voltage profile and ensures system stability and reliability (Kansal, et al. 2011) (Borges and Falcao 2006).

4.4.1 Optimal location for wind turbine

According to wind speed measurements recorded by CRES, the location that has the best possible wind power generation potential is at the place of highest altitude on the island where the 20 kW wind turbine has already been installed (CRES 2011).

The transformer between wind farm and grid (WPP TR) in the existing system is rated at 50 kVA. For the model development of the hybrid power system, this transformer is assumed to be replaced with a larger one (500 kVA) in order to carry the power flow from the wind farm without being overloaded.

4.4.2 Optimal location for the photovoltaic station

Apart from active power supply, PV generators are capable of providing reactive power as well. In practice it is equal to the reactive power capability of the converter connected between the PV and grid and is largely dictated by the converter's voltage and current ratings. In general, as the nominal reactive power output increases, the converter's apparent power rises according to the following formula.

$$S = \sqrt{P^2 + Q^2} \tag{4.1}$$

So, assuming P and Q output at the converter terminals equal to 1 pu (100 kW) and 0.5 pu (50 kvar) respectively, the apparent power is 1.12 pu (12% increase).

Two possible locations are investigated. As illustrated in Figure 35, the first location is close to the residential area which is the main load center of the island and the second location is close to the wind farm.

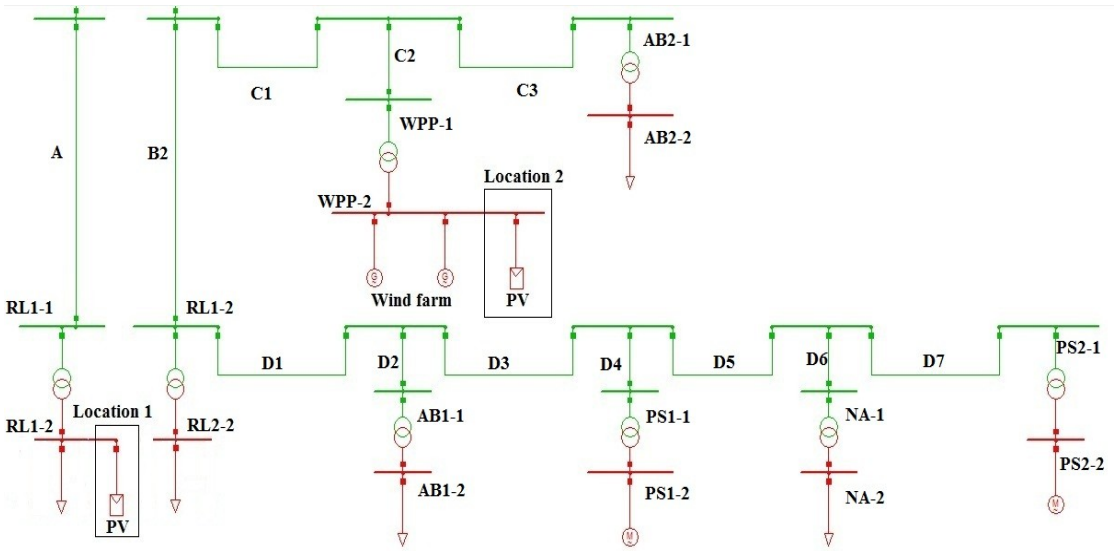

Figure 35 Illustration of the two possible places for the location of the PV station

The voltages at the buses for both locations are shown in Figure 36 and Figure 37. For the simulations, three different cases of demand have been considered in order to observe the effect of PV location under various loading conditions. The first case is the high demand (360 kW) period of August. The second case is the low demand period of August (150 kW) and the third one is the low demand period of January (80 kW). Moreover, it is assumed that all diesel generators are disconnected, the PV unit supplies its nominal active and reactive power (P=1 pu, Q=0.5 pu) and the rest of the demand is covered by the wind turbines.

As illustrated in Figure 36, when the PV unit is placed at location 1, voltage magnitude at MV buses is higher compared to when the solar panels are connected at location 2. The red line in Figure 36 shows that there is 3.5% voltage increase at bus RL1-1 where the PV is connected and around 1% at the other buses. Similar effect is demonstrated in (b) and (c) as well. Specifically in (c), the combination of very low local load and nominal power injection from the solar unit causes reverse power flow from LV side to MV side and brings overvoltage in all nodes and particularly in RL1-1.

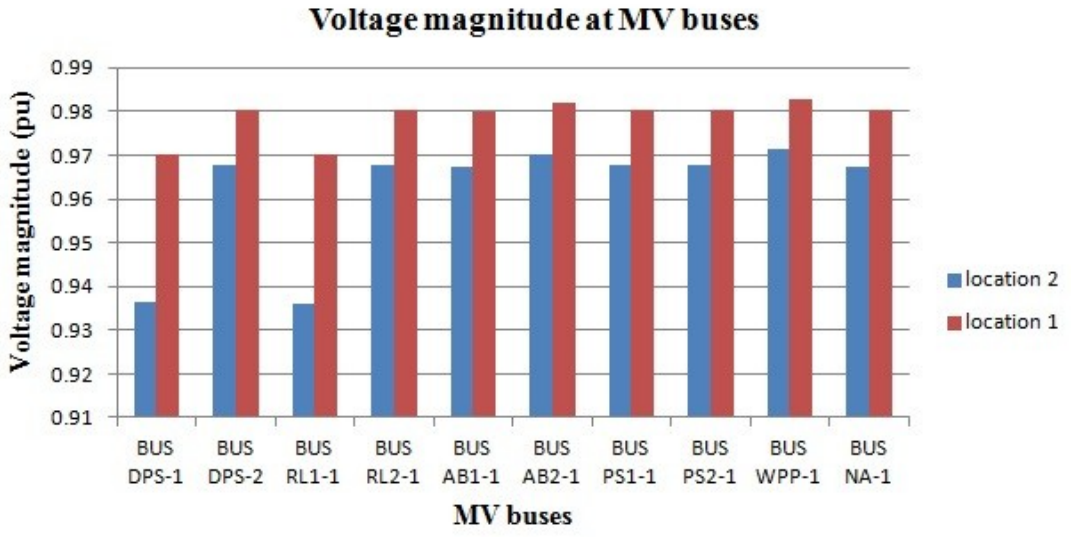

(a)

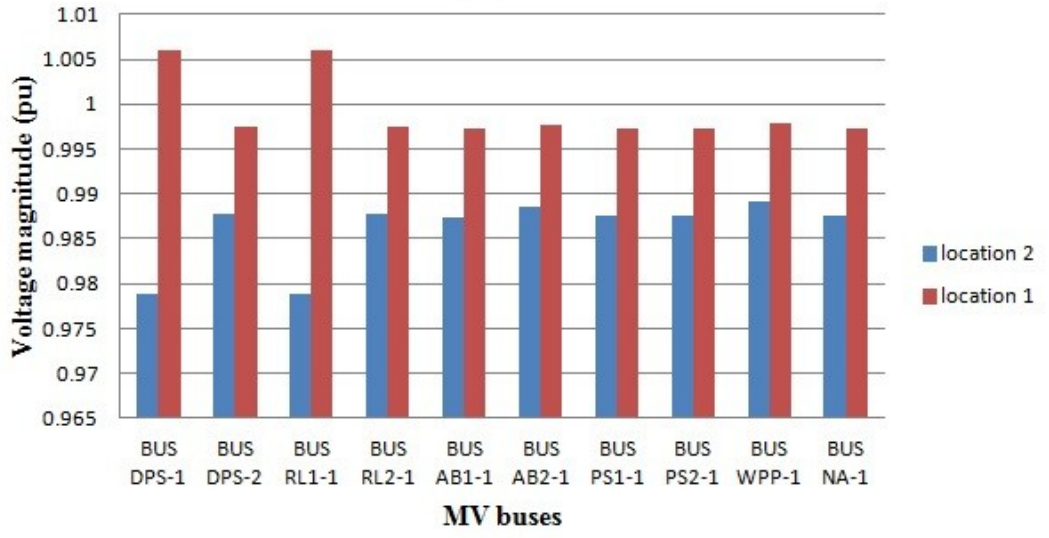

(b)

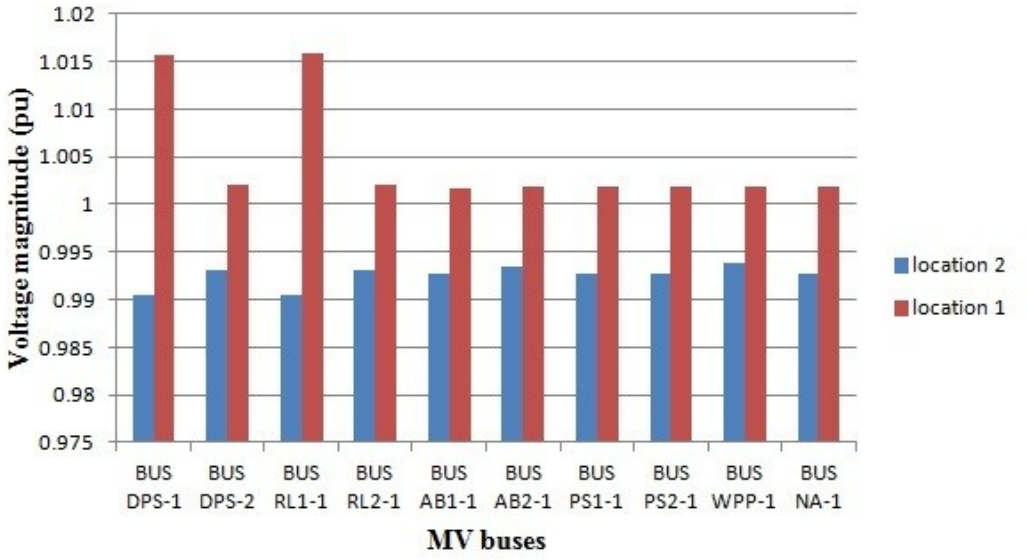

(c)

Figure 36 Voltage magnitudes at MV buses in case 1 (a), case 2 (b) and case 3 (c) for locations 1 & 2

Similar results can be obtained at LV buses as shown in Figure 37. When the PV unit is connected at bus RL1-2, the voltage steady-state level at one part of the residential area (buses N1-N7) can increase up to 6% in case 1 and 4% in cases 2 and 3. The overvoltage in case 3 is 2.5% more than the nominal. This is the maximum overvoltage that can take place and is within the acceptable limits. Moreover, at the same buses, voltage drops that are below the acceptable limits are likely to occur during high demand periods when the PV system is at location 2. Such significant voltage decrease takes place because of the large distance between power supply and load center and thus, larger voltage drop across the line. Consequently, the option of location 2 is not suggested.

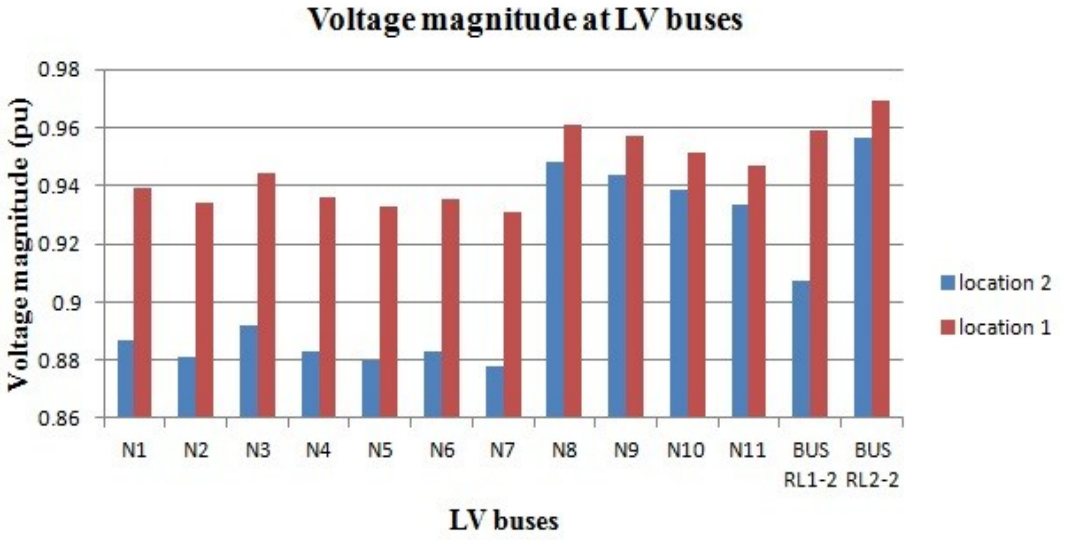

(a)

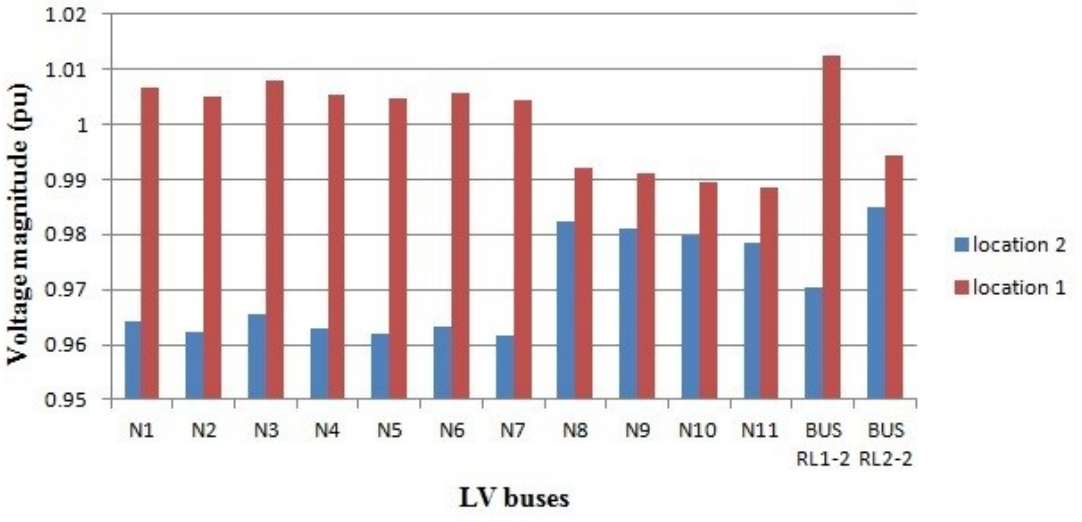

(b)

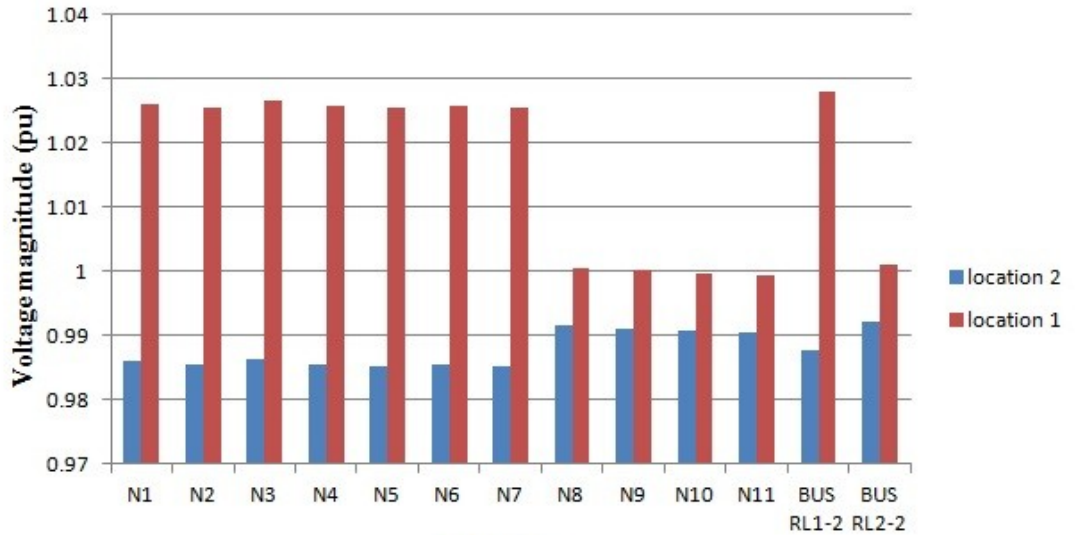

(c)

Figure 37 Voltage magnitudes at LV buses in case 1 (a), case 2 (b) and case 3 (c) for locations 1 & 2

Furthermore, when PV units are at location 2, the active and reactive power losses at the high demand case (case 1) are 26.2 kW and 45.1 kvar respectively. In case of location 1, the active power losses drop by 35% (17 kW) and the reactive power losses decrease by 65% (16.5 kvar). Therefore, distribution of generating units close to the consumers reduces the system's losses and improves the voltage profile.

Also, the level of voltage improvement depends from both active and reactive power capability of the PV. Assuming that reactive power supply increases from 0.5 pu to 1 pu, voltage grows further up to 2% at MV buses and up to 2.5% at LV buses.

Since placing the PV system closer to the loads has more advantages than the opposite, another option regarding the optimal location of solar panels is to divide their total capacity

into smaller units and place them at different feeders of the LV distribution network as shown in Figure 38 below.

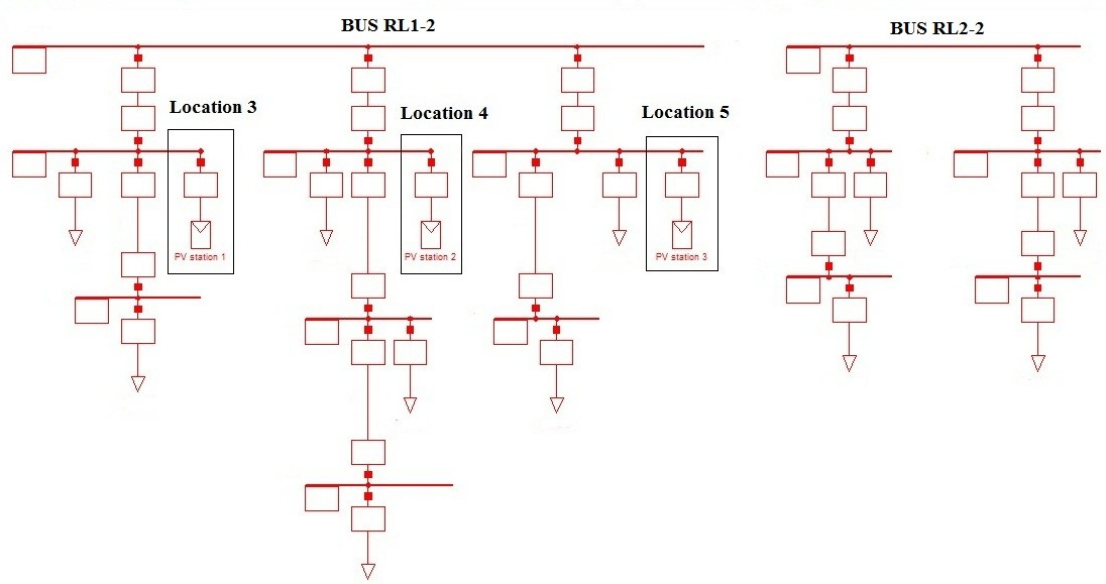

Figure 38 Illustration of separate distributed PV stations

Figure 39 shows, for the three cases of demand, the effect of PV units over voltage magnitude when the last ones are distributed at different parts of the residential area. In case 1, when separate units are placed at locations 3, 4 and 5 (red line), the voltage magnitude increases by 1% to 2% in buses N1-N7. The effect in buses located far from this location is negligible.

Regarding cases 2 and 3 which are illustrated in (b) and (c), the relatively low local load brings further increase in voltage level. In some of the buses it can reach 1.04 pu but this overvoltage phenomenon can be restrained through power output control of the solar units and/or power absorption from the storage. In Figure 55 at Appendix B, a snapshot of the radial LV residential area network is illustrated during an overvoltage case.

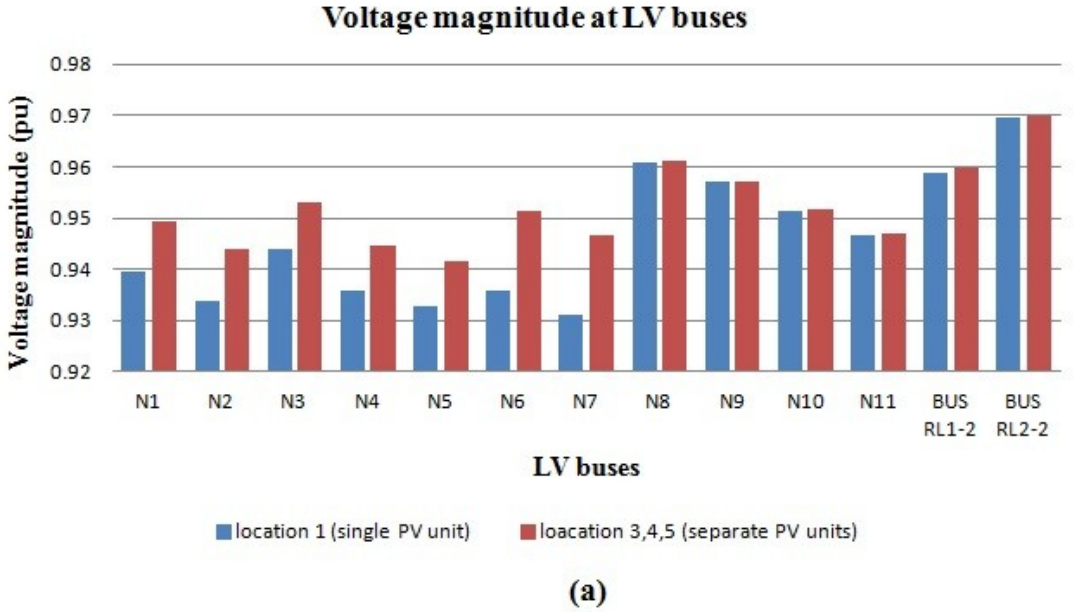

(a)

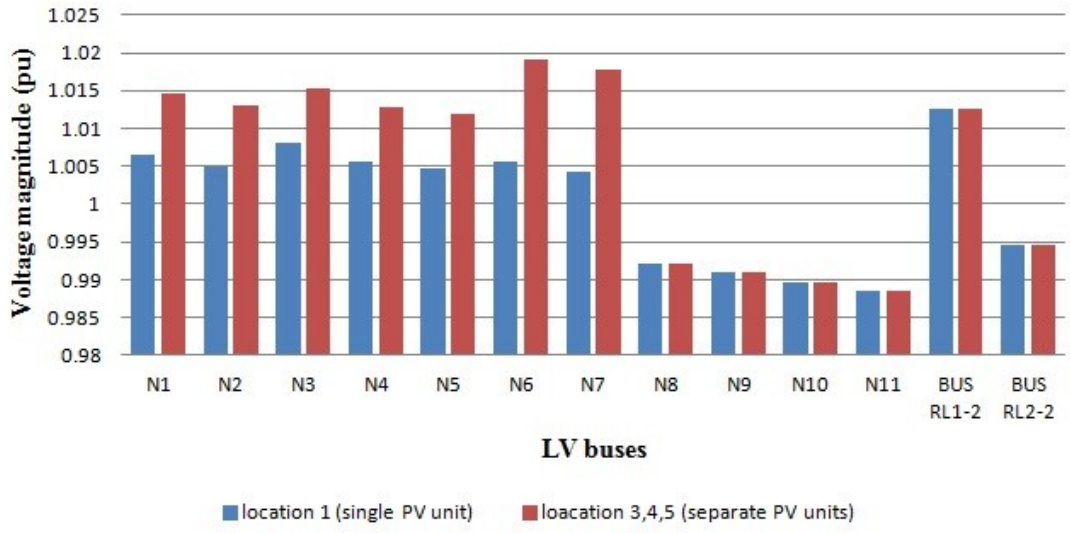

(b)

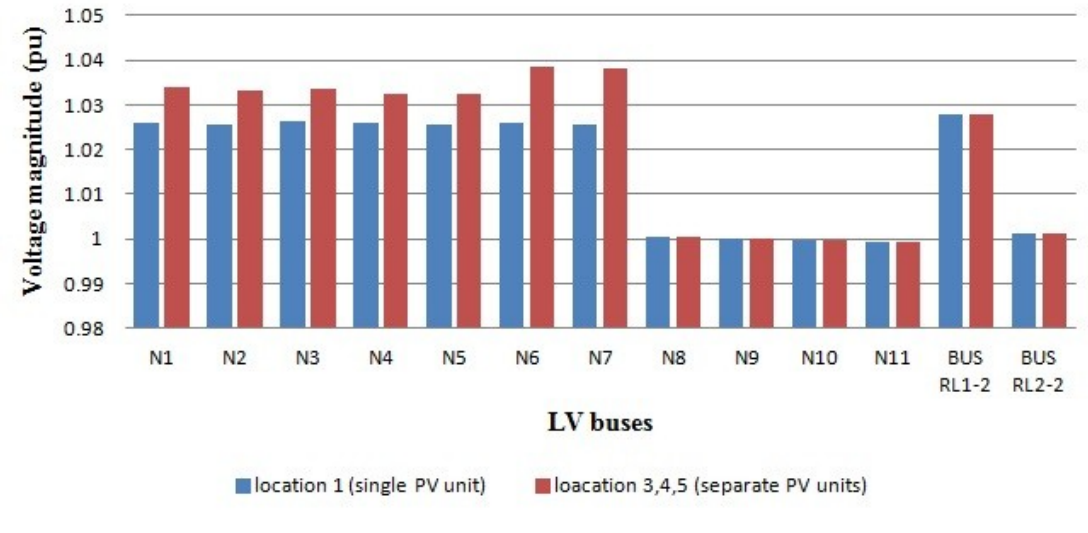

(c)

Figure 39 Voltage magnitudes at LV buses in case 1 (a), case 2 (b) and case 3 (c) for single and separate PV units

Although, from technical point of view, the case of distributing the PV units at many locations is more advantageous than placing them at one, there are further parameters, such as increased installation cost, that are likely to pose barriers but it is not within the scopes of this study to investigate them.

4.4.3 Optimal location for the ES unit

The conclusions regarding optimal location that were previously derived for the case of PV, apply to the case of battery as well.

Thus, splitting the batteries into different parts and placing them, along with the PV units, at locations 3, 4 and 5 is the optimal solution for storage placement for two major reasons. The first reason is that batteries, along with the PV unit, can further improve the grid's voltage

profile during both voltage drop and overvoltage. The second reason is that when solar power supply capability is limited, batteries are able to assist in voltage stability.

Batteries are able to provide active and reactive power supply which depends on the rating of the converter connected between them and grid.

4.5 Conclusions

In conclusion, a load flow analysis for the existing power system configuration was performed and demonstrated its loading conditions and voltage profile considering different seasonal demand. The highest loading and voltage drop take place at summer while, on the contrary, they are insignificant during winter. The voltage limits are not exceeded in all cases. Moreover, the optimal location for the proposed RES/ES components was investigated. Regarding the wind turbine, the sitting evaluation is related to the wind conditions along the island. For the PV and battery system, the best option is considered to separate them into smaller units and place them at different LV feeders of the residential area in order to reduce the losses and improve the voltage profile. The following chapter deals with the dynamic stability analysis of the hybrid system under normal generation/load conditions and fault cases.

Chapter 5 – Dynamic power system simulations with DIgSILENT

5.1 Introduction

In the previous chapter, a load flow analysis was performed for the existing power system of Agios Efstratios and optimal location for RES and ES units has been investigated.

The scope of this chapter is to analyze the system's dynamic behavior under various generation/load situations and contingencies and highlight the contribution of battery storage in frequency and voltage stability. Moreover, aims at demonstrating the importance of battery's balancing capability in stand-alone systems with high penetration of renewables.

Before proceeding to the dynamic modelling and simulations of the hybrid system, a brief definition of power system stability is discussed.

Power system stability is the ability of a power system to remain in a state of operating equilibrium after being exposed to a physical disturbance (Kundur 1994). The same author classifies and describes the different types of stability as shown in Figure 40.

Those disturbances initiate dynamic phenomena. The stability of the power system is strongly related to the magnitude and type of the disturbance as well as to the system's initial operating condition. Some of those dynamics are regarded as normal (switching, load variations, generation change) and do not endanger the system stability (like small-disturbance rotor angle stability), while some others like earth faults, disconnections and short-circuits have more serious impact and affect large parts of the system (transient stability). It is essential that the steady-state condition reached after the disturbance is acceptable. Moreover, it is not necessary that the system returns exactly at the same steady state condition it had before the disturbance.

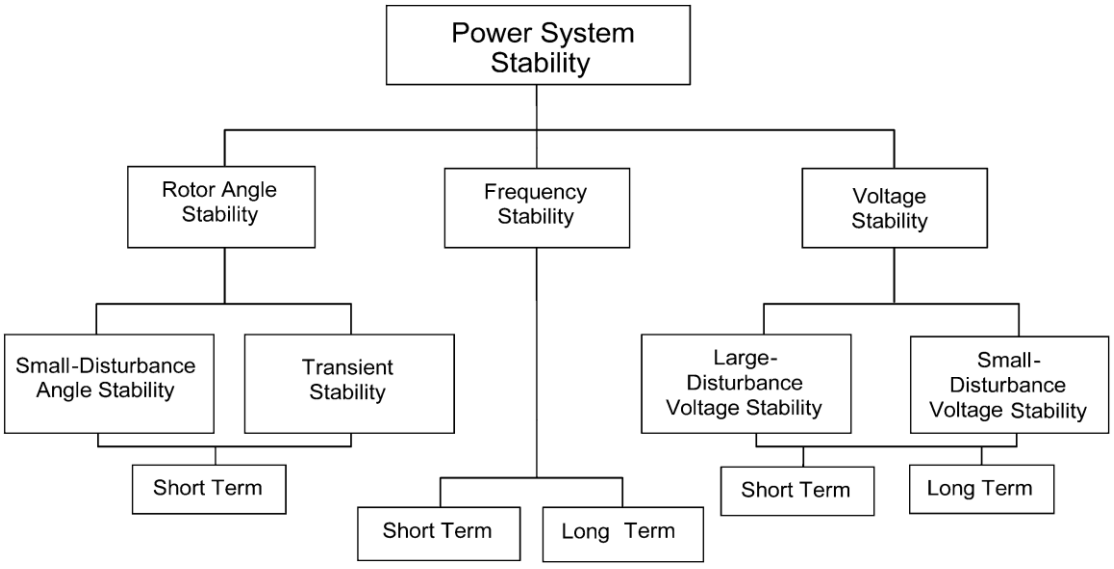

Figure 40 Classification of power system stability (Kundur, Paserba, et al. 2004)

This chapter deals with two types of power system stability, the frequency and the voltage stability.

Frequency stability is a display of the system's active power balance. When the total power fed into the system by the generators is less than the power consumption, the frequency level drops below its nominal value (50 Hz). If the power supply is more than the consumption, the frequency exceeds the nominal value. In both cases, the power output of the generating units adjusts in order to bring the frequency back to acceptable levels.

Voltage stability is the power system's ability to maintain steady state acceptable voltage level and depends on the reactive power balance at the network's nodes. When the injected reactive power is different from the required one, there is voltage instability. Overvoltage is mostly related to low load conditions while voltage drop to high loading.

5.2 DIgSILENT standard models

This section describes the dynamic model development of the proposed hybrid power system. The system configuration is the one illustrated in Figure 26. Built-in models from DIgSILENT library are used for the implementation of the hybrid system. It is not within the scopes of this part to analyze those models in detail but to present the main structure and configuration parameters of the simulation blocks.

Loads

The low voltage loads of the residential areas are modeled as two separate aggregated voltage-dependent loads (Elmlodlv) placed at buses RL1-2 and RL2-2. The load profile is the high demand (August) which is shown in Table 16.

Wind power station

A built-in model illustrated in Figure 56, contained in template library, of a wind turbine generator equipped with fully rated converter is connected in bus WPP2. The parameters of the control blocks are presented in tables 18-20 at Appendix C. Its power rating is 350 kW and the power factor is equal to 0.9. The transformer which connects it with the grid (TR WPP) is rated at 500 kVA.

Diesel generation units

The diesel generation units are modeled as synchronous generators. Their rating is shown in Table 8 of the previous chapter and they are equipped with a governor and an automatic voltage regulator (AVR). The governor regulates the output power and the speed of the generator. The governor model used in this thesis is a built-in model included in DIgSILENT library. It is named as "DEGOV1" and based on an IEEE model (DIgSILENT GmbH). The AVR regulates the generator's excitation current and, thus, the terminal voltage through adjustment of the excitation voltage of the rotor windings. The library model is named as "IEEET1" (IEEE 2006). The parameters for both governor and AVR models are presented in Table 21 and Table 22 at Appendix C.

Photovoltaic system

The PV system is connected in the LV bus RL1-2. The PV array and the power converter are represented by a static generator included in the template library of DIgSILENT and illustrated in Figure 57 at the Appendix C (DIgSILENT GmbH). This built-in model comprises of the PV generator whose apparent power is 0.11 MVA and power factor is 0.95 and also from measurement and control blocks. Their parameters are also shown in tables 23-26.

Battery ES system

The battery ES system (BESS) that is used in this section is also contained in the template library and its model frame is shown in Figure 58 at Appendix C (DIgSILENT GmbH). This model consists of:

- The generic battery model which provides the input signals for the charge controller. Those signals are the SOC, the DC cell voltage and DC cell current.
- The converter which determines the active and reactive power output for frequency and voltage control respectively.
- Three controllers (frequency controller, voltage - power controller and a charge controller). The frequency controller regulates the active power in case of frequency deviation according to the droop value. In the voltage – power controller, the voltage and active power deviation is balanced. The output from this controller is used as input signal for charge controller. The last one controls the charging/discharging according to the SOC. A current limiter is also included in this block in order to restrain the value of current according to a maximum current limit.
- Three measurement blocks (frequency, AC-voltage and PQ).

The configuration parameters for all blocks are presented in tables 27-30. Furthermore, the BESS is connected in bus RL1-2 in parallel to the PV system.

5.3 Simulation and results

This part presents the simulation results for various generation/load conditions and fault cases concerning the BESS response and also the system's voltage and frequency stability.

Case 1: Wind generator outage event

The first case to be investigated is an outage event. Initially, the wind generator supplies steady power to the consumers and 20 seconds after the simulation start, it is suddenly disconnected from the grid. Three levels of RES penetration are taken into account. For each RES penetration level, wind power share is 90% while the rest (10%) comes from the PV system. Moreover, three different cases of BESS operation are considered. In the first case the BESS is deactivated and only the DG is responding to the disturbance. In the second and third case, the battery is activated and its power rating is 0.5 MW and 1 MW respectively. The following figures 41-44 illustrate the voltage and frequency profile and the power output of the battery and DG.

As shown in Figure 41, there are more significant voltage and frequency variations after the disturbance in case that BESS is not included in the hybrid system. Moreover, the increment of batteries' power rating restrains the magnitude and length of fluctuations and leads to better steady-state conditions. The improved dynamic performance occurs because of the BESS balancing capability and is due to the time constants of the battery controller blocks.

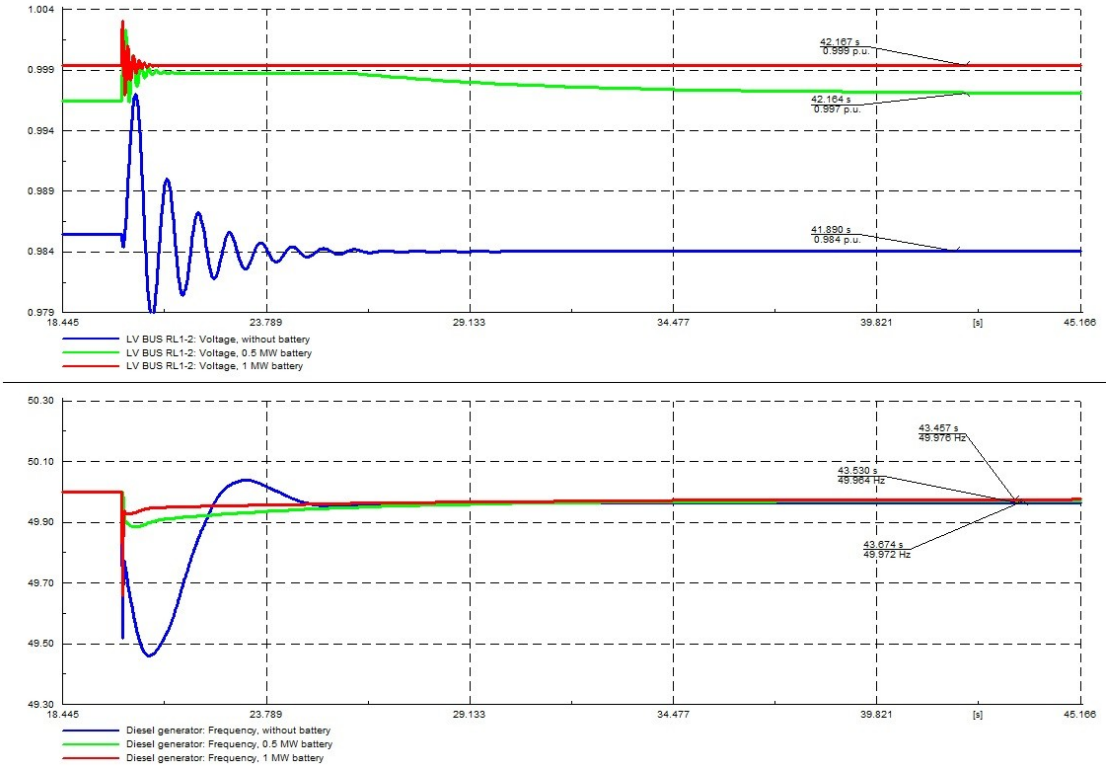

Figure 41 Simulation results for outage event in high RES penetration (90%) case

Also, Figure 42 illustrates that as the battery's power capacity grows, its power supply increases as well. On the other hand, the DG's output drops.

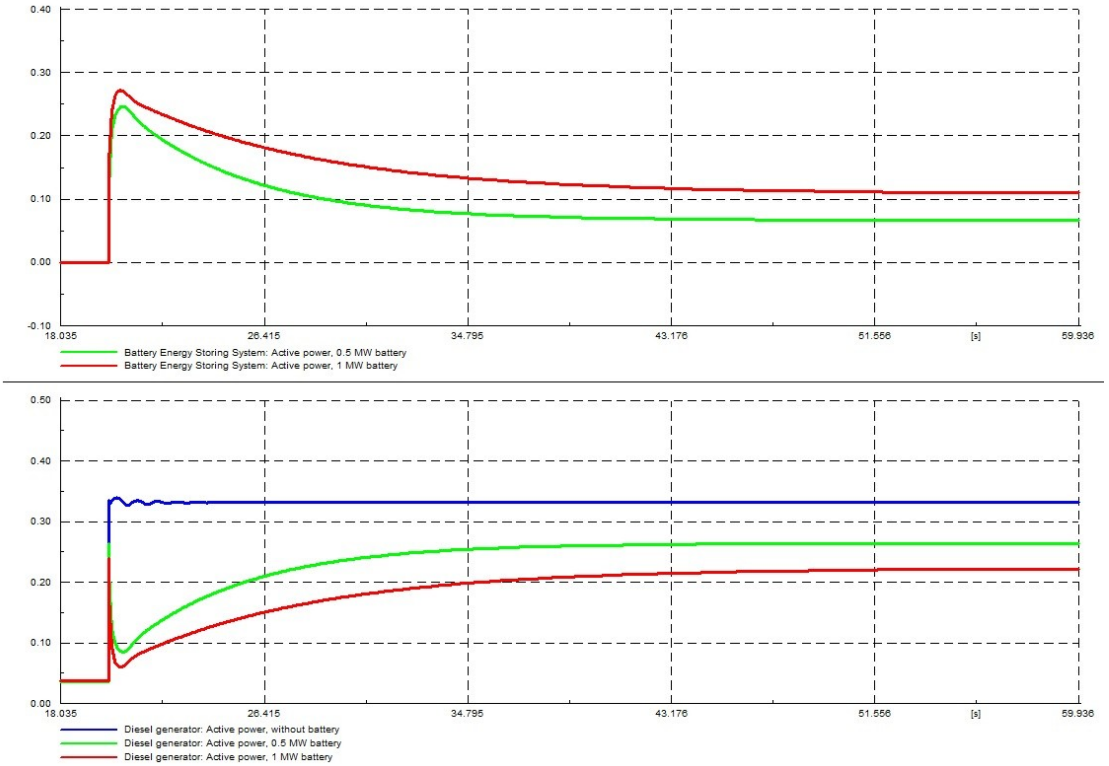

Figure 42 Power output from BESS and DG during outage event in high RES penetration (90%) case

The voltage and frequency profiles in the cases of medium and low RES share are demonstrated in Figure 43 and Figure 44.

Those figures show that as RES power participation in the energy mix grows, more significant instabilities are likely to take place in the grid during a sudden wind power supply interruption and also, there are larger deviations of steady-state frequency values from the nominal (50 Hz). This issue is common in energy systems with limited participation from synchronous generators, due to low inertia of the system. Therefore, the presence of BESS in hybrid systems with high penetration from renewables is very important in order to negotiate the generation/load unbalances and as storage power rating increases, the achievement of high RES fractions becomes more feasible.

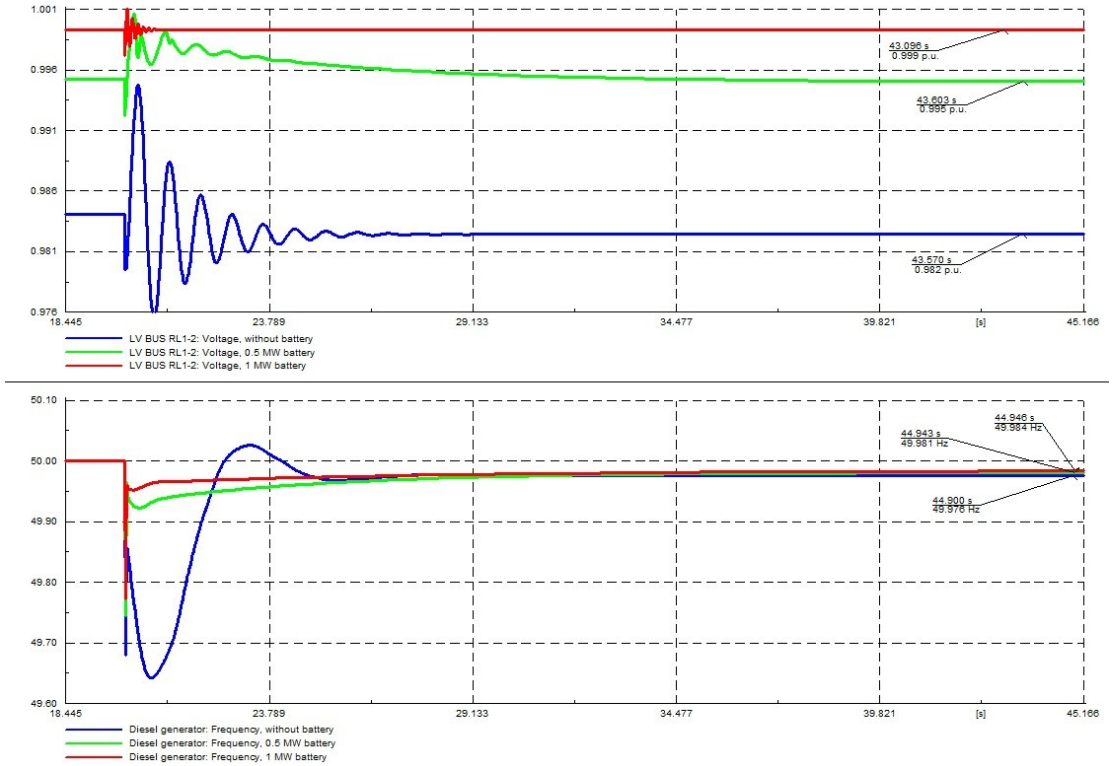

Figure 43 Simulation results for outage event in medium RES penetration (60%) case

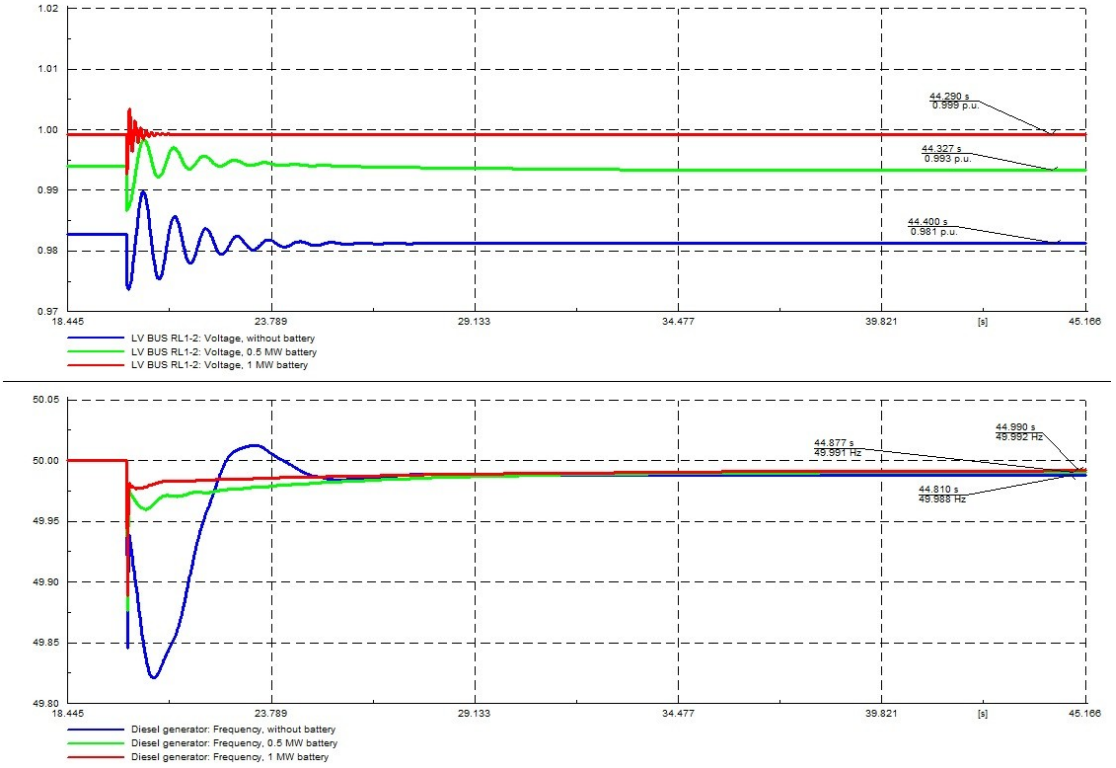

Figure 44 Simulation results for outage event in low RES penetration (30%) case

Case 2: Residential load reduction event

This case discusses the battery behaviour and system stability during a load reduction event that takes place at the 20th second of the simulation. During this event, batteries absorb the exceeding power in order to maintain balancing conditions. Three different levels of load drop are assumed: 20%, 30% and 40%. It is also assumed that wind and solar generators cover 90% of the demand and the power rating of BESS is 1 MW. The results are illustrated in Figure 45 and Figure 46.

During the event, the voltage and frequency variations which are illustrated in Figure 45, show that the magnitude of the fluctuations and the steady-state condition after the disturbance are related to the percentage of load drop and grow with the increment of reduction. Moreover, the acceptable ranges are not exceeded during the events. Also, Figure 46 shows that battery charging increases according to the load drop and DG output is adjusted as well.

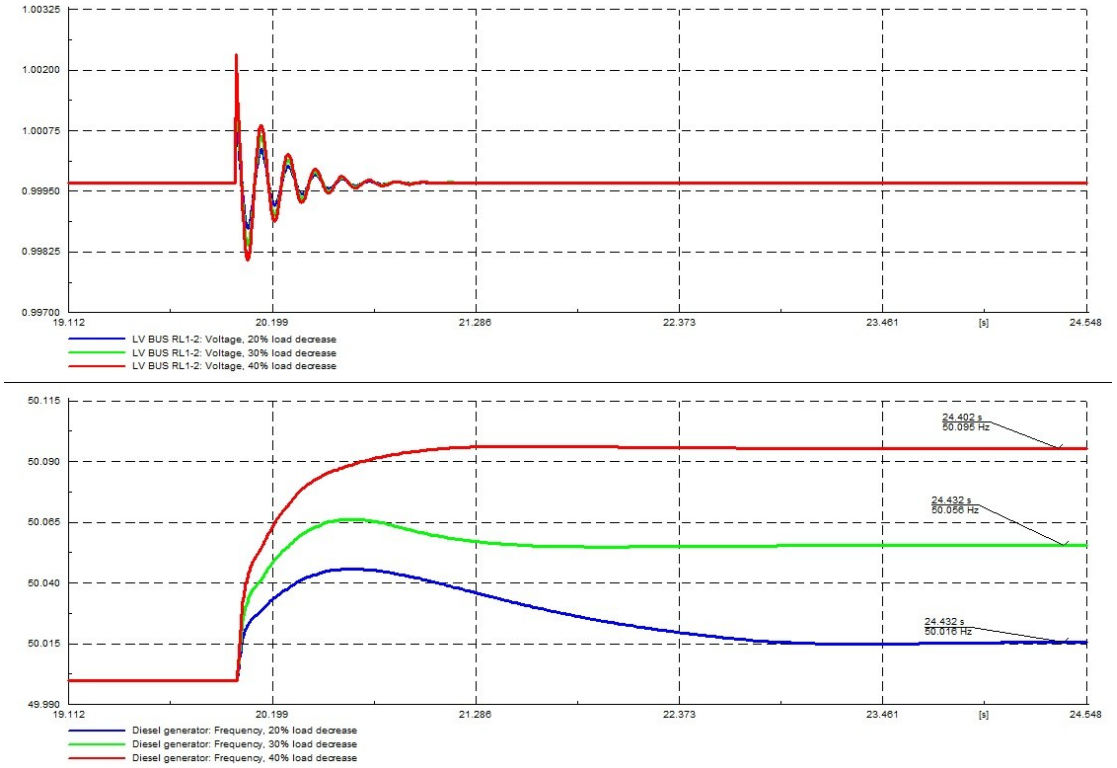

Figure 45 Simulation results for different levels of load reduction

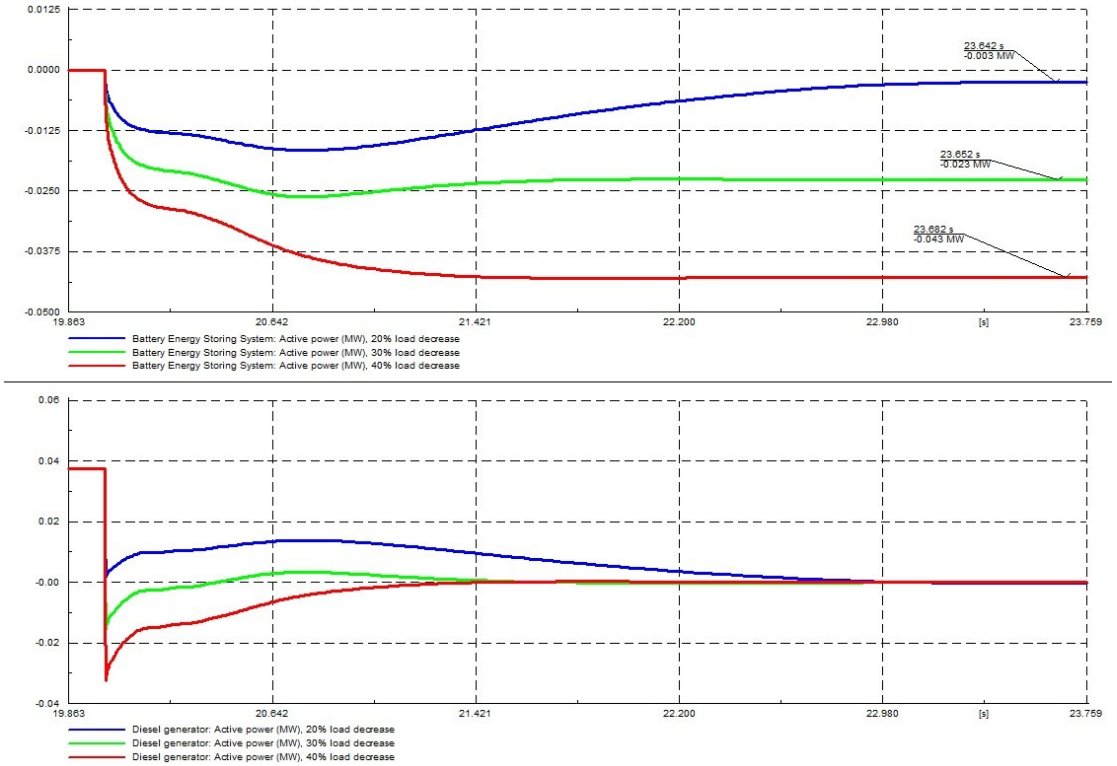

Figure 46 Power output from BESS and DG during load reduction event

Case 3: DG outage event

In this case it is assumed that the demand is covered 40% by wind and solar units and the rest by one DG that supplies its nominal power (220 kW). The DG is suddenly disconnected from the grid 30 seconds after the initialization of simulation. The disturbances are negotiated by the BESS and other DG units which are in stand-by mode. Three cases are considered: one case where BESS is not included in the system and two other cases with different battery power capacities (0.5 MW/1 MW). Figure 47 shows the simulation results for this event with respect to the frequency and voltage variations.

As expected, more important deviations take place when there isn't ES in the system. Moreover, larger power ratings bring better balancing capability. It is also found that during such important DG contingencies in cases of increased conventional power supply in the energy mix, the system stability is improved when a BESS operates in parallel with the stand-by DG reserves. Therefore, the operation of batteries in stand-alone systems has many advantages and not only when it comes to achievement of high RES shares.

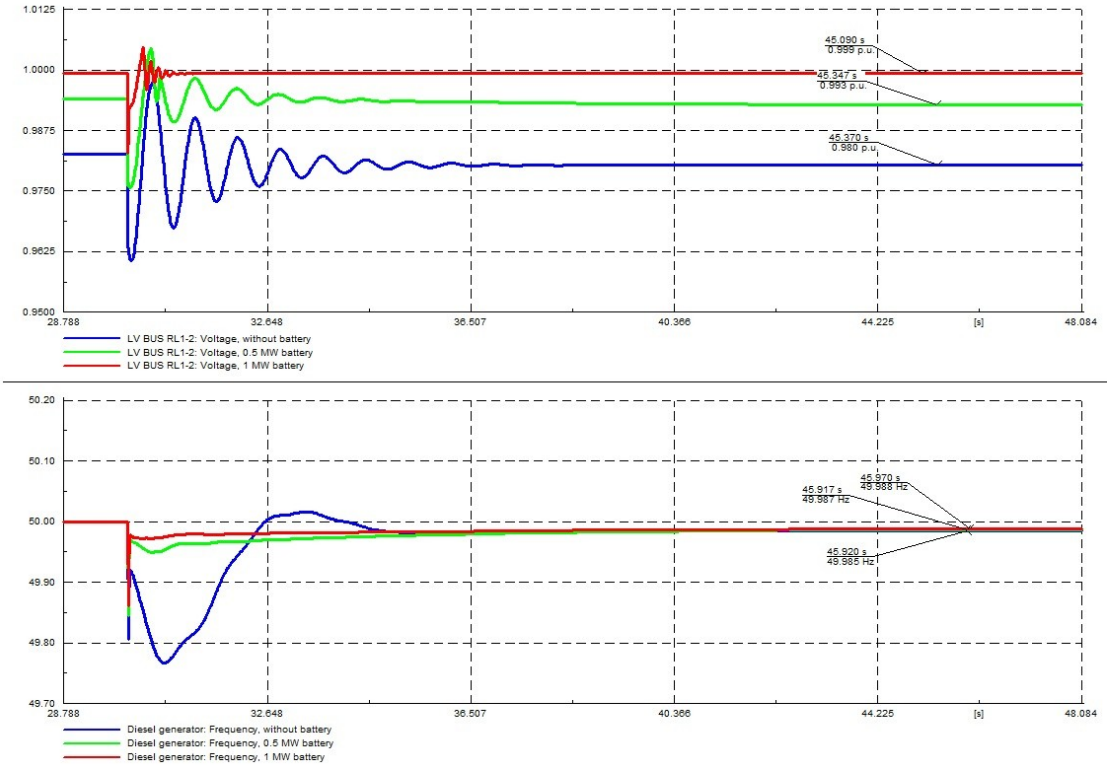

Figure 47 Simulation results for DG outage event

5.4 Conclusions

In conclusion, this chapter investigated the dynamic behaviour of the proposed hybrid power system under different generation/load variations and faults. Through simulation of various events, it was found that the BESS plays a very significant role in system stability and keeps the grid within acceptable frequency and voltage ranges. Also, the power system's unbalances, during sudden changes of demand and/or renewable power supply, are amplified in cases of high RES penetration due to low system inertia. For this reason, in renewable-based stand-alone systems, it is considered very important to include BESS. Furthermore, the problems related to low system inertia are likely to pose technical barriers in the level of achievable RES share since a DG unit must be running all the time. Finally, the benefits from battery usage were also demonstrated during a DG unit disconnection event and results showed that batteries can improve the stability in cases of high DG participation (low RES fraction) due to their faster response compared to the DG units.

Chapter 6 – Conclusions and future work

The initial goal for this thesis was sizing an ES system for a hybrid renewable-based power station in the islanded system of Agios Efstratios. Utilization of ES technologies in autonomous power systems is a popular method for improving power quality and negotiating the power output fluctuations. For this reason, the first step was to evaluate the available ES technologies according to their capability to provide applications suitable for renewable stand-alone islanded systems. The main characteristics of the ES types have been presented and compared. According to this assessment, battery technologies are the most suitable ones to support RES integration in Agios Efstratios due to their technical maturity, flexibility and wide range of applications. Furthermore, a number of studies and cases demonstrating the benefits of ES utilization in autonomous power systems have been included.

Secondly, the size of hybrid system has been optimized with respect to its NPC and considering a number of technical and economic constraints. Moreover, the optimization process took into account different types of wind turbines and a range of wind, solar and storage capacities. The results were categorized according to three scenarios, each of them representing a different policy approach (scenarios). It was found that the solution of the objective function is a system comprising of one WT rated at 330 kW, a PV plant of 100 kWp and 1 MWh battery energy capacity. The drawback of this hybrid system is the large energy excess that is generated due to the size of WT and the incapability of ES to absorb it. The NPC is 2,966 k€ and comparing it to the costs that were derived from combinations with smaller wind turbines, it was found that the first one was less. Also, by removing the constraint of obligatory PV participation, photovoltaics are not included in the optimal solution and the NPC drops by 9%. The high RES policy constraint (scenario 2) is satisfied with the same wind (330 kW) and solar (100 kWp) ratings and by increasing the battery capacity to 3 MWh. The cost for that system is 67 k€ more than scenario 1 but on the other hand it has the advantage of diesel reduction by 32%. Moreover, it has been proved that a total renewable scenario (scenario 3) is economically feasible since the cost for that system is less than the diesel station's cost for the same period. Further, it was calculated that interconnection is not a feasible option due to high capital and installation cost. The next step was a battery type assessment including four types (LA, Li-ion, VRB and NaS) which are suitable for RES integration. The results showed that LA is the most economic choice, has good efficiency level and cycle lifetime close to the nominal float life.

Another objective of this thesis was to analyze the existing power system (base case topology) and its voltage profile during normal operation. For that scope, a static model of the power network was developed in DIgSILENT and load flow analysis was performed considering various demand profiles (summer – winter). The results showed that the voltage steady-state magnitude is maintained within acceptable range and the system's components (lines and transformers) are low loaded during the largest part of the year. Only during peak demand there is high loading in one of the transformers of residential area. The next target was to investigate the optimal placement for renewable and ES units. Regarding the WT, its sitting depends on the wind conditions of the island and it is proposed to be located at the existing wind farm. For the PV and battery plants, the best option is to place separate smaller units at different LV feeders of the residential area. In that way, the power losses are minimized and the voltage profile is improved.

Finally, this thesis aimed at demonstrating the hybrid system's dynamic behavior under generation and demand variations and the battery's capability for frequency and voltage stability improvement. A dynamic model was developed using DIgSILENT standard library models and simulations showed that BESS operation is very important in autonomous renewable-based power systems. Moreover, the BESS balancing capability is improved with the increment of its power capacity and thus, achievement of high RES share becomes more feasible. Moreover, high levels of RES penetration bring limited tolerance against disturbances due to low inertia in the system and power quality deviations are amplified as the magnitude of disturbances increases. Through the results it was proved that the constant DG operation is important in order to maintain the system inertia. Therefore, the potential RES penetration levels are likely to be restrained and a total renewable scenario might be infeasible for the island. A possible solution can be to use a smaller DG unit so that it will not suppress the renewables fraction that much.

A possible future work may be to apply demand side management actions for further system optimization. Also, a sensitivity analysis can be performed regarding renewable resources data, demand time series and diesel prices and observe the changes that are brought in optimization results and grid breakeven point. Another option is to expand the dynamic analysis for further dynamic events (short-circuits, LVRT etc.) and develop a controller which can enable 100% RES penetration. Finally, another potential is to investigate the techno-economic feasibility of implementing hybrid power stations in more islanded systems.

APPENDIX A

Diesel power system cost calculation

The total discounted costs and main technical characteristics for the diesel power system are presented in Figure 48 and Table 10.

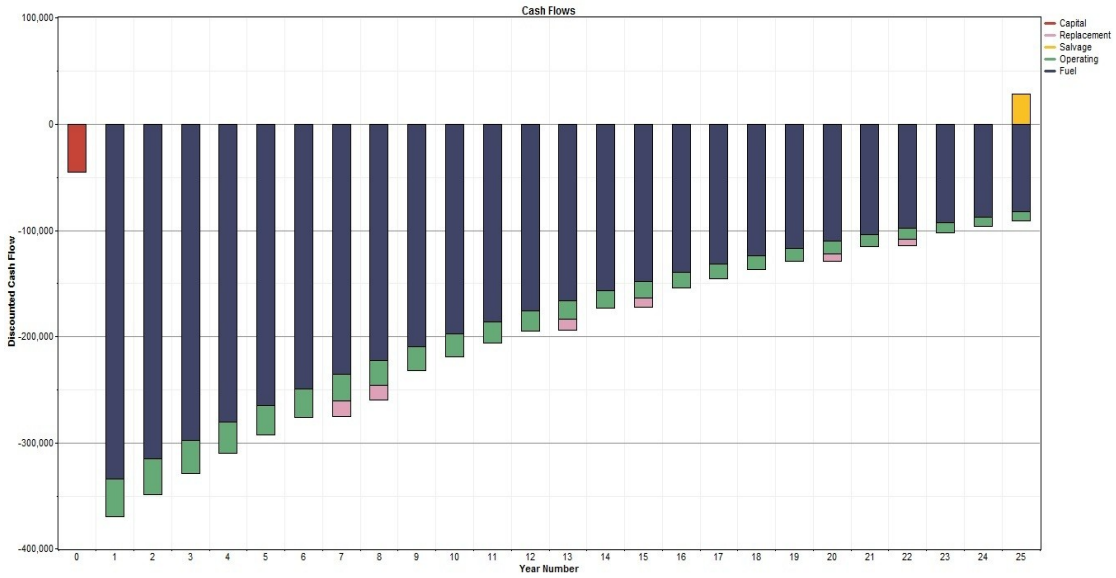

Figure 48 Discounted case flows for the diesel power station

Table 10 Operational data and total costs of the diesel power station

	Capital (€)	Replacement (€)	Salvage (€)	Operating (€)	Fuel (€)	Total (€)
System	45,000	60,501	-27,828	478,485	4,530,300	5,086,459
Diesel Unit	**Fuel consumption (L/yr)**	**Specific fuel consumption (L/kWh)**	**Electrical production (kWh/yr)**	**Hours of operation (hr/yr)**	**Fuel Cost (€)**	
DG1	203,666	0.345	589,673	7,810	2,082,828	
DG2	135,898	0.395	344,027	6,928	1,389,783	
DG3	103,424	0.360	287,254	1,796	1,057,689	
DG4	0	0	0	0	0	
DG5	0	0	0	0	0	

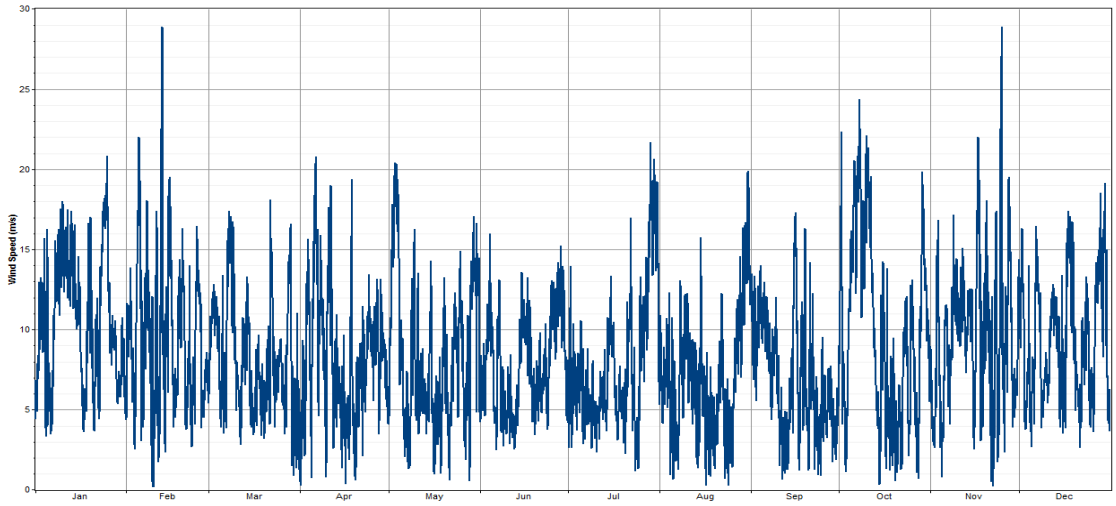

Figure 49 Wind speed annual time series in average hourly values

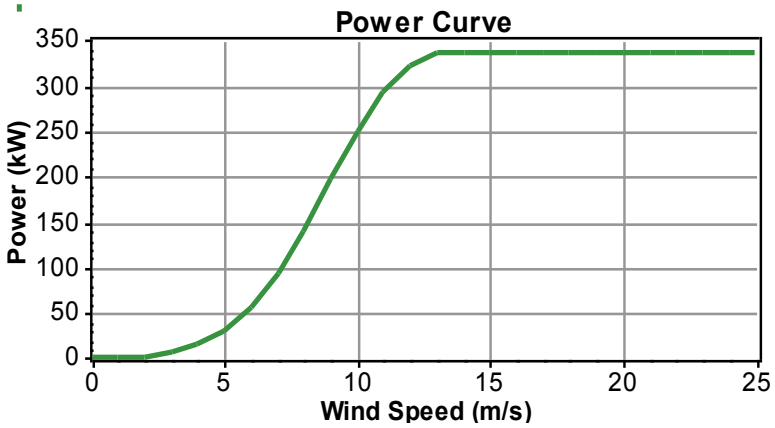

Figure 50 Power curve of E-33 / 330 kW wind turbine

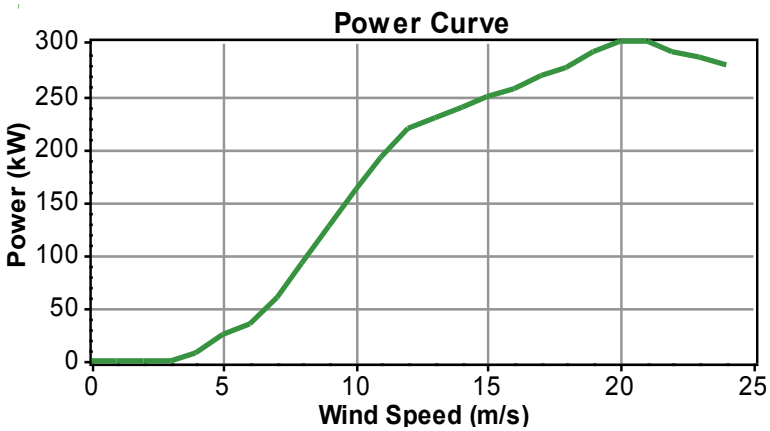

Figure 51 Power curve of F250 / 250 kW wind turbine

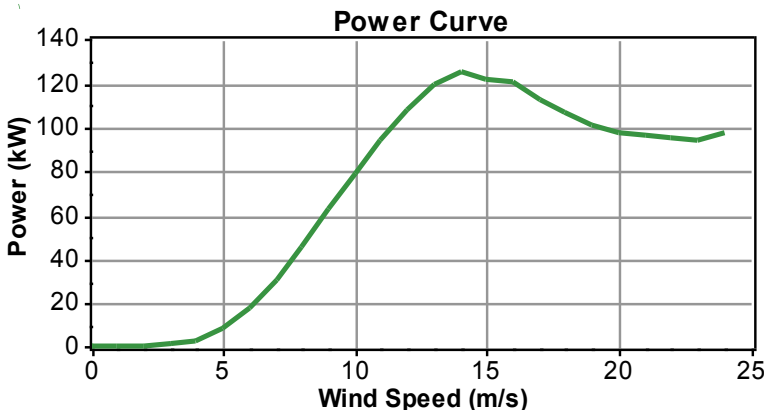

Figure 52 Power curve of F100 / 100 kW wind turbine

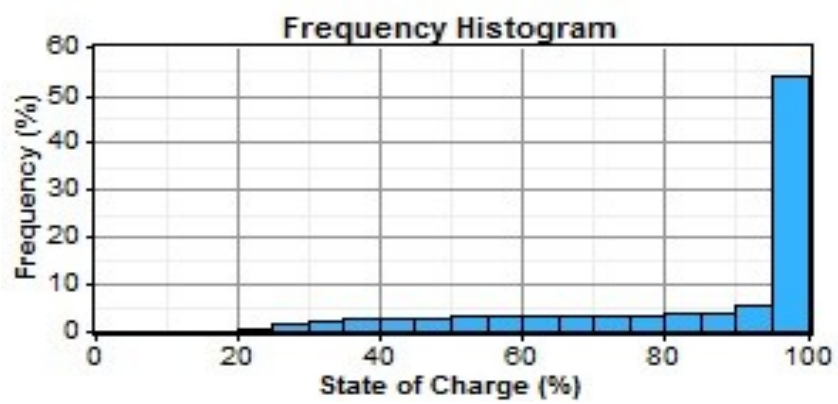

Figure 53 Frequency histogram for battery SOC

Table 11 Optimization results for case 1

WT power (kW)	Battery (MWh)	PV power (kW)	Capital cost (M€)	Total NPC (M€)	COE (€/kWh)	RES fraction	Excess energy (MWh/yr)	Diesel (L/yr)
330	1	100	1.678	2.966	0.190	0.89	937	72,709
		200	2.078	3.284	0.210	0.91	1,043	61,032
		300	2.478	3.640	0.233	0.93	1,162	52,807
	3	100	2.037	3.033	0.194	0.93	846.542	48,945
		200	2.437	3.324	0.213	0.95	948.822	34,483
		300	2.837	3.667	0.235	0.97	1,064.3	24,855
	6	100	2.577	3.499	0.224	0.95	798.8	35,701
		200	2.976	3.829	0.245	0.97	912.367	24,738
		300	3.377	4.186	0.268	0.98	1,033.3	16,407
	9	100	3.116	4.045	0.259	0.96	772.312	29,644
		200	3.516	4.392	0.281	0.97	895	20,385
		300	3.916	4.755	0.304	0.98	1,018	12,592
	12	100	3.655	4.593	0.294	0.96	750.575	23,868
		200	4.055	4.964	0.318	0.98	880.222	16,809
		300	4.455	5.342	0.342	0.99	1,010.4	10,387
	15	100	4.194	5.184	0.332	0.97	743.09	22,079
		200	4.594	5.552	0.355	0.98	872.634	14,695
		300	4.994	5.921	0.379	0.99	1,000.7	7,506
660	1	100	2.368	3.347	0.214	0.98	2,573.6	28,615
		200	2.768	3.707	0.237	0.98	2,696.3	20,927
		300	3.168	4.108	0.263	0.99	2,828.4	16,643
	3	100	2.638	3.520	0.225	0.99	2,531.2	16,896
		200	3.038	3.914	0.25	0.99	2,664.6	11,904
		300	3.438	4.327	0.277	0.99	2,800.9	8,691
	6	100	3.177	4.065	0.26	0.99	2,508.2	10,792
		200	3.577	4.479	0.287	0.99	2,648.5	7,740
		300	3.977	4.910	0.314	1	2,790.9	6,085
	9	100	3.716	4.632	0.296	0.99	2,492.2	6,803
		200	4.116	5.061	0.324	1	2,637.2	5,046
		300	4.516	5.488	0.351	1	2,779.1	3,098
	12	100	4.255	5.216	0.334	1	2,482.2	4,331
		200	4.655	5.640	0.361	1	2,626.5	2,147
		300	5.055	6.079	0.389	1	2,772.6	1,332
	15	100	4.794	5.807	0.372	1	2,475.2	2,471
		200	5.194	6.244	0.4	1	2,623.7	1,495
		300	5.594	6.676	0.427	1	2,767.8	0

Table 12 Optimization results for case 2

WT power (kW)	Battery (MWh)	PV power (kW)	Capital cost (M€)	Total NPC (M€)	COE (€/kWh)	RES fraction	Excess energy (MWh/yr)	Diesel (L/yr)
250	1	100	1.468	3.093	0.198	0.83	506.517	103,49
		200	1.868	3.365	0.215	0.86	598.792	87,070
		300	2.268	3.699	0.237	0.89	707.820	76,033
	3	100	1.828	3.178	0.203	0.85	422.897	83,801
		200	2.228	3.379	0.216	0.9	498.432	60,557
		300	2.628	3.665	0.235	0.93	597.355	45,026
	6	100	2.367	3.584	0.229	0.88	354.274	65,015
		200	2.767	3.843	0.246	0.92	449.862	47,006
		300	3.167	4.138	0.265	0.95	551.995	32,407
	9	100	2.906	4.139	0.265	0.89	329.342	59,946
		200	3.306	4.352	0.279	0.93	413.942	37,744
		300	3.706	4.680	0.299	0.96	527.896	26,051
	12	100	3.445	4.672	0.299	0.9	301.926	52,740
		200	3.845	4.907	0.314	0.94	393.869	32,578
		300	4.245	5.265	0.337	0.96	518.463	23,681
	15	100	3.984	5.223	0.334	0.91	281.608	47,295
		200	4.384	5.518	0.353	0.94	393.49	32,608
		300	4.784	5.877	0.376	0.96	517.066	23,786
500	1	100	1.858	3.173	0.203	0.94	1639.618	60,054
		200	2.258	3.507	0.224	0.95	1750.18	49,377
		300	2.658	3.883	0.249	0.96	1873.917	42,511
	3	100	2.218	3.251	0.208	0.96	1545.874	35,880
		200	2.618	3.588	0.23	0.97	1661.455	25,070
		300	3.018	3.964	0.254	0.98	1786.768	17,917
	6	100	2.757	3.740	0.239	0.97	1502.479	24,731
		200	3.157	4.108	0.263	0.98	1628.889	16,726
		300	3.557	4.500	0.288	0.99	1761	10,980
	9	100	3.296	4.299	0.275	0.98	1480.781	19,891
		200	3.696	4.655	0.298	0.99	1606.356	10,905
		300	4.096	5.084	0.325	0.99	1751.578	8,510
	12	100	3.835	4.840	0.31	0.99	1456.515	13,507
		200	4.235	5.249	0.336	0.99	1599.556	9,315
		300	4.635	5.665	0.363	0.99	1740.494	5,828
	15	100	4.374	5.424	0.347	0.99	1446.357	11,064
		200	4.774	5.833	0.373	0.99	1589.903	6,897
		300	5.174	6.256	0.4	1	1733.401	3,947
750	1	100	2.248	3.523	0.225	0.97	2840.101	39,911
		200	2.648	3.887	0.249	0.98	2961.987	32,196
		300	3.048	4.287	0.274	0.98	3093.343	27,558
	3	100	2.608	3.656	0.234	0.99	2759.905	18,489
		200	3.008	4.054	0.259	0.99	2894.744	13,316
		300	3.408	4.468	0.286	0.99	3030.272	9,559
	6	100	3.147	4.190	0.268	0.99	2732.447	11,405
		200	3.547	4.612	0.295	0.99	2875.477	8,434
		300	3.947	5.042	0.323	1	3017.046	6,210
	9	100	3.686	4.758	0.305	0.99	2715.928	7,455
		200	4.086	5.192	0.332	1	2862.969	5,572
		300	4.486	5.625	0.36	1	3006.343	3,591
	12	100	4.225	5.342	0.342	1	2705.457	5,012
		200	4.625	5.779	0.37	1	2853.988	3,436
		300	5.025	6.214	0.398	1	2998.831	1,645

	15	100	4.764	5.929	0.379	1	2696.944	2,822
		200	5.164	6.373	0.408	1	2848.053	1,833
		300	5.564	6.808	0.436	1	2992.688	0

Table 13 Optimization results for case 3

WT power (kW)	Battery (MWh)	PV power (kW)	Capital cost (M€)	Total NPC (M€)	COE (€/kWh)	RES fraction	Excess energy (MWh/yr)	Diesel (L/yr)
100	1	100	1.458	3.746	0.24	0.6	26.447	173,35
		200	1.858	3.927	0.251	0.68	63.156	143,29
		300	2.258	4.127	0.264	0.75	122.32	118,01
	3	100	1.727	3.983	0.255	0.6	14.473	171,98
		200	2.127	4.034	0.258	0.69	37.141	135,66
		300	2.527	4.172	0.267	0.77	75.226	104,31
	6	100	2.267	4.596	0.294	0.6	4.2	172,24
		200	2.667	4.583	0.293	0.7	12.725	130,02
		300	3.067	4.638	0.297	0.79	39.993	94,179
	9	100	2.806	5.203	0.333	0.6	1.509	171,83
		200	3.206	5.141	0.329	0.71	0.742	125,20
		300	3.606	5.212	0.334	0.8	29.925	90,807
	12	100	3.345	5.803	0.371	0.6	0	170,91
		200	3.745	5.764	0.369	0.71	1.92	126,35
		300	4.145	5.816	0.372	0.8	24.828	90,205
	15	100	3.884	6.412	0.41	0.6	0	170,69
		200	4.284	6.382	0.408	0.71	2.299	127,01
		300	4.684	6.376	0.408	0.81	11.733	85,494
200	1	100	1.748	3.483	0.223	0.81	383.918	105,10
		200	2.148	3.689	0.236	0.85	464.309	85,168
		300	2.548	3.992	0.255	0.89	561.2	70,961
	3	100	2.017	3.559	0.228	0.83	335.095	92,896
		200	2.417	3.734	0.239	0.88	401.081	67,754
		300	2.817	3.999	0.256	0.91	493.275	50,954
	6	100	2.557	3.942	0.252	0.86	259.101	71,971
		200	2.957	4.171	0.267	0.91	344.508	51,818
		300	3.357	4.466	0.286	0.93	446.762	37,818
	9	100	3.096	4.497	0.288	0.87	237.679	66,898
		200	3.496	4.699	0.301	0.92	314.281	44,243
		300	3.896	4.988	0.319	0.95	416.424	29,624
	12	100	3.635	5.048	0.323	0.88	215.482	61,424
		200	4.035	5.254	0.336	0.93	295.877	39,107
		300	4.435	5.560	0.356	0.95	403.969	26,036
	15	100	4.174	5.610	0.359	0.89	199.327	56,921
		200	4.574	5.847	0.374	0.93	289.668	37,452
		300	4.974	6.178	0.395	0.95	404.863	26,739
300	1	100	2.038	3.585	0.229	0.89	871.069	78,237
		200	2.438	3.859	0.247	0.92	961.288	61,401
		300	2.838	4.186	0.268	0.94	1,069.811	49,953
	3	100	2.307	3.628	0.232	0.92	799.35	58,680
		200	2.707	3.919	0.251	0.94	901.854	44,234
		300	3.107	4.238	0.271	0.96	1,010.125	32,346
	6	100	2.847	4.100	0.262	0.93	750.727	45,924
		200	3.247	4.386	0.281	0.96	853.97	31,000

		300	3.647	4.724	0.302	0.97	968.344	20,919
	9	100	3.386	4.606	0.295	0.95	713.474	36,293
		200	3.786	4.937	0.316	0.96	830.665	25,527
		300	4.186	5.306	0.34	0.98	957.056	18,217
	12	100	3.925	5.156	0.33	0.95	691.265	30,643
		200	4.325	5.507	0.352	0.97	815.237	21,735
		300	4.725	5.880	0.376	0.98	942.826	14,824
	15	100	4.464	5.707	0.365	0.96	670.72	25,235
		200	4.864	6.090	0.39	0.97	806.064	19,209
		300	5.264	6.453	0.413	0.98	931.319	11,395
400	1	100	2.328	3.838	0.246	0.93	1,388.403	61,790
		200	2.728	4.133	0.265	0.95	1,488.757	47,466
		300	3.128	4.477	0.287	0.96	1,602.825	37,641
	3	100	2.597	3.918	0.251	0.95	1,327.239	44,716
		200	2.997	4.221	0.27	0.97	1,432.58	31,344
		300	3.397	4.569	0.292	0.98	1,549.52	22,198
	6	100	3.137	4.370	0.28	0.96	1,274.047	30,096
		200	3.537	4.705	0.301	0.98	1,389.578	19,738
		300	3.937	5.086	0.325	0.99	1,517.977	13,549
	9	100	3.676	4.924	0.315	0.97	1,250.54	24,920
		200	4.076	5.283	0.338	0.98	1,376.043	16,663
		300	4.476	5.658	0.362	0.99	1,504.553	9,959
	12	100	4.215	5.461	0.349	0.98	1,224.05	18,078
		200	4.615	5.832	0.373	0.99	1,355.327	10,991
		300	5.015	6.248	0.4	0.99	1,496.384	8,102
	15	100	4.754	6.028	0.386	0.98	1,209.033	14,030
		200	5.154	6.411	0.41	0.99	1,343.876	8,049
		300	5.554	6.826	0.437	0.99	1,485.594	5,069

Table 14 Total annualized costs of the hybrid system components

Case	Scenario	Total Annualized Costs (€/year)					
		WT	**PV**	**Diesel gen**	**Battery**	**Converter**	**Total**
Case 1	Sc. 1	77,503	35,043	59,462	20,790	35,347	232,146
	Sc. 2	77,503	35,043	38,056	47,780	35,347	236,293
	Sc. 3	142,872	105,130	4,144	95,561	35,347	383,334
Case 2	Sc. 1	46,510	35,543	97,477	21,535	35,347	242,152
	Sc. 2	105,154	35,543	49,569	19,346	35,347	248,294
	Sc. 3	151,663	106,630	5,074	95,561	35,347	394,618
Case 3	Sc. 1	81,244	35,043	92,335	21,740	35,347	271,919
	Sc. 2	115,779	35,043	48,168	47,780	35,347	285,384
	Sc. 3	254,019	105,130	5,571	95,561	35,347	496,006

Table 15 Comparison of optimization results with respect to policy constraints and without them

Case	Scenario 1	Wind power (kW)	PV power (kWp)	ES capacity (MWh)	NPC (M€)	Diesel (L/yr)	RES fraction (%)	Excess energy (MWh)
Case 1	With constraints	1x330	100	1	2.966	72,709	89	937 (42%)
	Without constraints	1x330	-	1	2.705	88,286	87.4	835.5 (39%)
Case 2	With constraints	1x250	100	1	3.093	103,500	83	506.5 (28%)
	Without constraints	2x250	-	1	2.891	75,129	92	1,536 (55%)
Case 3	With constraints	2x100	100	1	3,483	105,100	81	383.9 (24%)
	Without constraints	2x100	-	1	3,303	136,857	74.5	345 (21%)

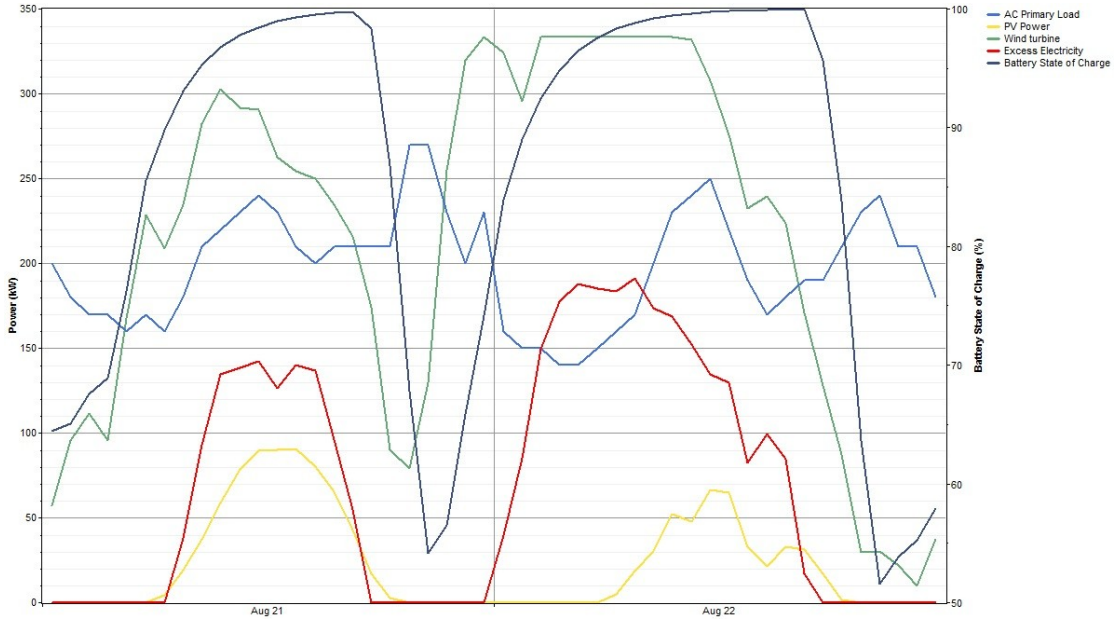

Figure 54 Typical example of excess electricity production

APPENDIX B

Table 16 List of cable lengths and load values for all cases and seasons

Line	Length (m)	Load type	August High demand (kW)	August Average demand (kW)	August Low demand (kW)	January Average demand (kW)	January Low demand (kW)
A	543	**Load 1**	40	23	13	8	4
B1	312	**Load 2**	30	17	10	6	3
B2	231	**Load 3**	35	20	11	7	3.5
C1	1,857	**Load 4**	25	14.4	8	5	2.5
C2	976	**Load 5**	20	11.5	7	4	2
C3	37	**Load 6**	25	14.5	8	5	2.5
D1	1,351	**Load 7**	25	14.5	8	5	2.5
D2	1,940	**Load 8**	20	9.7	5	3	1.6
D3	49	**Load 9**	12.5	6	4	2	1
D4	7	**Load 10**	25	12.1	7	4	2
D5	285	**Load 11**	25	12.1	7	4	2
D6	2,021	**PS1**	15	15	15	15	15
D7	43	**PS2**	7.5	7.5	7.5	7.5	7.5
V1	150	**AB1**	20	17.5	15	12.5	12.5
V2	100	**AB2**	30	25	20	17.5	17.5
V3	100	**MNA**	5	5	5	5	5
V4	100						
V5	80						
V6	250						
V7	100						
V8	150						
V9	170						
V10	200						
V11	100						

Table 17 Technical characteristics for MV and LV OHL cables (Papathanassiou and Papadopoulos 2006)

Cable type	R (Ohm/km)	X (Ohm/km)	C (nF/km)
MV OHL 3x35 mm²	0.591	0.393	5
LV OHL 4x120+25 mm²	0.253	0.069	610

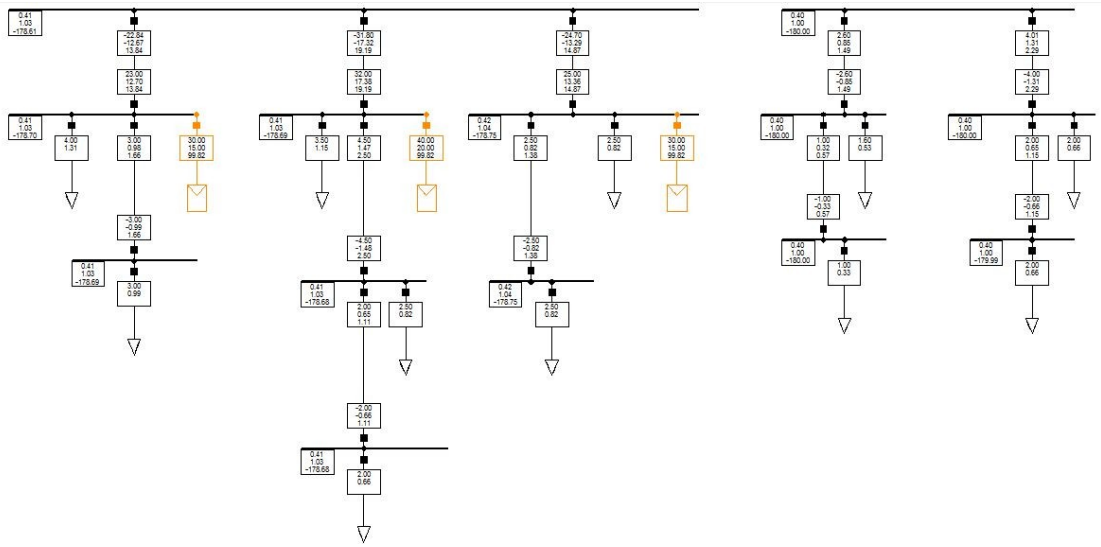

Figure 55 Voltage profile at the LV feeders of the residential area

APPENDIX C

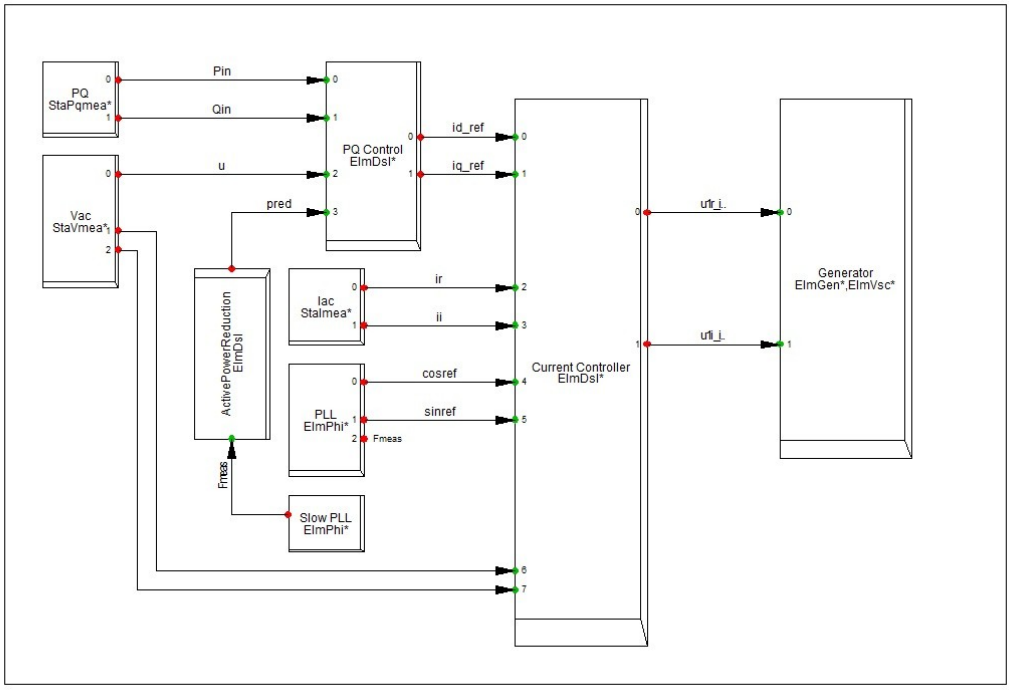

Figure 56 Wind turbine generator frame including current controller

Table 18 Parameters for the PQ controller of wind turbine generator

Parameter	Value
Kp, Gain of active power control (pu)	0.5
Tp, Time constant of the active power control (s)	0.002
Kq, Gain of reactive power control (pu)	0.5
Tq, Time constant of the reactive power control (s)	0.02
Xm, Magnetizing reactance at Pbase (pu)	0
deltaU, Voltage deadband (pu)	0.1
i_EEG: 0=acc. E.ON; 1=acc. SDLWindV	1
Tudelay, Voltage support delay (s)	0.01
K_deltaU, Reactive support gain	2
i_max, Combined current limit (pu)	1
Ramp, Active power ramp (%/s)	500
u_max, Maximum allowed internal voltage (pu)	1.1
X, Coupling reactance (%)	10
id_max, id current limit (pu)	1
iq_max, iq current limit (pu)	1

Table 19 Parameters for the current controller of wind turbine generator

Parameter	Value
Kq, Gain of reactive current controller	1
Tq, Integrator time constant of the reactive current controller (s)	0.002
Kd, Gain of active current controller	1
Td, Integrator time constant of the active current controller (s)	0.002
Tm, Current filter time constant (s)	0

Table 20 Parameters for the active power reduction block of wind turbine generator

Parameter	Value
fUp, Start of active power reduction (Hz)	50.2
fLow, End of active power reduction (Hz)	50.05
PHz, Gradient of active power reduction (%/Hz)	40
Tfilter, PT1-filter time constant (s)	0.05
nedGrad, Negative gradient for power change (pu/s)	-0.25
posGrad, Positive gradient for power change (pu/s)	0.25

Table 21 Parameters of the model of the diesel governor

Parameter	Value
K, Actuator gain	30
T4, Actuator derivative time constant (s)	0.35
T5, Actuator first time constant (s)	0.002
T6, Actuator second time constant (s)	0.015
TD, Combustion delay (s)	0.024
Droop, Frequency deviation/active power change	0.002
TE, Time constant power feedback (s)	0.5
T1, Electric control box first time constant (s)	0.018
T2, Electric control box second time constant (s)	0.0001
T3, Electric control box derivative time constant (s)	0.38
Droop control, 0=Throttle feedback, 1=Electric power feedback	1
Tmin, Minimum torque (pu)	0
Tmax, Maximum torque (pu)	1.2

Table 22 Parameters of the model of AVR

Parameter	Value
Tr, Measurement delay (s)	0.02
Ka, Controller gain (pu)	175
Ta, Controller time constant (s)	0.03
Ke, Excitor constant (pu)	1
Te, Excitor time constant (s)	0.266
Kf, Stabilization path gain (pu)	0.0025
Tf, Stabilization path time constant (s)	1.5
E1, Saturation factor 1 (pu)	4.5
Se1, Saturation factor 2 (pu)	1.5
E2, Saturation factor 3 (pu)	6
Se2, Saturation factor 4 (pu)	2.46
Vrmin, Controller output minimum (pu)	-12
Vrmax, Controller output maximum (pu)	12

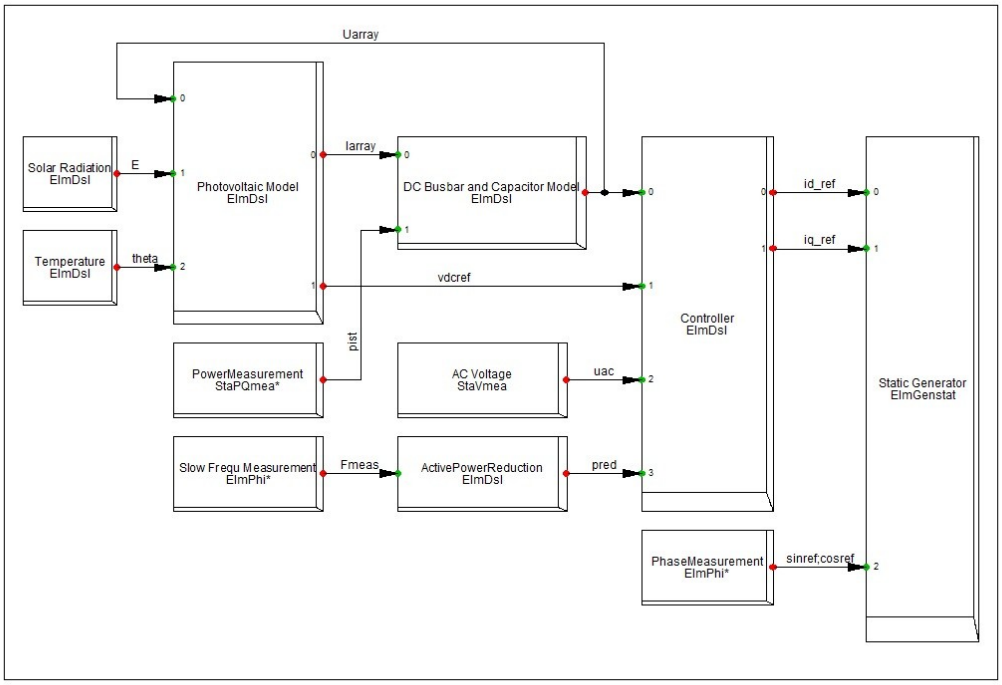

Figure 57 Frame of PV system

Table 23 Parameters of the PV array

Parameter	Value
UI0, Open-circuit voltage of module (V)	32.9
Ummp0, MPP voltage of module (V)	26.3
Immp0, MPP current of module (A)	7.61
Ik0, Short-circuit current of module (A)	8.21
au, Temperature correction factor (voltage) (1/K)	-0.0039
ai, Temperature correction factor (current) (1/K)	0.0004
nSerial, Number of series modules	20
nParallel, Number of parallel modules	25
Tr, Time constant of module (s)	0

Table 24 Parameters for the DC busbar and capacitor

Parameter	Value
Capacity, capacity of capacitor on DC busbar (s)	0.0172
Udc0, Initial DC voltage (V)	700
UdcN, Nominal DC voltage (kV)	1
Pnom, Rated power (MW)	0.1

Table 25 Parameters for the Vdc controller

Parameter	Value
Kp, Gain of active power PI – controller	0.005
Tip, Integration time constant of the active power PI - controller	0.03
Tr, Measurement delay (s)	0.001
Tmpp, Time delay MPP tracking (s)	5
Deadband, Deadband for AC voltage support (pu)	0.1
Droop static for AC voltage support (pu)	2
i_EEG: 0=acc. TC2007; 1=acc. SDLWindV	1
id_min, Minimum active current limit (pu)	0
U_min, Minimum allowed DC voltage (V)	333
iq_min, Minimum reactive current limit (pu)	-1
id_max, Maximum active current limit (pu)	1
iq_max, Maximum reactive current limit (pu)	1
maxAbsCur, Maximum allowed absolute current (pu)	1
maxIq, Maximum absolute reactive current in normal operation (pu)	1

Table 26 Parameters for active power reduction block

Parameter	Value
fUp, Start of active power reduction (Hz)	50.2
fLow, End of active power reduction (Hz)	50.05
Gradient, Gradient of active power reduction (%/Hz)	40
Tfilter, PT1-filter time constant (s)	0.01

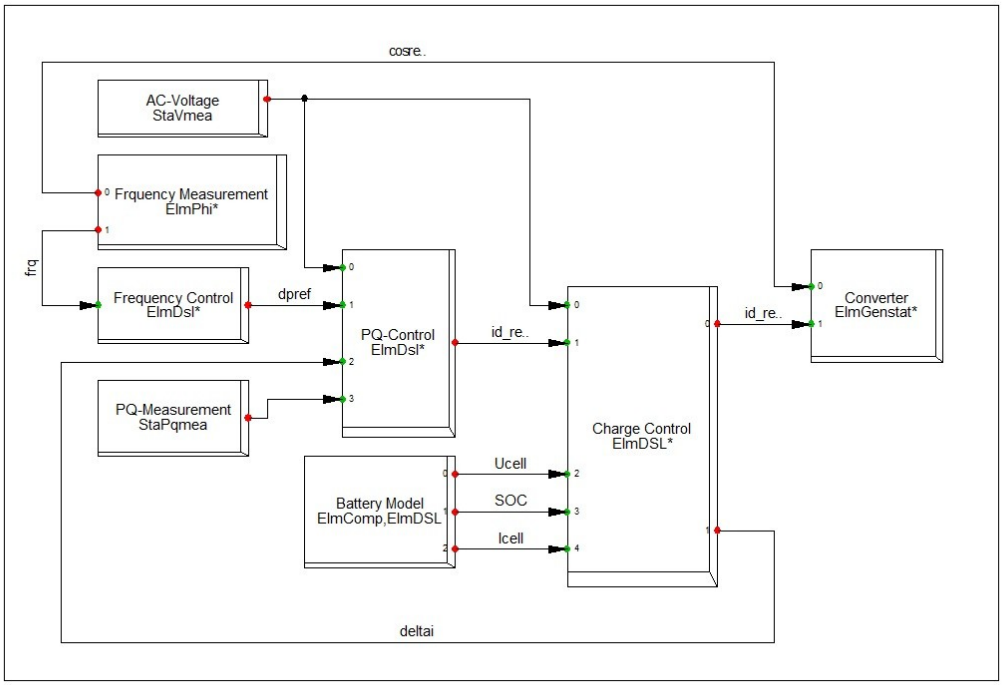

Figure 58 Model frame of the battery ES system

Table 27 Parameters of the battery common model

Parameter	Value
SOC0, State of charge at initialization	0.8
CellCapacity, Capacity per cell (Ah)	3000
u_min, Voltage of empty cell (V)	1.7
u_max, Voltage of full cell (V)	2.4
CellsParallel, Amount of parallel cells	20
CellsInRow, Amount of cells in row	25
RiCell, Internal resistance per cell (ohm)	0.001

Table 28 Parameters of the frequency controller of the battery ES system

Parameter	Value
droop, The droop value of active power	0.004
db, Deadband for frequency control (pu)	0.0002

Table 29 Parameters of the voltage and power controller of the battery ES system

Parameters	Value
Tr, Filter time constant, active path (s)	0.01
Trq, Filter time constant, reactive path (s)	0.1
Kp, Proportional gain -id – PI – controller (pu)	2
Tip, Integrator time constant – id – PI – controller (s)	0.2
AC_deadband, Deadband for proportional gain (pu)	0
Kq, Proportional gain for AC – voltage support (pu)	1
Tiq, Integrator time constant – iq – I – controller (s)	0.002
id_min, Minimum real part of current (pu)	-0.4
iq_min, Minimum imaginary part of power (pu)	-1
id_max, Maximum real part of current (pu)	1
iq_max, Maximum imaginary part of current (pu)	1

Table 30 Parameters of the charge controller of battery ES system

Parameters	Value
ChargeCur, Minimum charging current (pu)	0.05
minSOC, Minimal SOC, discharging will be stopped (pu)	0.2
maxSOC, Maximal SOC, charging will be stopped (pu)	1
deltaU, Threshold for iq preference (pu)	0.9

Bibliography

Barton, John, and David Infield. "Energy Storage and Its Use with Intermittent renewable Energy." *IEEE TRANSACTIONS ON ENERGY CONVERSION, VOL. 19, NO. 2*, June 2004: 441-448.

Bognar, Kristina, and Frank Behrendt. "Water Desalination in Micro Grids Based on Renewable Energies ." *Micro Perspectives for Decentralized Energy Supply.* Berlin: Technische Universität Berlin, 2011. 73-80.

Boretti, Alberto. "Stoichiometric H2ICE with water injection and exhaust and coolant heat recovery through organic Rankine cycles." *International Journal of Hydrogen Energy vol. 36*, 2011.

Borges, Carmen, and Djalma Falcao. "Optimal distributed generation allocation for reliability, losses, and voltage improvement." *Electrical Power and Energy Systems 28* , February 23, 2006: 413–420.

Braun, Philipp, Maciej Swierczynski, Robert Diosi, Daniel Stroe, and Remus Teodorescu. "Optimizing a Hybrid Energy Storage for a Virtual Power Plant for Improved Wind Power Generation: A Case Study for Denmark." *Proceedings of the 6th International Renewable Energy Storage Conference and Exhibition.* 2011.

Chen, Haiseng, Ngoc Kong Thang, Yang Wei, Tan Chunqing, Li Yongliang, and Ding Yulong. "Progress in electrical energy storage system: A critical review." *Progress in Natural Science 19*, 2009: 291-312.

Connolly, David. "A Review of Energy Storage Technologies for the Integration of Fluctuating Renewable Energy." University of Limerick, August 17, 2009.

CRES. *Center for Renewable Energy Sources and Savings.* July 25, 2011. http://www.cres.gr/kape/news/deltia/deltio_typoy_prasino_nisi.htm (accessed March 11, 2012).

DIgSILENT GmbH. "PowerFactory User's Manual DIgSILENT PowerFactory, Version 14 ." Manual, Gomaringen, Germany, 2008.

Divya, K.C., and Jacob Ostergaard. "Battery energy storage technology for power systems - An overview." *Electric Power Systems Research vol. 79*, December 11, 2009: 511-520.

E.S.A. *Electricity Storage Association.* 2009. http://www.electricitystorage.org/technology/storage_technologies/technology_comparison (accessed March 2012, 4).

Electropaedia. http://www.mpoweruk.com/zebra.htm (accessed February 20, 2012).

EPRI DOE. *EPRI DOE Handbook Supplement of Energy Storage for Grid Connected Wind generation Applications.* Technical report, Palo Alto: EPRI DOE and U.S Department of Energy, 2004.

EPRI. *Handbook of Energy Storage for Transmission and Distribution Applications.* Technical update, Palo Alto, CA: EPRI, 2002.

Espinar, Bella, and Didier Mayer. "The role of energy storage for mini grid stabilization." International Energy Agency, Photovoltaic Power Systems Program, July 2011.

EURELECTRIC. *Application Guide to the European Standard EN 50160 on "Voltage Characteristics of Electricity Supplied by Public Distribution Systems".* Technical Standards, Eurelectric, Union of the Electricity Industry, 1995.

European Commission. *The EU climate and energy package.* October 2010. http://ec.europa.eu/clima/policies/package/index_en.htm (accessed March 2012, 10).

European Environmental Agency (EEA). *NATURA 2000 Viewer.* 2011. http://natura2000.eea.europa.eu/# (accessed March 11, 2012).

Garimella, Niraj, and N-K.C. Nair. "Assessment of Battery Energy Storage Systems for Small-Scale Renewable Energy Integration." *TENCON 2009.* Singapore: Conference Publications, 2009. 1-6.

Giannoulis, E.D., and D.A. Haralambopoulos. "Distributed Generation in an isolated grid: Methodology of case study for Lesvos - Greece." *Applied Energy 88*, February 2011: 2530 - 2540.

Global Energy Network Institute. *G.E.N.I.* 2012. http://www.geni.org/globalenergy/library/renewable-energy-resources/world/europe/wind-europe/wind-greece.shtml (accessed March 10, 2012).

Gomis-Bellmunt, Oriol, Adria Junyent-Ferre, Andreas Sumper, and Joan Bergas-Jane. "Ride-Through Control of a Doubly Fed induction Generator Under Unbalanced Voltage Sags." *IEEE Transactions on Energy Conversion vol. 23 No. 4*, December 2008: 1036-1045.

Gonzalez, Diaz Francisco, Andreas Sumper, Gomis Oriol Bellmunt, and Villafafila Roberto Robles. "A review of energy storage technologies for wind power applications." *Renewable and Sustainable Energy Reviews 16*, 2012: 2154-2171.

Greek Transmission System Operator. "Study for the upgrade of the transmission network 2010-2014." Report, 2010.

Hu, Guozhen, Shanxu Duan, Tao Cai, and Changsong Chen. "Sizing analysis of PV system with VRB storage." 2012.

Ibrahim, Hussein, Adrian Ilinca, and Jean Perron. "Energy Storage Systems - Characterisitcs and Comparisons." *Renewable and Sustainable Energy Reviews 12*, 2008: 1221-1250.

IEEE. *IEEE Recommended Practice for Excitation System Models for Power System Stability Studies, IEEE Std 421.5-2005.* New York: IEEE, 2006.

Joint Research Centre. *PVGIS.* February 2012. http://re.jrc.ec.europa.eu/pvgis/ (accessed March 12, 2012).

Kaldellis, I., and D. Zafirakis. "Optimum energy storage techniques for the improvement of renewable energy sources-based electricity generation economic efficiency." *Energy 32*, May 30, 2007: 2295-2305.

Kaldellis, Ioannis, Dimitrios Zafirakis, and Kosmas Kavadias. "Minimum cost solution of wind - photovoltaic based stand - alone power systems for remote consumers." *Energy Policy 42*, December 21, 2011: 105-117.

kaldellis, Ioannis, Dimitrios Zafirakis, kosmas Kavadias, and Eleni Kaldelli. "Cost benefit analysis of a photovoltaic-energy storage electrification solution for remote islands." *Renewable Energy 34*, 2009: 1299-1311.

Kansal, Satish, B.B.R. Sai, Barjeev Tyagi, and Vishal Kumar. "Optimal placement of distributed generation in distribution networks." *International Journal of Engineering, Science and Technology, Vol. 3, No. 3*, April 2011: 47-55.

Karri, Vishi, Wai Yap, and John Titchen. "Simulation and Configuration of Hydrogen Assisted Renewable Energy Power Systems." *Engineering and Technology 47*, 2008: 269-276.

Khan, M.J., and M.T. Iqbal. "Pre-feasibility study of stand-alone hybrid energy systems for applications in Newfoundland." *Renewable Energy 30*, December 8, 2004: 835-854.

Kintner-Meyer, M., et al. *Energy Storage for Power Systems Applications: A Regional Assessment for the Northwest Power Pool (NWPP).* Report, Washington: Pacific Northwest National Laboratory, 2010.

Komor, Paul, and John Glassmire. *Electricity Storage and Renewables for Island Power: A Guide for Decision Makers.* Report, International Renewable Energy Agency, 2012.

Kundur, Prabha. *Power System Stability and Control.* Palo Alto: McGraw-Hill, 1994.

Kundur, Prabha, et al. "Definition and Classification of Power System Stability ." *IEEE Transactions on Power Systems, vol. 19, no. 2*, May 2004: 1387-1401.

Lorax Energy Systems LLC. "Windpoweringamerica." *Fuhrlander Wind Turbine Overview.* September 29, 2004. http://www.windpoweringamerica.gov/winddiesel/pdfs/2004_wind_diesel/company/lorax.pdf (accessed March 29, 2012).

Lund, Henrik, David Connolly, Brian Vad Mathiesen, and Martin Leahy. "A review of computer tools for analysing the integration of renewable energy into various energy systems." *Applied Energy 87*, 2010: 1059 - 1082.

Makarov, Y.V., et al. *Wide-Area Energy Storage and Management System to Balance Intermittent Resources in the Bonneville Power Administration and California ISO Control Areas.* report, Pacific Northwest National Laboratory, 2008.

Marin, Cipriano, Manuel Luis Alves, and Arthouros Zervos. *100% RES, A challenge for Island Sustainable Development.* Lisbon: Instituto Superior Tecnico, 2005.

Martin, James. *Solar Choice.* 2010. http://www.solarchoice.net.au/blog/batteries-for-stand-alone-solar-power-systems/ (accessed February 15, 2012).

Naish, Chris, Ian McCubbin, Oliver Edberg, and Michael Harfoot. *Outlook of Energy Storage Technologies.* study, Brussels: European Parliament, Commitee on Indusrty, Research and Energy, 2008.

National Renewable Energy Laboratory (NREL). "HOMER energy." 2012. http://homerenergy.com/ (accessed March 25, 2012).

Papathanasiou, Stavros, and Eleni Karamanou. *Investigation of Photovoltaic Penetration Capability at Non Interconnected Islands and Effects over the Operation of Installed Wind Farms.* Technical Report, Athens: National Technical University of Athens, 2007.

Papathanassiou, Stavros, and Michael Papadopoulos. "Harmonic Analysis in a Power System with Wind Generation." *IEEE Transaction on Power Delivery vol. 27*, October 2006: 2006-2016.

PPC. *Public Power Corporation.* December 2011. http://www.dei.gr/ (πρόσβαση March 9, 2012).

Rodrigues, Luis, and Ana Estanqueiro. "Integration of Renewable Sources in the Electric System using Virtual Renewable Power Plants." Lisbon: Laboratório Nacional de Energia e Geologia - LNEG.

Roussakis, G., A.P. Karageorgis, N. Conispoliatis, and V. Lykousis. "Last glacial–Holocene sediment sequences in N. Aegean basins: structure, accumulation rates and clay mineral distribution." *Geo-Marine Letters*, March 10, 2004: 97-111.

Saadat, Hadi. *Power System Analysis.* McGraw-Hill, 2002.

Schoenung, Susan. *Energy Storage Systems Cost Update, A Study for the DOE Energy Storage Systems Program.* Report, SANDIA National Laboratories, 2011.

Singh, Bhim, and Zakir Hussain. "Applications of Battery Energy Storage System (BESS) in Voltage Control and Damping of Power Oscillations." *5th International Conference on Industrial and Information Systems, ICIIS 2010.* 2010.

Souissi, Ahmed, Othman Hasnaoui, and Anis Salami. "Optimal Sizing of a Hybrid System of Renewable Energy for a Reliable Load Supply without Interruption." *European Journal of Scientific Research Vol. 45 No. 4*, 2010: 620-629.

Steward, D., Saur. G., M. Penev, and T. Ramsden. *Lifecycle Cost Analysis of Hydrogen Versus Other Technologies for Electrical Energy Storage .* Technical Report NREL/TP-560-46719, Golden, Colorado: NREL, 2009.

Sudworth, J.L. "The sodium/nickel chloride (ZEBRA) battery." *Journal of Power Sources*, 2001: 149-163.

Swierczynski, Maciej, Remus Teodorescu, Claus Nygaard Rasmussen, Pedro Rodriguez, and Henrik Vikelgaard. "Overview of the Energy Storage System for Wind Power Integration Enhancement." *2010 IEEE International Symposium on Industrial Electronics (ISIE).* 2010. 3749-3756.

Tsikalakis, Antonios, et al. *Market applications in specific island power systems.* Report, Intelligent Energy Europe, 2009.

Turconi, Alberto. *Developments and Improvements in Zebra Nickel Sodium Chloride Batteries.* report, MES-DEA S/A.

Vassillakos, Nikolaos, Nikolaos Karapanagiotis, Dimitrios Fertis, and Kostas Tigkas. *Methods of financing renewable energy investments in Greece.* Report, Athens: Center for Renewable Energy Sources and Savings, 2003.

Wright, D. Sally, L. Anthony Rogers, F. James Manwell, and Anthony Ellis. "Transmission options for offshore wind farms in the united states." University of Massachuccets, Department of Mechanical and Industrial Engineering, Renewable Energy Research Lab, June 2002.

Yang, Zhenguo, et al. *Electrochemical Energy Storage for Green Grid.* review, Pacific Northwest National Laboratory, USA, 2010.

Zafirakis, Dimitrios, and Ioannis Kaldellis. "Present situation and future prospects of electricity generation in Aegean Archipelago islands." *Energy Policy 35*, May 23, 2007: 4623-4639.

Zoulias, Emmanuel, and Nikos Lymperopoulos. *Hydrogen-based Autonomous Power Systems, Techno-Economic Analysis of the Integration of Hydrogen in Autonoum Power Systems .* Springer, 2008.